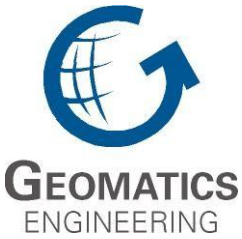

UCGE Reports
Number 20393

Department of Geomatics Engineering

Four-constellation GNSS Reliability and the Estimation of Inter-system Time-offsets for Improved Performance in Challenging Signal Environments

(URL: http://www.geomatics.ucalgary.ca/graduatetheses)

by

Rasika Winit

December 2013

UNIVERSITY OF CALGARY

Four-constellation GNSS Reliability and the Estimation of Inter-system Time-offsets for Improved Performance in Challenging Signal Environments

By

Rasika Winit

A THESIS

SUBMITTED TO THE FACULTY OF GRADUATE STUDIES

IN PARTIAL FULFILMENT OF THE REQUIREMENTS FOR THE

DEGREE OF MASTER OF SCIENCE

DEPARTMENT OF GEOMATICS ENGINEERING

CALGARY, ALBERTA

December 2013

ABSTRACT

The new GNSS constellations such as Galileo and BeiDou being planned and launched will result in a greatly increased number of available ranging sources, hence, improvement in constellation geometry and coverage. When using signals from multiple constellations, however, the challenges are not only to maximize the benefit from the additional ranging observations but also to deal with the differences among satellite systems such as the time-offset between the constellations. Also, challenges exist when using the ranging signal in GNSS degraded environments where GNSS users potentially see a limited number of satellites from multiple GNSS constellations. This work investigates the accuracy and reliably of position solutions when using ranging signals from combined GPS, GLONASS, BeiDou and Galileo constellations in urban environments. Furthermore, this study assesses the benefits of using a priori inter-system clock-offset information.

The positioning performance of multiple GNSS constellations has been examined through covariance simulation and with live data. The benefit of using a priori clock-offset constraints has been demonstrated. It has been found that the benefits of using a priori clock-offset constraints to help enhance the availability of position solutions and fault detection and exclusion capabilities are particularly significant when the receiver is located in areas where limited GNSS signals are available such as in the urban-canyon environment.

ACKNOWLEDGEMENTS

I would like to express my deepest appreciation to my supervisor, Dr. Kyle O'Keefe, for his gracious support, guidance and continuous encouragement during my studies. I would like to thank him for providing me with this opportunity to learn and explore my interests in the field of satellite navigation.

I would like to express my gratitude to Dr. Mark Petovello for his vast knowledge and his kind support in software development for this research. I would also like to thank my colleagues in Position Location And Navigation (PLAN) Group for their instructive discussions and for providing an enjoyable and cooperative work environment. Special thanks to Srinivas Bhaskar, Anup Dhital, G.S. Naveen, Vimal Bhandari, Bernhard Aumayer and Vijay Bellad.

Finally, I am most grateful to my parents for their boundless love, support and encouragement. What I have achieved would not have been possible without them.

To my parents,

If I am an eagle, you are my wings

TABLE OF CONTENTS

LIST OF TABLES

LIST OF FIGURES AND ILLUSTRATIONS

LIST OF SYMBOLS

Symbol	Definition
α	Significance level
b	Receiver-GNSS time-offset
β	Power of the test parameter
c	Speed of light in vacuum
C_r	Covariance matrix of the residuals
cdt	Receiver-GNSS clock-offset in distance units
d	Clock drift
dt	Receiver-GNSS clock-offset in time units
Δb	Inter-system time-offset
$\Delta\hat{x}$	Protection level
δ_0	Non-centrality parameter
$\delta\boldsymbol{z}$	Misclosure vector
el	Elevation angle
(E, N, U)	Local-level coordinate frame, for example East, North and up
ε	Range measurement error
η	Element in design matrix as a function of receiver and satellite positions
f	Carrier phase frequency
$h(\boldsymbol{x})$	Mathematical model as a function of the state vector
H	Design matrix

Symbol	Definition
H_0	Null hypothesis
H_1	Alternative hypothesis
i	Observation index
I_ρ	Ionospheric delay
j	GNSS system index
k	Iteration number
ξ_{global}	Global test statistic
ξ_{local}	Local test statistic
χ^2	Chi-square test statistic
$\boldsymbol{M}$	Column vector uses to map blunder into observations
M_a	Ionospheric code delay correction factor
$Max(\bullet)$	Maximum function
∇_{MDB}	Minimum detectable blunder
μ	Dilution of precision state
$N(\bullet)$	Statistical threshold
N_j	Maximum number of satellites in view from j constellation
$OF(\bullet)$	Obliquity factor
P	Pseudorange measurement
P_C	Estimated state covariance matrix
(ϕ, λ, h)	Curvilinear geodetic coordinate with latitude, longitude and elevation
Φ	Doppler measurements

Symbol	Definition
q	Element in pure geometry dilution of precision matrix
Q_G	Pure geometry dilution of precision matrix
Q_R	Cofactor matrix of an observation covariance matrix
$\boldsymbol{r}$	Residual vector
$\boldsymbol{r_s}$	Standardized residuals vector
R	Observation covariance matrix
ρ	Geometric range between satellite and receiver
σ	Standard deviation
σ^2	Variance
σ_0^2	A priori variance factor
$\hat{\sigma}_0^2$	A posteriori variance factor
$\sigma_{clock\ \&\ ephemeris}$	Error due to satellite clock and ephemeris errors
σ_{iono}	Error due to ionosphere code delay
$\sigma_{multipath}$	Error due to multipath
σ_{noise}	Error due to noise
$\sigma_{noise\ +\ small\ multipath}$	Error due to noise and small multipath
σ_{tropo}	Error due to tropospheric effects
$\sigma_{UERE\ iono,tropo\ only}$	Nominal range observation error due to ionosphere and tropospheric effects only
σ_{URA}	Standard deviation of User Range Accuracy
σ_{UERE}^2	Nominal range observation error

Symbol	Definition
τ_{GPS}	Time-offset between GPS and GLONASS systems
$\boldsymbol{x}$	State vector
$\hat{\boldsymbol{x}}$	Estimated state vector
x_0	Point of expansion
(x, y, z)	Earth-centered Earth-fixed coordinate
$\boldsymbol{z}$	Observation vector
$\hat{\boldsymbol{z}}$	Estimated measurement vector
$(\bullet)_R$	Receiver position
$(\bullet)^s$	Satellite position
$\dot{(\bullet)}$	Velocity parameter

LIST OF ABBREVIATIONS

Abbreviation	Definition
AL	Alert Limit
BDS	BeiDou Navigation Satellite System
BDT	BeiDou Time
BIPM	Bureau International des Poids et Mesures (The International Bureau of Weights and Measures)
C/A	Coarse/Acquisition
CGCS2000	China Geodetic Coordinate System 2000
CS	Control Segment
DoF	Degrees of Freedom
DOP	Dilution of Precision
ECEF	Earth-centered Earth-fixed
EDOP	East Dilution of Precision
EGNOS	European Geostationary Navigation Overlay Service
EOP	Earth Orientation Parameters
EOPP	Earth Orientation Parameters Prediction
ESA	European Space Agency
ETS	Electronic Tolling Systems
EU	European Union
FAA	Federal Aviation Administration
FDE	Fault Detection and Exclusion

Abbreviation	Definition
FDMA	Frequency Division Multiple Access
GDOP	Geometric Dilution of Precision
GEAS	Global Navigation Satellite System Evolutionary Architecture Study
GEO	Geostationary Earth Orbit
GGTO	GPS-Galileo Time-offset
GLONASS	Global Navigation Satellite System
GLONASST	Global Navigation Satellite System Time
GNSS	Global Navigation Satellite System
GPS	Global Positioning System
GPST	Global Positioning System Time
GSNRx	Global Navigation Satellite System Software Navigation Receiver
GST	Galileo System Time
GTRF	Galileo Terrestrial Reference Frame
HMI	Hazardously Misleading Information
HPL	Horizontal Protection Level
ICD	Interface Control Document
IERS	International Earth Rotation and Reference Systems Service
IGS	International Global Navigation Satellite System Service
IGSO	Inclined Geosynchronous Orbit
LS	Least-squares
MCS	Master Control Station

Abbreviation	Definition
MDB	Minimal Detectable Blunder
MEO	Medium Earth Orbit
MI	Misleading Information
NDOP	North Dilution of Precision
NIORAIM	Novel Integrity-Optimized Receiver Autonomous Integrity Monitoring
NTSC	National Time Service Center
OCS	Operational Control System
P(Y)	Precision codes
PDOP	Position Dilution of Precision
PHMI	Probability of Hazardously Misleading Information
PL	Protection Level
PLAN	Position Location And Navigation
PRN	Pseudo Random Noise
PTF	Precise Timing Facility
QZSS	Quasi-Zenith Satellite System
RAIM	Receiver Autonomous Integrity Monitoring
RMS	Root Mean Square
RUC	Road User Charging
SBAS	Satellite-based Augmentation System
SI	Systeme International d'Unites (International Systems of Units)
SISA	Signal in Space Accuracy

Abbreviation	Definition
SISRE	Signal in Space Range Error
SU	Soviet Union
SV	Space Vehicle
TAI	Temps Atomique International (International Atomic Time)
TDOP	Time Dilution of Precision
TECu	Total Electron Content Units
TTA	Time to Alert
UDOP	Vertical Dilution of Precision
UDRE	User Differential Range Error
UERE	User Equivalent Range Error
URA	User Range Accuracy
USNO	United States Naval Observatory
UT	Universal Time
UTC	Universal Time Coordinated
VDOP	Vertical Dilution of Precision
VPL	Vertical Protection Level
VTEC	Vertical Total Electron Content
WAAS	Wide Area Augmentation System
WGS 84	World Geodetic System 1984
XDOP	X-direction Dilution of Precision
YDOP	Y-direction Dilution of Precision
ZDOP	Z-direction Dilution of Precision

CHAPTER ONE: BACKGROUND AND INTRODUCTION

New Global Navigation Satellite System (GNSS) constellations such as Galileo and BeiDou are either nearing completion or on their way to deployment and will provide promising improvements to the satellite navigation users. As a result of increased numbers of available satellites, more ranging observations, improved user-satellite geometry, and increased coverage can be expected in open sky environments as well as in locations with degraded GNSS signals. When using signals from multiple constellations, however, the challenges are not only to maximize the benefit from the additional ranging observations but also to deal with the differences among satellite systems such as the time-offset between the systems when working without differential corrections.

When GNSS is used as a stand-alone navigation system in safety-critical or liability-critical applications, the aspects related to GNSS measurement reliability need to be properly addressed and the environment in which the receiver operates also needs to be considered. The performance of receivers in open sky conditions is well understood, however challenges exist when using the ranging signal in GNSS degraded environments.

The overall goal of this work is to investigate the reliability of the position solution using ranging signals from combined GPS, GLONASS, BeiDou and Galileo constellations. The aim of this study is also to examine the benefits of using a priori clock-offset constraints when computing position solutions with signals from multiple GNSS constellations.

The following subsections present a brief introduction to the use of multiple GNSS constellations, GNSS orbital structure and integrity requirement when using satellite navigation. Moreover, the challenges involved using multi-constellation GNSS to obtain position solution are also discussed.

1.1 Multi-constellation GNSS and GNSS Modernization

The modernization of GNSS provides promising improvements to satellite navigation users across the globe. The new GNSS constellations such as Galileo and BeiDou being planned and launched will result in a greatly increased number of available ranging sources, hence, improvement in constellation geometry and coverage.

The aviation industry sees a great potential in the use of modernized GNSS in aircraft navigation. In 2006, the Federal Aviation Administration (FAA) had established the GNSS Evolutionary Architecture Study (GEAS) Panel with the aim to explore the possibility of using new GNSS systems to provide robust aircraft navigation services worldwide (Lee & Cashin 2010). Taking advantages of multi-constellation GNSS and increasing number of ranging sources, much research (Blanch et al. 2013, Lee & Cashin 2010, Neri et al. 2011, Walter et al. 2013, Walter et al. 2008,) had been carried out with the aim to use GNSS for aircraft navigation during the critical phases of flight (such as final approach) with stringent requirements that have not been met before. With additional satellites in orbit, the improvement in positioning accuracy is also expected in environments with degraded GNSS signals such as vehicle and pedestrian navigation in dense foliage or in urban-canyons. With the increasing number of satellite constellations,

however, the challenge of the GNSS navigation is to deal with the differences among satellite systems as well as to maximize the benefit from the additional signal sources (Feng et al. 2011).

1.2 GNSS Constellations

The following sections describe GPS, GLONASS, Galileo and BeiDou orbital parameters including reference coordinate system and reference time adopted by each system. A brief history of the development of each of the GNSS constellations is also discussed.

1.2.1 GPS

The core constellation of the American Global Positioning System (GPS) is composed of 24 satellites evenly spread across 6 orbital planes. The GPS underwent a constellation expansion which was completed in June 2011 resulting in a new baseline constellation of 27 satellites (GPS.GOV 2013b). Currently, there are approximately 30 healthy GPS satellites transmitting signals. With a designed orbital inclination angle of 55^{o} and orbital altitude of approximately 20,200 km, the GPS satellites have an orbital period of approximately 11 hours 58 minutes and a repeat geometry period of one sidereal day (Bhatta 2011, GPS.GOV 2013b, Van Diggelen 2009). GPS adopts the World Geodetic System 1984 (WGS 84) as reference coordinate system (IS-GPS-200G 2012).

The first generation of operational GPS satellites, known as Block II satellites, were launched starting in 1989 and transmitted L1 Coarse/Acquisition (C/A) code for civil users as well as L1 and L2 Precision P(Y) codes for military users. The central frequencies for L1 and L2 signals are 1575.42 MHz and 1227.60 MHz respectively. The Block IIA, the upgrade version of Block II,

was first launched in 1990 and transmitted the same signals as the GPS Block II. The series "A" stands for *advanced* version of Block II. The GPS Block IIR which was first launched in July 1997 was produced to replace the degraded or aged Block II/IIA series (hence the series "R" stands for *replenishment*). An on-board clock monitoring feature had been implemented in this satellite series. In September 2005, the first upgraded version of Block IIR, known as Block IIR-M, where "M" stands for *modernized* was first launched. The Block IIR-M is the first satellite series to transmit a second civilian GPS signal, L2C ("C" stands for *civilian*), which broadcasts at higher effective power than the L1 C/A signal. Two new military signals which enhance jam-resistance are also transmitted by the Block IIR-M satellites (Bhatta 2011, GPS.GOV 2013a, GPS.GOV 2013b, IS-GPS-200G 2012).

The first GPS Block IIF ("F" stands for *follow-on*) satellite was launched in May 2010 and is the first GPS satellite series to transmit a third civil signal at a frequency protected for safety-of-life transportation (1176.45 MHz) known as L5 signal. The L5 signal is transmitted at a higher power than L2C signal and has greater bandwidth for improved multipath and jam-resistance. The improvement in Block IIF compared to the earlier GPS satellite series include the use of more accurate onboard clocks and improved signal strength. Currently, the newest GPS series, GPS Block III, are in the development phase with first launches expected in 2014. The fourth civilian GPS signal, L1C, which was designed for international GNSS interoperability as well as aeronautical radio navigation is planned to be transmitted by GPS Block III (Bhatta 2011, GPS.GOV 2013a, GPS.GOV 2013b, IS-GPS-200G 2012, IS-GPS-800C 2012, IS-GPS-705C 2012, Lockheed Martin Press Release 2012).

1.2.2 GLONASS

The originally planned Russian's Global Navigation Satellite System (GLONASS) constellation consists nominally of 24 Medium Earth Orbit (MEO) satellites in 3 orbital planes with 8 satellites equally spaced apart in each plane. With the nominal orbiting altitude of 19,100 km at 64.8^{o} inclination angle, the orbital period of GLONASS is about 11 hours 15 minutes and the ground track repeat geometry period is 7 days 23 hours 27 minutes (equal to 17 orbital periods) (GLONASS-ICD 2008).

The full constellation was initially completed in 1995, consisting of the first generation GLONASS satellites with a design operational life-time of 3 years. Following that, however, due to financial difficulties, the GLONASS constellation was not maintained. Also, the short life-span of GLONASS satellites meant that expensive and frequent launches were required to maintain the complete constellation which was not possible during periods of financial difficulty. After the Russian economic recovery in the early 2000s, a plan to restore the GLONASS constellation was established. The launch of the modernized Russian navigation satellites, GLONASS-M, commenced in 2003 (Bhatta 2011). The GLONASS-M has a design operating life of 7 years and uses a more stable clock (Bhatta 2011, GLONASS-ICD 2008).

In the early 2010s the complete constellation of 24 Russian navigation satellites was restored. The first of the latest generation of Russian navigation satellite, GLONASS-K, was launched in 2011 and has a design life-time of 10 years. One GLONASS-K satellite is currently being tested in-orbit (Dumas 2011, Inside GNSS 2011, Russian Federal Space Agency 2013). A redesigned version of GLONASS-K satellite known as GLONASS-K2 and a modernized GLONASS-K

satellite known as GLONASS-KM are under research and development (Revnivykh 2010). As of May 2013, there are 29 satellites in the constellation with 24 operational, 4 spares, and 1 being tested (Russian Federal Space Agency 2013). The future plan for GLONASS is to have a total of 30 satellites, 10 in each orbital plane. There will be 24 operational and 6 operational spares (Bhatta 2011).

The GLONASS satellites transmit in two bands, L1 and L2. However, unlike GPS, GLONASS uses Frequency Division Multiple Access (FDMA), meaning that each satellite transmits on its own channel or sub-band. The sub-bands for L1 frequencies range from 1598.0625 MHz to 1605.3750 MHz with a 0.5625 MHz spacing; the nominal central frequency is at 1602.0 MHz. The sub-bands for L2 frequencies range from 1242.9375 MHz to 1248.6250 MHz with a 0.4375 MHz spacing; the nominal central frequency is at 1246.0 MHz (GLONASS-ICD 2008). A new signal in the L3 frequency band will be added to GLONASS-K satellites (Bhatta 2011, Dumas 2011, Inside GNSS 2011). GLONASS uses PZ-90.02 as system reference frame (GLONASS-ICD 2008).

1.2.3 Galileo

The European Galileo GNSS is being developed in collaboration between the European Union (EU) and the European Space Agency (ESA). The complete Galileo constellation will consist of 30 MEO satellites in three orbital planes at an inclination of 56^{o} from the equatorial plane. Each orbital plane consists of 10 satellites including 27 operational and 3 spares orbiting at an altitude of 23,222 km; the orbital period is around 14 hours and a repeat geometry period of approximately 10 days. Each orbital plane will contain one active spare satellite. The inclination

was chosen to ensure improved coverage over polar region; these regions are not well covered by the GPS system due to its lower orbital inclination angle (ESA 2013a, ESA Fact Sheet 2013, Galileo ICD 2010, Van Diggelen 2009). The Galileo satellites transmitted signals in four frequency bands: E1 at 1575.420 MHz, E6 at 1278.750 MHz, E5a at 1176.450 MHz and E5b at 1207.140 MHz. The Galileo's E1 and E5a frequencies are coincided with GPS' L1 and L5 respectively (Galileo ICD 2010). The Galileo system uses the Galileo Terrestrial Reference Frame (GTRF) (Galileo ICD 2010).

1.2.4 BeiDou

The initial phase of Chinese satellite navigation system BeiDou (BDS) constellation is composed of five Geostationary Earth Orbit (GEO) satellites, five Inclined Geosynchronous Orbit (IGSO) satellites and four MEOs. This phase was completed by the end of October 2012. When fully deployed, the BeiDou constellation will consist of five GEO satellite and three IGSO satellites to provide enhanced navigation signals in the Asia-Pacific region and 27 MEO satellites to provide global positioning services (BDS-ICD 2012, Ge et al. 2012, He et al. 2013, Zhao et al. 2013).

The GEO satellites are positioned at 58.75^{o}E, 80^{o}E, 110.5^{o}E, 140^{o}E and 160^{o}E respectively and are operating in orbit at an altitude of 35,786 km. The IGSO satellites are operating in orbit at an altitude of 35,786 km at an inclination of 55° and the longitude bands of the IGSO range from 90^{o} to 125^{o}. The MEO BeiDou satellite orbits are at an altitude of 21,528 km with an inclination of 55° and have an orbital period of 12 hours and 53 minutes. The repeat geometry period of MEO BeiDou is approximately seven days. All the BeiDou satellites transmit navigation signal at three central frequencies which are 1,561.098 MHz (B1), 1,207.140 MHz (B2) and 1,268.520

MHz (B3) (BDS-ICD 2012, He et al. 2013, Van Diggelen 2009). According to BDS-ICD (2012), China Satellite Navigation Office (2012a) and China Satellite Navigation Office (2012b), the BeiDou satellites adopt the China Geodetic Coordinate System 2000 (CGCS2000).

1.3 Universal Time Standard and GNSS Times

When using GNSS as navigation and positioning tool, ability to accurately and precisely measure the elapsed time between transmission and reception of GNSS signal is a critical factor to obtain accurate position solution. This section provides brief information regarding international time standard and the various GNSS reference times.

The *Universal Time* (UT) standard is a time scale which based on the rotation of the Earth. The UT was introduced as an international time scale standard. There are three forms of UT standard which are UT0, UT1 and UT2. The UT0 is a time obtained from direct astronomical observation (ITU-R TF.460-5 1997). The UT1 is UT0 corrected for the effect of the Earth motion relative to the axis of rotation (polar variation), the UT1 is commonly known us a time based on Earth rotation (ITU-R TF.460-5 1997, Lewandowski & Arias 2011). The UT2 is UT1 corrected for the effects of a small seasonal fluctuation in the rate of the Earth rotation (ITU-R TF.460-5 1997).

The *International Atomic Time* (Temps Atomique International – TAI) was introduced after the measurements with atomic standards first became possible in 1955 through the use of resonant frequency of cesium atom (Essen & Parry 1955, Guinot & Arias 2005, Lewandowski & Arias 2011). The origin of TAI was set on 1st January 1958 (ITU-R TF.460-5 1997, Lewandowski & Arias 2011). TAI is a continuous atomic time scale which calculated at the International Bureau

of Weights and Measures (Bureau International des Poids et Mesures – BIPM) using data from some 200 atomic clocks in over 50 national laboratories around the world (BIPM 2013b).

The *Universal Time Coordinated* (UTC) is an atomic time scale maintained by the BIPM. The UTC is adjusted to ensure approximate agreement with UT1. An integer leap second adjustment is performed on UTC upon a recommendation by the International Earth Rotation and Reference Systems Service (IERS) based on astronomical observations of the Earth's rotation. The difference between UTC from UT1 will not exceed 0.9 seconds. UTC is based on the continuous TAI time scale but differs from it by a number of leap seconds (ITU-R TF.460-5 1997, Lewandowski & Arias 2011). Local realizations of UTC have been computed and are maintained at a regional level including the local representation of UTC maintained by the U.S. Naval Observatory, UTC (USNO); UTC maintained by National Time Scale of Russian Federation, UTC (SU); and the local representation of UTC maintained by National Time Service Center, China Academy of Science, UTC (NTSC). The differences between the UTC and the local representations of UTC are illustrated in Figure 1.1.

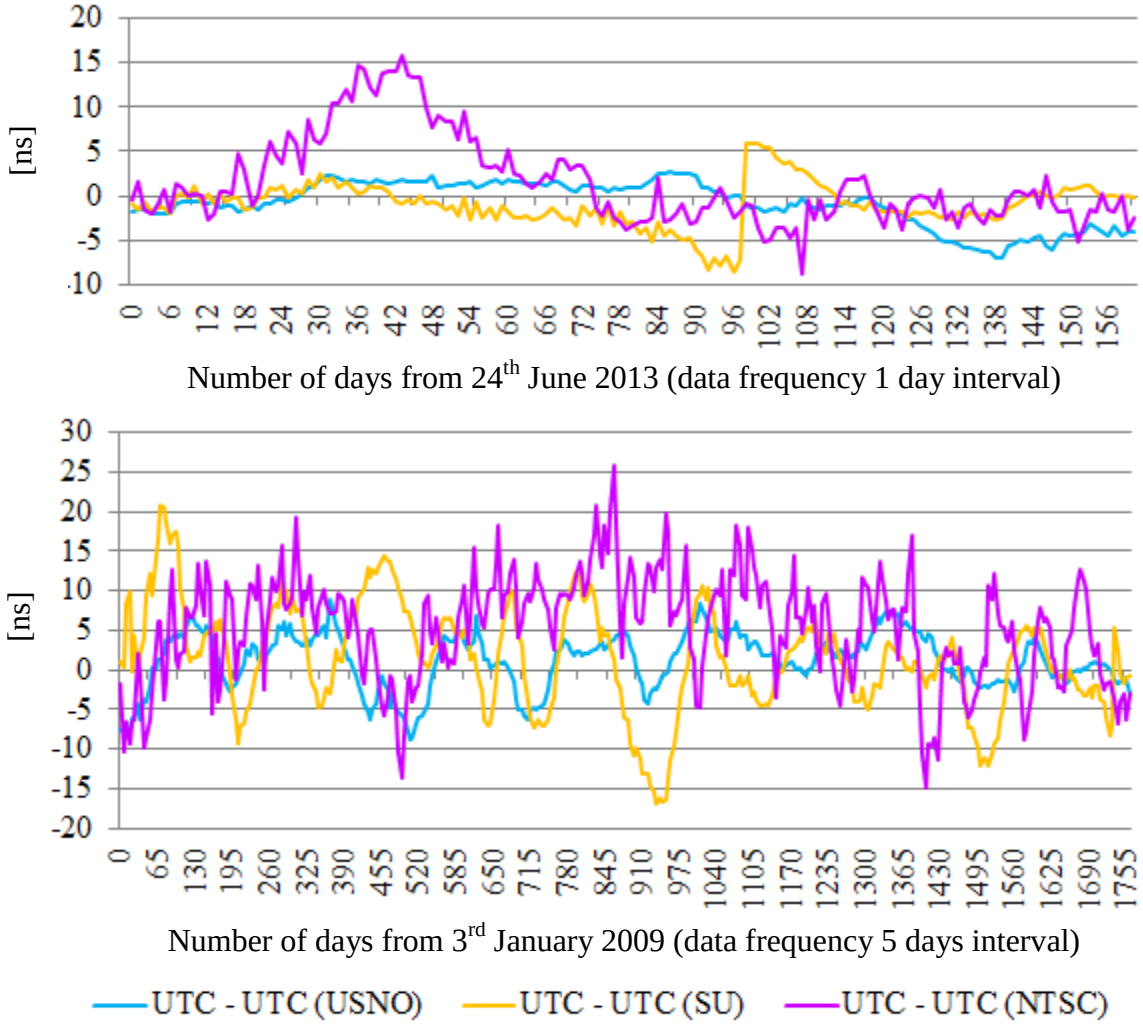

Figure 1.1: The short term (top) and long term (bottom) difference between UTC and local representation of UTC (BIPM 2013a)

As previously mentioned, the ability to accurately measure time is essential in order to obtain accurate position solution when using GNSS. Each GNSS are required to have reference time scale. The following subsections describe GPS, GLONASS, Galileo and BeiDou system reference time.

1.3.1 GPS Time

The GPS system uses the GPS time (GPST) standard which increments from a reference epoch starting at midnight on the night of 5th January 1980 and morning of 6th January 1980 in Universal Time Coordinated as maintained by the U.S. Naval Observatory, UTC (USNO). The GPST is maintained by the Master Control Station (MCS) of the Control Segment (CS). Unlike the UTC (USNO) which applies integer leap second corrections, the GPS time standard operates on a continuous time scale (IS-GPS-200G 2012). The difference between the UTC and UTC (USNO) is illustrated in Figure 1.1. The Operational Control System (OCS) keeps the GPS time scale to be within 1 μs of UTC (USNO), modulo 1 second. Over the past few years, however, the difference between GPST and UTC (USNO) had been within tens of nanoseconds (IS-GPS-200G 2012, Lewandowski & Arias 2011). Data between 1999 and 2005 show that the GPS average daily clock stability is within 3×10^{-14} most of the time for Block IIR satellites and within 1×10^{-13} for Block II/IIA satellites (Phelan et. al. 2005).

1.3.2 GLONASS Time

GLONASS adopts GLONASS time (GLONASST) as reference time which is based on the National Time Scale of Russian Federation, UTC (SU), with integer second corrections. This means that there are no integer-second difference between GLONASS time and UTC (SU), there is, however, a constant three-hour difference between these time scales. The difference between the UTC and UTC (SU) is illustrated in Figure 1.1, the difference between GLONASST and UTC (SU) are kept within 1 μs (GLONASS-ICD 2008, Lewandowski & Arias 2011). An accuracy of the synchronization of GLONASS time scale is within 20 ns for GLONASS and 8 ns for the GLONASS-M satellites. The GLONASS and GLONASS-M satellites have daily

instability not worse than 5×10^{-13} and 1×10^{-13} respectively (GLONASS-ICD 2008). The planned GLONASS-M navigation message will also transmit corrections and parameters related to differences between GPS and GLONASS times, the difference between these time scales is targeted to be maintained within 30 ns (GLONASS-ICD 2008).

1.3.3 Galileo Time

The Galileo system adopts Galileo System Time (GST) as reference time which is generated by the Precise Timing Facility (PTF) at the Galileo Control Centre in Fucino, Italy (ESA 2013b, Inside GNSS 2013). The Galileo System Time initial epoch is at midnight between 21st and 22nd August 1999. At the start epoch, the GST was ahead of UTC by 13 seconds, the GST is a continuous time without leap second adjustments (Galileo ICD 2010). The Galileo time is derived independently of the UTC as maintained by BIPM. The offset between these two times is continuously being monitored (ESA 2013c) and the Galileo system timing accuracy with respect to the UTC will be within 30 ns (ESA 2002). The offset between the GPS and Galileo time, known as GPS-Galileo time-offset (GGTO), is calculated on a continuous basis by PTF and the GST and GPST are kept within 50 ns (ESA 2013b, Inside GNSS 2013). Galileo will broadcast both GST-GPS and GST-UTC conversion parameters in its navigation message (Galileo ICD 2010).

1.3.4 BeiDou Time

The reference time for the BeiDou system is BeiDou Time (BDT) which is a continuous time without leap seconds. The BDT is related to the Universal Time Coordinated through UTC (NTSC) which is a UTC time maintained by National Time Service Center, China Academy of

Science. The difference between the UTC and UTC (NTSC) is as illustrated in Figure 1.1. The BDT time offset with respect to UTC will be maintained within 100 ns, modulo 1 second. The start epoch of BDT was at 00:00:00 on 1st January 2006 UTC. The planned BeiDou navigation message will broadcast time parameters relating BDT to UTC, GPS, GLONASS and Galileo time, the accuracies of the broadcast offset parameters are however not stated in the current BeiDou ICD (BDS-ICD 2012, China Satellite Navigation Office 2012b).

Finally, it should be noted that each of the GNSS system times are merely averages of all of the clocks involved in the system (both on the satellites and in the ground control stations) that are computed after the fact and compared to each local representation of UTC which itself is an average of an ensemble of clocks. Each GNSS satellite clock has its own error with respect to its GNSS system reference time. Each GNSS system reference time has its own error with respect to its local representation of UTC and each local representation of UTC has its own error with respect to UTC maintained by BIPM. The differences between GNSS satellite clocks and the corresponding GNSS system time can be computed from global tracking data and can also be predicted. Prediction is done by the operational control segments of each GNSS in order to include clock error parameters in the ephemeris messages. Prediction and post processing are also undertaken by national and international agencies including the International GNSS Service (IGS) which produces predicted and various levels of post-mission clock products, as well as by commercial service providers needing to provide better clock error values to enable positioning and/or precise timing services. Currently, the IGS real-time service provides GPS-only clock corrections. The GPS and GLONASS corrections are in an experimental stage and corrections for Galileo and BeiDou are not currently available (IGS 2013).

1.4 Inter-system Time-offset Issue

Although the use of multiple GNSS constellations can lead to improvements in receiver-satellite geometry and availability of position solutions, problems may result from the way different GNSS constellations use different reference-time systems. Because of this, the inter-system time-offset must be considered when solving for the position solution. One method that can be used to overcome this problem is by treating the unknown time differences between each system as parameters to be estimated. When using this method, for each additional signal from a new GNSS constellation, one more unknown parameter is introduced to the estimation algorithm. This means that the time-offset can be obtained at the cost of the first satellite from each additional system being added.

The problem of the difference between system reference-time has been considered by GNSS providers. As a result, various system providers are intending to broadcast system time-offsets to other systems. For Galileo it is proposed to broadcast a time-offset (GGTO) with a standard deviation of 0.75 m or 2.5 ns (5 ns 2σ) (ESA 2013b, Hahn & Powers 2005, Vanschoenbeek et al. 2007). For GLONASS, the time offset between GPS and GLONASS systems called τ_{GPS} are planned to be transmitted by GLONASS satellites (GLONASS-ICD 2008). According to GLONASS-ICD 2008, τ_{GPS} will not exceed 30 ns but the accuracy of the offset is not stated. The inter-system time-offsets are, however, currently not broadcast by all the satellites (Petovello 2013).

The broadcast time-offset can be treated as additional measurement by position estimation algorithm enabling solution to be obtained from a minimum of four satellites with any

combination. In some cases, the inter-system time-offset can be estimated by third-party service provider and sent to users via alternative data links. Alternatively, as has been discussed by Moudrak et al. (2005) and demonstrated by Cai (2008), the inter-system time-offset parameter can be initially estimated by the receiver when the number of satellites is sufficient. Then, when the receiver-satellite geometry changes and the number of satellites in view is no longer sufficient to perform inter-system time-offset estimation, the receiver can continue using the previously estimated inter-system time-offset value until the number of satellites improve.

1.5 Integrity Parameters and Reliability Requirements

Types of ranging signal errors, integrity requirements and reliability parameters are introduced in this section. The importance of ensuring the reliability of position solutions is also discussed.

1.5.1 Threat Space and Types of Ranging Signal Errors

In satellite navigation, there are three main types of faults: *nominal errors*, *independent* (*narrow*) *faults* and *wide failure errors* (Blanch et al. 2011, Lee & Cashin 2010). The *nominal errors* are referred to the errors when all operational segments including satellites, ground and user segments are functioning normally. In this case, the ranging error occurs as a result of accuracy limitations in orbital and clock determination processes performs by ground segment. This type of error can also occur as a result of accuracy limitations in on-board clock prediction model. The tropospheric and ionospheric errors as well as the code noise and multipath also contribute to nominal errors (Blanch et al. 2011). It must be noted that, when the GNSS signal travels through ionosphere, the code and carrier phase are affected in different ways; this results in code

delay and phase advanced. Also, multipath can lead to erroneous pseudorange measurements and cycle slips in carrier phase signals (Ren et al. 2012, Ren et al. 2011).

The *independent fault* or *narrow failure* is referred to errors which occur independently on a single or more satellites (simultaneous occurrence of independent faults). The fault in one satellite will not affect navigation signals sent out by other satellites. The sources of this type of fault include change in satellite orbit, clock failure and the broadcast of erroneous signal due to satellite malfunction or component failure. These types of faults can likely be considered independent across different satellites (Blanch et al. 2011).

The *wide failure* corresponds to errors introduce into the satellite system by the ground segment as a result of inadequate manned operations which may take place during an update of the operational ground segment. This type of fault simultaneously affects navigation signals of multiple satellites (Blanch et al. 2011).

The *wide failure* also includes *consistent fault* which leads to a corruption in the navigation messages transmitted from multiple satellites in such a way that large errors in the navigation solution would occur while consistency between solutions from all-in-view satellites and position estimates from subset satellites are maintained (Lee & Cashin 2010). The threats that could potentially cause consistent errors include the use of an erroneous gravitational constant, erroneous Earth Orientation Parameters (EOP), or erroneous EOP Prediction (EOPP) (Blanch et al. 2011, Lee & Cashin 2010).

In satellite navigation, the *threat space* is defined as a set of assumptions about the environment in which the positioning algorithm is applied and the *threat model* must take into consideration the nature of threats that could occur including magnitude, duration and the possibility of occurrence (Blanch et al. 2011, Blanch et al. 2007, Ene et al. 2006). The main contributions to signal errors vary depending on the user environment. When using navigation signals in aeronautical applications, the largest source of nominal error is due to ionospheric delay (Ene 2006). Also, rare but possible independent fault due to satellite malfunction could occur. If undetected, this type of fault could leads to catastrophic consequence if the navigation solution is used in safety critical applications such as aircraft navigation. When the GNSS is used as navigation aid in signal challenging environment such as in urban-canyon, the position errors due to signal multipath becomes the major concern. Multipath can affect multiple ranging signals at the same time.

1.5.2 Integrity Requirements and Protection Levels

Usually, the accuracy of navigation solution is the main focus in satellite navigation. When the GNSS is to be used as a stand-alone navigation method in safety-critical applications such as in aviation, however, system integrity becomes a major concern. For applications which required position estimation such as in surveying, reliability testing is carried out to detect outliers in measurements and determine whether the position solution is reliable. When the position estimate is to be used in safety-critical applications, the reliability test is carried out as a method to monitor integrity of the system. The integrity parameters can be used as indications of how dependable the navigation solution is at a particular time. The dependable solutions referred to

solutions which errors are bounded within system's specified level of accuracy (Petovello et al. 2008).

The importance of system integrity also extend to liability-critical applications such as road user charging (RUC) application using GNSS-based electronic tolling systems (ETS). In this case, an excessive error in the estimated user position may leads to incorrect tolling bills which further leads to either loss of avenue or negative legal consequence (Salós et al. 2010c).

The concept of integrity can be quantitatively expressed by three parameters which are *integrity risk*, *alert limit* and *time to alert* (Petovello et al. 2008). The *integrity risk* refers to the possibility that the system generates an excessively large error without providing a user with timely warning about degraded solution. When this happened, the solution output from the system is called *Misleading Information* (MI). If the potential consequence of Misleading Information can potentially imposed life threatening situation then the term *Hazardously Misleading Information* (HMI) is used (Petovello et al. 2008). The *Probability of Hazardously Misleading Information* (PHMI) is therefore referred to the probability that the true position lies outside the maximum error bound determined by the user. The integrity is verified if the PHMI is below the allowable integrity budget (Blanch et al. 2011).

The *Alert Limit* (AL) refers to the largest error that the system can tolerate. It is represented by the maximum magnitude of error that can occurred without violating safety requirement and is commonly expressed in terms of position error bounds. When the alert limit is exceeded, the *Time to Alert* (TTA) parameter is referred to the time between the occurrence of potential

misleading information and the time when the system issues a warning to the user of the problem. The *integrity risk*, thus, denotes a probability that the error in the output of the system may exceed the AL without providing user with a warning within maximum TTA limit (Murphy 2005). Systems with high integrity generally have the ability to issue a warning to the user with minimal time to alert before the potential misleading information become hazardous.

The *internal reliability* refers to an ability to detect measurement outliers. This parameter is measured by *Minimal Detectable Bias* or *Minimum Detectable Blunder* (MDB) which is the smallest bias or error that can be detected when performing statistical testing. In practice, it is the *external reliability*, which measures by *protection level* (PL) to indicate the effect of MDB on the estimated position, which becomes an interest to satellite navigation users. The PL parameter is further divided into *horizontal protection level* (HPL) and *vertical protection level* (VPL). These PL parameters can be used as an indication of the position solution's reliability.

The integrity of the system can be ensured by comparing protection level and the corresponding alert limit. The integrity is warranted when the protection level is smaller than alert limit (PL < AL). When the protection level exceeded the alert limit (PL > AL), the system should provide warning message to the user about possible misleading information.

1.6 Use of Satellite-based Augmentation System (SBAS)

In order to improve the accuracy and reliability of position solutions, Satellite-based Augmentation System (SBAS) such as Wide Area Augmentation System (WAAS) in the USA and European Geostationary Navigation Overlay Service (EGNOS) in Europe can be used to

provide corrections to GNSS measurements. The SBAS helps provide integrity messages and differential corrections such as ionospheric information which can be used by GNSS/SBAS receivers to improve the accuracy of GNSS receivers (EGNOS SDD 2013, European Space Agency 2005, Federal Aviation Administration 2010, GNSS Supervisory Authority 2011).

The use of SBAS helps to improve *User Equivalent Range Error* (UERE) which is an indication of ranging accuracy for each satellite signal. SBAS plays an essential role in safety-critical application as well as applications where accuracy and integrity are crucial; examples include the guidance of agricultural machinery, and on-road vehicle fleet management (GNSS Supervisory Authority 2011).

1.7 Overview of Receiver Autonomous Integrity Monitoring (RAIM)

In order to ensure system reliability, an integrity monitoring algorithm is required to detect and exclude faulty satellite measurements from a set of measurements that will be used to compute navigation solutions. To achieve this, Receiver Autonomous Integrity Monitoring (RAIM) was proposed in 1986 to perform integrity check on the satellite navigation system (Lee 1986, Lee & Cashin 2010). Due to its self-contained nature, RAIM has become a commonly used integrity monitoring method.

When misleading information occurs, the faulty signal might not immediately trigger GNSS to sending out a satellite unhealthy flag to the users. During this time, the user will continue to assume that there is no fault in navigation signal. It is the RAIM algorithm that must detect and protect the user against the fault. Due to its potential in enhancing integrity of navigation system

and its self-contain nature, RAIM has been explored and adopt by the FAA for GPS integrity monitoring in avionics since 1992 (Lee 2006). The use of RAIM also has great potential benefits to the users in non-aviation applications. The studies of the use of RAIM in road user charging has been carried out by Salós et al. (2010a) and Salós et al. (2010c).

Unlike integrity monitoring in aeronautical application where the integrity of navigation system are monitored by ground segments, in urban-canyon environment such as ETS application, local effects such as multipath become a major contribution to ranging signal error and cannot be monitored by ground segment. This means that, in urban-canyon environment, the integrity monitoring and the detection of local effects have to be done at the user level (Simon et al. 2010).

The RAIM algorithm uses measurement redundancy to perform consistency check and monitor system integrity. Generally, the integrity monitoring algorithm can be categorized into two major classes: *residual-based* scheme which performs consistency testing in the range domain, and *solution separation* method which performs consistency check in position domain (Chan & Pervan 2010, Lee & Cashin 2010).

When using RAIM to detect faulty signal in single GNSS constellation, the algorithm requires a minimum of five satellites in view. To perform fault elimination process, at least six satellites are required. When a position solution is computed using range measurements from multiple GNSS constellations without using inter-system broadcast time-offset as measurement, the number of satellites required is further complicated by the fact that the first additional satellite from each

additional constellation does not contribute to the position solution; rather, the first satellites used in the solving of inter-system time-offset. Thus, when using range measurements from two GNSS constellations, five satellites in any combination between the two systems are required to obtain a position solution. This fact further complicates receiver autonomous integrity schemes as at least seven satellites from two GNSS constellations with at least three satellites from each system are required if fault detection and exclusion (FDE) is to be performed on these measurements (Hewitson & Wang 2006, O'Keefe et al. 2011). The use of a priori inter-system time-offset parameters as measurements or constraints would, however, result in the reduction of number of satellites required.

At each epoch, the RAIM algorithm first checks the availability of the fault detection and exclusion algorithm and computes the protection level. If the protection level does not satisfy an operational requirement, the RAIM will issue a notification to the user. If the protection level requirement is met and the availability of FDE is verified, upon detecting a fault, the algorithm will exclude faulty measurements from being used in the position solution. With the increasing number of satellites, various studies (Angus 2006, Miaoyan et al. 2008, Yun & Kee 2013) had been carried out with the aim to use RAIM to detect multiple-faults.

The availability and performance of RAIM are closely related to the number of satellites uses by the algorithm. New constellations result in increased numbers of satellites which enhance measurement redundancy and receiver-satellite geometry. This raises the possibility of using RAIM in applications which have stringent integrity requirement as well as the use of RAIM in challenging signal environment such as in urban-canyon areas. The use of multiple GNSS

constellation RAIM also helps in the detection of wide failure or consistent faults which affect the navigation signals from every satellite in a given constellation. To detect this type of fault and eliminate faulty satellites, multiple GNSS constellations are required (Lee & Cashin 2010). More recent work in the field of detecting constellation-wide faults using signals from multiple GNSS constellations has been carried out by Lee (2013).

1.8 Limitation of Previous Works

With the planned launches of new satellite navigation systems, much research has been carried out to investigate the integrity performance of existing and future multi-constellation GNSS. The reliability performance of GPS and GLONASS constellations was demonstrated using real data by Choi et al. (2011). This work was carried out to validate availability, VPL, and accuracy of position solution from GPS and GLONASS measurements using 10 days of data collected at Stanford University. The performance of single, and combined GNSS constellations were compared. Another work which was done to investigate the performance of combined GPS and GLONASS constellations including a simulation study was performed by Madonna et al. (2010). In this study, Novel Integrity-Optimized RAIM (NIORAIM) was used as the integrity monitoring scheme.

In order to investigate the integrity performance of future constellations, various simulation studies of triple and dual GNSS constellations have also been carried out. The availability of GPS and Galileo signals under various user range accuracy (URA) and probability of failures were investigated by Blanch et al. (2010). The system availability as a function of URA and failure probability was presented in this research. The system integrity of the combined GPS and

Galileo constellations was also investigated by Ene (2006). In this study, the reliability of position solution using signals from the combined constellations when number of satellites in each constellation was altered between 12 and 30 satellites were examined. When investigating the effect of faulty satellite on positioning performance, the worst case scenario was considered in this studied to be a situation where a single fault is occurs on the most geometrically-critical satellite.

Other simulations were carried out to examine the positioning performance of the combined GPS and Galileo constellations including a global simulation studied by Ene et al. (2006), local-scale simulations for receiver located at a location in Sydney, Australia, and Portland, USA, performed by Hewitson (2003), and work carried out by Qian & Jun (2011) to investigate the availability of the combined GPS and Galileo constellation in China. The performance evaluation of dual-GNSS constellation, Galileo and GPS, was also studied by Lee (2004).

The performance of triple-constellation GNSS was carried out by Blanch et al. (2011). In this study, the VPL obtained from stand-alone Galileo system, GPS and Galileo systems and combined GPS, Galileo and GLONASS constellations under various prior probabilities of satellite failure were investigated. The receiver-satellite geometry and performance of the RAIM algorithm when applied to the combined GPS, Galileo and GLONASS systems was also examined by Sun & Zhang (2009) for a fixed receiver location in Beijing.

Although much research has been carried out to examine the performance of dual and triple-constellation GNSS as discussed above, these researches did not consider the effect of GNSS

performance in urban-canyon environments. Also, apart from the study performed by Ene (2006), none of the works discussed above have considered the imbalanced number of satellites in each constellation. As new GNSS constellations such as BeiDou and Galileo are underway and the signals from complete constellation are not yet available, examining the availability and reliability of position solution when using signals from partial constellations can be a useful indicator of when the new constellation will begin to benefit users before the complete constellation is in operation.

One of the detailed integrity performance studies on combining GPS, GLONASS and Galileo was carried out by Hewitson & Wang 2006. The investigation was conducted for stand-alone GPS, GPS-GLONASS constellations, GPS-Galileo systems and combined GPS, GLONASS and Galileo constellations. In the global snapshot simulation conducted in this study, an elevation mask angle of 15^{o} was used. The 24-hours temporal simulation was carried out to evaluate the reliability performance at a single location in Sydney, Australia using 15^{o} and 30^{o} mask angles to simulate the effect of urban-canyons. For each simulation, the number of visible satellites, minimum separable bias, correlation coefficient and maximum internal reliability were determined. The external reliability was also examined in temporal simulation.

In this study, however, the position solution from only one single epoch was used in the performance analysis of the global simulation and the effect of urban-canyon on performance of the triple-constellation GNSS had not been considered. The effect of urban environment and external reliability was only considered for a single location in Sydney, Australia. In both global

and temporal simulations, the positioning performance when using signals from partial Galileo constellation had not been considered.

Few studies have been carried out to evaluate positioning and reliability performance of multi-constellation GNSS for sub-urban and urban-canyon environments. Studies using software simulation were carried out by O'Keefe (2001) and O'Keefe et al. (2002) to investigate the availability and reliability of position solutions achievable by using stand-alone and combined GPS and Galileo systems. High elevation mask angles were chosen to simulate an urban-canyon environment.

One integrity monitoring scheme called FDE+PL (Fault Detection and Exclusion and Protection Level) was developed and used by Simon et al. (2010) to detect multiple faults and compute protection level in non-aeronautical environment taking into consideration of moderate to harsh multipath conditions. This algorithm was applied to stand-alone Galileo constellation and combined GPS and Galileo constellations under simulated urban-canyon (assumed 12 m to 20 m high building), sub-urban (assumed 6 m to 15 m high building), rail, maritime and rural environments. Assumptions regarding outliers and characteristics of multipath were varied during algorithm testing to examine the effect of these parameters on system performance. The reliability performance when using signals from partial Galileo constellations, however, was not considered in these studied.

The use of the combined GPS and Galileo signals for urban-canyon environment with emphasis on road tolling application was studied by Salós et al. (2010c). Simulation with one day period

was carried out to examine number of satellites that would be visible to a moving vehicle in study areas with an average building height of 15 meters was examined. Similar study for road user charging applications using the combined GPS and Galileo systems was done by Salós et al. (2010a). The study was focused on the visibility of the combined GPS and Galileo systems in open sky, sub-urban environment with building heights between 4 m to 20 m and urban-canyon environment with building height between 4 m to 50 m. In these two studies, however, further investigation on protection level is required. Also, the performance using a partial Galileo constellation was not considered.

As the Chinese's satellite navigation system become closer to full operation capability and with the release of the first official BeiDou Interface Control Document (BDS-ICD) in December 2012, more recent studies have focused on examining the performance of the new system using real data. Performance of BeiDou in aiding river navigation, ship positioning, and vessel traffic monitoring in China was investigated by Qian & Yuan (2013). Also, the accuracy of single point positioning obtained from single frequency code observations using combined GPS and BeiDou signals under various surrounding environments and visibility conditions were examined by Cai et al. (2013) for a study location in Changsha, China. As the final phase of BeiDou development is to be a global navigation system, it would be of interest to investigate the performance of this constellation outside China and Asian locations. A simulation study was performed by Duan et al. (2011) to investigate the performance of combined GPS, Galileo, and BeiDou constellations outside China. The effect of urban-canyons and the availability of signals from partial constellation are, however, not considered in this research.

Previous studies have also been carried out to investigate the performance of GPS augmented with SBAS and multiple GNSS constellations. Lee et al. (2005) investigated performance of combined GPS and Galileo systems with WAAS corrections for vertically guided approaches and Chin et al. (1997) investigated system availability for CAT I precision approach when GLONASS and GPS signals are used with WAAS corrections. The performance of EGNOS augmented GPS-only, and EGNOS augmented GPS and GLONASS signals in urban-canyon environments was investigated by Alcantarilla et al. (2006) using the existing GLONASS constellation – at that time, GLONASS had an average visibility of about 4 satellites – and by Bonet et al. (2009) using 30 GPS and 14 operational GLONASS satellites. Receiver-satellite geometry, coverage and reliability of a multiple GNSS constellations consisting of GLONASS, EGNOS and a set of three geosynchronous satellites similar to Quasi-Zenith Satellite System (QZSS) was investigated by Angrisano et al. (2009) for urban-canyon environments. Work has also been done by Bestmann et al. (2012) to examine the performance of SBAS in urban-canyon environments when SBAS data are shared between multiple rover receivers in a local area. Also, the availability and receiver-satellite geometry when using signals from GPS, GLONASS and QZSS was examined by Sakai et al. (2012) for open sky and urban-canyon scenarios.

As the GLONASS constellation of 24 satellites had recently been restored in the early 2010s, it would be of interest to investigate the availability and reliability of position solutions obtain using signals from combined GPS and GLONASS constellations when SBAS corrections applied to GPS measurements in GNSS signal challenging locations. Also, the use of SBAS and the use of additional ranging signals from new constellations can help improve the reliability of position solution. As new satellite systems are well underway to become fully operational, it

would be of interest to compare the improvements in reliability performance that is obtainable from using addition range measurements of new constellations to the improvement in reliability performance that would be achieved by applying SBAS corrections to the existing constellation.

1.9 Objectives and Contributions

With regard to the limitations of the existing research mentioned in the previous section, the objectives of this thesis is to perform in-depth analysis of the positioning and reliability performance of the combined GPS, GLONASS, BeiDou and Galileo constellations and the benefit of using a priori inter-system (or receiver-GNSS) clock-offset constraints. The main objectives and contributions of this research include:

1) Examination of the reliability of position solutions obtained from the existing GPS and GLONASS constellations with and without SBAS corrections applied to GPS measurements in open sky and semi-urban environments.
2) Investigation of the availability and reliability of position solution when using signals from existing GPS and GLONASS constellations and additional range measurements from the new Galileo and BeiDou constellations.
3) Determining the benefits of using a priori clock-offsets as constraints when computing position solution using ranging signals from multiple GNSS constellations. The focus of this study is to assess the availability and reliability of position solutions in challenging GNSS signal environments such as in urban-canyon where GNSS users potentially see limited number of satellites from multiple GNSS constellations.

4) Investigation of fault detection and exclusion capabilities when position solutions are computed using a limited number of range measurements from multiple GNSS constellations with a priori clock-offsets constraints.

Covariance simulations are carried out to achieve objectives 1) to 3). Analysis using real measurements from GPS, GLONASS, BeiDou and Galileo are carried out to achieve objectives 3) and 4).

1.10 Author's Contribution

Parts of the work described in this thesis have been published in Winit & O'Keefe (2013). Also, the author's contribution to Winit et al. (2013) was to assess the benefits of using EGNOS corrections which are applied to GPS measurements when using pseudorange observations from GPS and GLONASS constellations in challenging GNSS signals environments. The work presented in Winit et al. (2013) was conducted as part of a research contract with Telespazio S.p.A. in the context of a commercial project to monitor shipping containers on European highways.

1.11 Thesis Outline

The thesis is organized in five chapters and the outline of the remaining chapters is as follows:

Chapter 2 provides a review of the estimation algorithm and reliability parameters. The significance of receiver-satellite geometry in the estimated solution is discussed in this section. Also, the pseudorange observation model and design matrix, when using measurements from

multiple GNSS constellations, are explained in this section. Furthermore, the use of statistical testing to detect and identify measurement blunders are discussed in detail.

Chapter 3 describes the simulation scenarios and presents simulation results. First, the model parameters used in the covariance simulation and the GNSS constellations used to compute position solutions are explained in this section. Following these, an in-depth analysis on covariance simulation results is presented. The reliability performance of GPS and GLONASS with and without SBAS corrections applied to GPS measurements is investigated. This chapter then examines the availability and reliability of position solution obtains from GPS, GLONASS, BeiDou and Galileo, with and without using a priori inter-system clock-offsets constraints.

Chapter 4 first describes measurements from GPS, GLONASS, BeiDou and Galileo used in algorithm testing to examine position accuracy when using a priori receiver-GNSS clock-offset constraints. The software modifications required to process real data using a priori clock-offsets are also discussed in this chapter. Following these, a detailed analysis on position solutions obtained from the limited number of satellites from multiple GNSS constellations is presented. The accuracy of position solutions obtained with and without using a priori receiver-GNSS clock-offset constraints are compared in this chapter. The stability of clock-offset parameters when using a priori clock-offset constraints in position computation is also analysed in this section. In order to see the benefit of using a priori clock-offset constraints, the fault detection and exclusion capabilities are investigated for scenarios when using a limited number of satellites from multiple GNSS constellations to compute a position.

Chapter 5 summarizes the key findings from this research and provides conclusions of this work. Recommendations for possible future works are also discussed in this chapter.

CHAPTER TWO: ESTIMATION ALGORITHM AND RELIABILITY PARAMETERS

The receiver-satellite geometry is an important factor in determining the quality of a position solution. The receiver's surrounding environment such as open sky or urban-canyon influences the geometry and the number of satellites visible to the receiver. Poor receiver-satellite geometry results in imprecise position solutions. Once the position solution is obtained, it is also important to examine the reliability of the solution. The influence of receiver-satellite geometry on the estimated solution accuracy and reliability is discussed in this chapter. The estimation algorithms used and the statistical tests to detect and identify measurement biases are also explained.

2.1 Receiver-satellite Geometry and Design Matrix

The receiver-satellite geometry information is contained in the design matrix (also known as the observation matrix or the geometry matrix), H. The design matrix in Earth-centered Earth-fixed (ECEF) coordinates when using measurements from a single GNSS constellation can be expressed as:

$$H_i = \begin{bmatrix} \frac{\partial P_i}{\partial x_R} & \frac{\partial P_i}{\partial y_R} & \frac{\partial P_i}{\partial z_R} & \frac{\partial P_i}{\partial cdt} \end{bmatrix} \tag{2.1}$$

The subscript i represents the i^{th} satellite used in the position computation, the $(\cdot)_R$ is unknown receiver position (x_R, y_R, z_R) in (x, y, z) coordinates, cdt is the receiver-GNSS clock-offset, in distance units, and P_i is the i^{th} pseudorange which can be modelled as:

$$P_i = \rho_i + c \cdot dt + \varepsilon_i \tag{2.2}$$

where

P is the pseudorange measurement

ρ is the geometric range between satellite and receiver

c is the speed of light in vacuum

dt is the receiver-GNSS clock-offset term and

ε is the ranging error

The geometric range ρ can be expanded further as:

$$\rho_i = \sqrt{(x_i^s - x_R)^2 + (y_i^s - y_R)^2 + (z_i^s - z_R)^2} \tag{2.3}$$

where $(\cdot)_i^s$ denotes the satellite's position in (x^s, y^s, z^s) coordinated which is assumed to be known. The partial derivative in (2.1) can be evaluated with respect to the unknown receiver position (x_R, y_R, z_R) and clock-offset to obtain:

$$H_i = \begin{bmatrix} \frac{x_i^s - x_R}{\rho_i} & \frac{y_i^s - y_R}{\rho_i} & \frac{z_i^s - z_R}{\rho_i} & 1 \end{bmatrix} \tag{2.4}$$

Let

$$\eta(\bullet) = \frac{(\bullet)_i^s - (\bullet)_R}{\rho_i} \tag{2.5}$$

and (2.4) can be rewritten as:

$$H_i = \begin{bmatrix} \eta x_i & \eta y_i & \eta z_i & 1 \end{bmatrix} \tag{2.6}$$

Also, let $b = c \cdot dt$ represent receiver-GNSS clock-offset (or clock-bias) term, then (2.2) can be rewritten as

$$P_i = \rho_i + b + \varepsilon_i \tag{2.7}$$

The design matrix can also expressed in terms of curvilinear geodetic coordinates with latitude, longitude and height or elevation (ϕ, λ, h). Alternatively the design matrix can also be expressed in a local-level coordinate frame, for example East, North and up (E, N, U).

2.2 Least-squares Estimation

The position solution can be computed using least-squares (LS) estimation. Least-squares estimation is a method that is used to obtain *estimated state*, $\hat{\boldsymbol{x}}$, of *state vector*, $\boldsymbol{x}$, using a set of *observations*, $\boldsymbol{z}$. In the linear case, $\boldsymbol{z}$ can be expressed using a linear observation model:

$$\boldsymbol{z} = H\boldsymbol{x} + \varepsilon \tag{2.8}$$

where ε represents measurement errors. In the satellite positioning application, the state estimates are receiver position and receiver-GNSS clock-offset:

$$\hat{\boldsymbol{x}} = \begin{bmatrix} x_R \\ y_R \\ z_R \\ b \end{bmatrix} \tag{2.9}$$

and observation vector contains range measurements from the satellites. However the observation question is non-linear in this case. As a result the observation model must be used to express the observation vector as:

$$\boldsymbol{z} = h(\boldsymbol{x}) + \varepsilon \tag{2.10}$$

where $h(\boldsymbol{x})$ is a mathematical model as a function of the state vector. If a point of expansion x_0 is chosen near to $\hat{x}$, then $h(\boldsymbol{x})$ can be approximated by its Taylor series expanded about that point. The first derivative of h can then be used in place of H and the result is the same as when using the linear-model, provided the point of expansion x_0 is close to $\hat{x}$.

In both cases, the equation for least-squares estimation is:

$$\hat{\boldsymbol{x}} = (H^T R^{-1} H)^{-1} H^T R^{-1} \boldsymbol{z} \tag{2.11}$$

where

$$R = \begin{bmatrix} \sigma_1^2 & 0 & \cdots & 0 \\ 0 & \sigma_2^2 & & \vdots \\ \vdots & & \ddots & 0 \\ 0 & \cdots & 0 & \sigma_n^2 \end{bmatrix} \tag{2.12}$$

is the observation covariance matrix which contains the information regarding the uncertainty, σ, associated with observation errors. In other words, each diagonal element, $R_{i,i}$, corresponds to a quantification of how accurate z_i had been measured. It must be noted that the assumption of independent, hence uncorrelated, measurements had been made; thus, the R matrix is a diagonal matrix with non-diagonal elements being zeros. The term $(H^T R^{-1} H)^{-1}$ in (2.11) is known as estimated state covariance matrix which can be expressed as:

$$P_C = (H^T R^{-1} H)^{-1} \tag{2.13}$$

If the design matrix for the ECEF frame is used to compute the state error covariance matrix, the elements in P_C matrix take the form:

$$P_C = \begin{bmatrix} \sigma_x^2 & \sigma_{xy} & \sigma_{xz} & \sigma_{xt} \\ \sigma_{yx} & \sigma_y^2 & \sigma_{yz} & \sigma_{yt} \\ \sigma_{zx} & \sigma_{zy} & \sigma_z^2 & \sigma_{zt} \\ \sigma_{tx} & \sigma_{ty} & \sigma_{tz} & \sigma_t^2 \end{bmatrix} \tag{2.14}$$

If the design matrix in local coordinates is used, the elements in state error covariance matrix take the form:

$$P_C = \begin{bmatrix} \sigma_E^2 & \sigma_{EN} & \sigma_{EU} & \sigma_{Et} \\ \sigma_{NE} & \sigma_N^2 & \sigma_{NU} & \sigma_{Nt} \\ \sigma_{UE} & \sigma_{UN} & \sigma_U^2 & \sigma_{Ut} \\ \sigma_{tE} & \sigma_{tN} & \sigma_{tU} & \sigma_t^2 \end{bmatrix} \tag{2.15}$$

The estimated correction vector of the least-square can be written as:

$$\delta\hat{\boldsymbol{x}} = (H^T R^{-1} H)^{-1} H^T R^{-1} \delta\boldsymbol{z} \tag{2.16}$$

Once the solution is computed, it is important to examine the quality of the final solution. In order to do this, *residuals*, $\boldsymbol{r}$, which are the difference between the actual measurements, $\boldsymbol{z}$, and the final predicted measurements can be examined. For the linear case, the residual vector is defined as:

$$\boldsymbol{r} = \boldsymbol{z} - H\hat{\boldsymbol{x}} \tag{2.17}$$

For the non-linear case, non-linear least-squares estimation can be applied and the solutions can be obtained using iterative process. In this case, the state estimates can be computed by:

$$\hat{\boldsymbol{x}}_{k+1} = \hat{\boldsymbol{x}}_k + \delta\hat{\boldsymbol{x}}_k \tag{2.18}$$

where subscript k denotes the iteration number. The estimated correction vector from (2.16) can be expressed for the iteration process as:

$$\delta\hat{\boldsymbol{x}}_k = (H_k^T R^{-1} H_k)^{-1} H_k^T R^{-1} \delta\boldsymbol{z}_k \tag{2.19}$$

The iteration process is continued until the elements in the correction vector $\delta\hat{\boldsymbol{x}}_k$ have a sufficiently small value within a pre-set threshold. The term $\delta\boldsymbol{z}$ in (2.19) is known as misclosure vector which is the difference between estimated $\hat{\boldsymbol{z}}$ and observed $\boldsymbol{z}$ values ($\delta\boldsymbol{z} = \boldsymbol{z} - \hat{\boldsymbol{z}}$). Once the correction vector converges and the iteration stops, the last value of the misclosure becomes the residuals.

A small magnitude residuals vector indicates high confidence in the solution. When the least-squares algorithm is applied to obtain an estimated value of the state vector, the goal is to minimize the weighted sum of squares of the residuals and to obtain a minimum variance estimate of the states.

2.3 Dilution of Precision

The dilution of precision (DOP) parameters can be used as indications of the goodness of receiver-satellite geometry. Good satellite geometry results in smaller DOP values. The dilution of precision can be divided in to x, y, z, east (E), north (N), up (U) (or vertical (V)), horizontal (H), time (T), position (P) and geometry (G) DOPs. The *pure geometry* DOPs can be computed from the design matrix which contains geometry information:

$$Q_G = (H^T H)^{-1} \tag{2.20}$$

where Q_G is a pure geometry DOP matrix. From the design matrix in ECEF coordinates, the DOP matrix is obtained to be:

$$Q_G = \begin{bmatrix} q_x^2 & q_{xy} & q_{xz} & q_{xt} \\ q_{yx} & q_y^2 & q_{yz} & q_{yt} \\ q_{zx} & q_{zy} & q_z^2 & q_{zt} \\ q_{tx} & q_{ty} & q_{tz} & q_t^2 \end{bmatrix} \tag{2.21}$$

Similarly, if the local-coordinate (ENU) design matrix is used, the Q_G matrix will contain the following:

$$Q_G = \begin{bmatrix} q_E^2 & q_{EN} & q_{EU} & q_{Et} \\ q_{NE} & q_N^2 & q_{NU} & q_{Nt} \\ q_{UE} & q_{UN} & q_U^2 & q_{Ut} \\ q_{tE} & q_{tN} & q_{tU} & q_t^2 \end{bmatrix} \tag{2.22}$$

The XDOP, YDOP, ZDOP, EDOP, NDOP, UDOP and TDOP can be computed from the diagonal terms of Q_G in relevant coordinate frames:

$$\mu DOP = \sqrt{q_\mu^2} \tag{2.23}$$

where μ is the state for which DOP is to be computed. The position and geometric DOPs can be calculated as:

$$PDOP = \sqrt{Q_{G_{1,1}} + Q_{G_{2,2}} + Q_{G_{3,3}}} \tag{2.24}$$

and

$$GDOP = \sqrt{Q_{G_{1,1}} + Q_{G_{2,2}} + Q_{G_{3,3}} + Q_{G_{4,4}}} \tag{2.25}$$

where Q_P can be either in ECEF or ENU frame. The local level horizontal DOP can be computed from DOP matrix in local-coordinate frame as:

$$HDOP = \sqrt{q_E^2 + q_N^2} \tag{2.26}$$

Note that, if the computation is done in the earth-centered earth-fixed frame, the HDOP and VDOP can be obtained from Q_G matrix in ECEF frame by transforming the matrix to the local level frame using a transformation matrix that rotates between the two frames. The north, east, horizontal and vertical DOPs can then be computed in the usual way as discussed. Also, the size of the Q_G matrix is dependent on the number of GNSS constellations used to compute position solution. The DOP matrices given in (2.21) and (2.22) are for the scenario when using signals from a single GNSS constellation. When using signals from multiple GNSS constellations, each satellite system has its own q_t element and the dimension of the Q_G matrix would expand accordingly.

2.4 Blunder Detection

The *Global* and *local* tests can be performed to detect and identify blunders in observations. The global test statistic can be expressed as:

$$\xi_{global} = \boldsymbol{r}^T R^{-1} \boldsymbol{r} \tag{2.27}$$

Assuming Gaussian measurement errors, global test statistic is tested against a threshold obtained from chi-square (χ^2) test statistic, which is a function of degrees of freedom (DoF) and significance level α:

$$\left|\xi_{global}\right| < \chi^2_{(DoF,\alpha)} \tag{2.28}$$

If ξ_{global} exceeds the threshold, this suggests that the sum-of-squares of the residuals does not follow the expected distribution of a sum of squares of zero-mean Gaussians and thus errors in one or more of the observations are suspected.

It must be noted that, in this case, the observation covariance matrix, R, is assumed to be known from estimated measurement accuracy. For a general case, matrix Rcan be expressed as:

$$R = \sigma_0^2 Q_R \tag{2.29}$$

where σ_0^2 is the *a priori* variance factor which assumed to be known and Q_R is the cofactor matrix of R. An approximation of for σ_0^2 which is *a posteriori* variance factor, $\hat{\sigma}_0^2$, can be computed by:

$$\hat{\sigma}_0^2 = \frac{\boldsymbol{r}^T Q_R^{-1} \boldsymbol{r}}{DoF} \tag{2.30}$$

The a posteriori variance factor can be statistically tested. In this case, the null hypothesis, H_0, is that the *a priori* and *a posteriori* variance factors agreed ($\hat{\sigma}_0^2 = \sigma_0^2$). The corresponding test statistic for this is:

$$\xi_{global} = \frac{\widehat{\sigma}_0^2}{\sigma_0^2} DoF \tag{2.31}$$

Thus,

$$\xi_{global} = \frac{\boldsymbol{r}^T Q_{\mathrm{R}}^{-1} \boldsymbol{r}}{\sigma_0^2} = \boldsymbol{r}^T R^{-1} \boldsymbol{r} \tag{2.32}$$

In this case, a failed statistical test implies either the *a priori* variance is incorrectly chosen, the observation model is wrong, or one or more of the residuals is not a zero-mean Gaussian process, suggesting that a blunder is present.

In the case when global test statistic indicates that there may be a blunder in one or more of the observations, the local test can be performed to identify the particular measurement containing the blunder. The null hypothesis, H_0, used in the blunder detection process is that each residual is normally distributed with zero mean with variance corresponding to its element of the covariance matrix of the residuals, C_r, which can be computed from the design matrix and observation covariance matrix as:

$$C_r = R - H(H^T R^{-1} H)^{-1} H^T \tag{2.33}$$

In the local test, the H_0 is accepted if the local test statistic, ξ_{local}, satisfies the condition

$$|\xi_{local}| = \left| \frac{r_i}{\sqrt{(C_r)_{i,i}}} \right| < N_{1-\frac{\alpha}{2}} \tag{2.34}$$

where $N(\alpha)$ is a statistic threshold as a function of significance level. The measurement is identified as blunder and will be rejected if the local test statistic exceeds the threshold, in which case an alternative hypothesis, H_1, is chosen.

2.5 Internal and External Reliability

Statistical tests can be carried out to examine the reliability of measurements given an assumed observation accuracy. Two reliability parameters, *internal* and *external* reliabilities, are explained in this subsection.

2.5.1 Internal Reliability

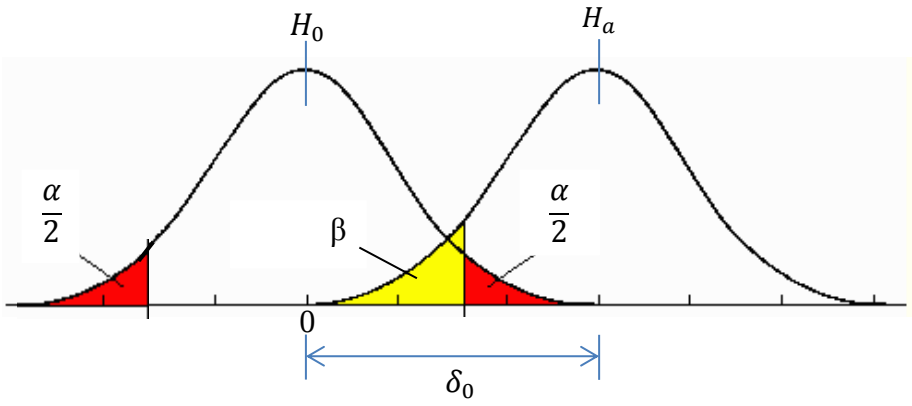

Figure 2.1: Relationship between Type I (red) and Type II (yellow) errors

Two types of errors, Type I and Type II, can occur during statistical hypothesis testing. Type I errors refer to a situation when a good measurement is incorrectly rejected. Type II errors, on the other hand, refer to the scenario when a bad observation is incorrectly accepted. The relationship between Type I and Type II errors are shown in Figure 2.1.

The Type I error occurs with a probability of α shown by the red regions. The parameter α is the significance level used in test statistic and blunder detection process. The Type II error occurs with a probability of β as indicated in the yellow region of the figure. The parameter β is often called "the power of the test" and is a design parameter which is used to assess the theoretical

reliability of the solution. This parameter is not implicitly used in blunder detection as the threshold is set based on significance level α only.

The non-centrality parameter, δ_0, represents a shift of the normal distribution of the standardized residual as a result of the presence of a blunder. The δ_0 can be computed using a given α and β probability level as

$$\delta_0 = N_{1-\frac{\alpha}{2}} + N_{1-\beta} \tag{2.35}$$

where $N(\alpha)$ and $N(\beta)$ are function of significance level and power of test respectively. Assuming uncorrelated measurements and a single blunder is present in a set of observations, the non-centrality parameter can be used to compute a minimum detectable blunder for the i^{th} observation, ∇_{MDB_i}, using the following equation:

$$\nabla_{MDB_i} = \frac{R_{i,i}}{\sqrt{(C_r)_{i,i}}}\,\delta_0 \tag{2.36}$$

The ∇_{MDB_i} denotes the smallest magnitude of blunder that can be detected by employing the local test for blunder detection on the i^{th} observation when using significance level α and power of test β.

2.5.2 External Reliability

The external reliability evaluates the effect of the undetected blunder on the estimated state parameters. The error in the states introduced by a blunder in the i^{th} observation can be computed by passing the error through LS solution:

$$\Delta\hat{x}_i = (H^T R^{-1} H)^{-1} H^T R^{-1}\, M_i \nabla_{MDB_i} \tag{2.37}$$

where M_i is a column vector $[0 \cdots 0 \;\; 1 \;\; 0 \cdots 0]^T$ with value of one located at the element corresponding to i^{th} observation and all zeros at other elements. The column vector $\boldsymbol{M}$ is used to map the blunder into the observations. In the general case, the protection level (PL), $\Delta\hat{x}_i$, obtained from (2.37) is a position error due to a single MBD, should it occurred in an observation, given α and β values. In this study, the PL refers to the largest value of $\Delta\hat{x}_i$ obtained from all MDBs in each epoch ($Max(\Delta\hat{\boldsymbol{x}})$).

2.6 Design Matrix Using Multiple GNSS constellations

When ranging signals from multiple GNSS constellations are available, the pseudorange measurement equations for each system can be written as:

$$\begin{aligned} P_{GNSS1_i} &= \rho_{GNSS1_i} + b_{GNSS1} + \varepsilon_{GNSS1_i} \\ P_{GNSS2_i} &= \rho_{GNSS2_i} + b_{GNSS2} + \varepsilon_{GNSS2_i} \\ P_{GNSS3_i} &= \rho_{GNSS3_i} + b_{GNSS3} + \varepsilon_{GNSS3_i} \end{aligned} \tag{2.38}$$

for the three GNSS constellation case. The clock-offset parameter of the second and third systems can be expressed in term of the bias of the first system as:

$$\begin{aligned} b_{GNSS2} &= b_{GNSS1} + \Delta b_{GNSS12} \\ b_{GNSS3} &= b_{GNSS1} + \Delta b_{GNSS13} \end{aligned} \tag{2.39}$$

where Δb is an inter-system time-offset between the two systems. In this case, the GNSS1 is the *reference system* for the time-offset. The representation is justified by assuming that there are constant, or at least very slowly changing, time-offsets between the various GNSS in addition to a single unknown user receiver clock-offset due to the actual clock in the receiver. The design

matrix when using signals from multiple GNSS constellations, when each of the system clock-offsets are estimated at the receiver at each epoch, can be written as:

$$H = \begin{bmatrix} \eta x_{GNSS1_i} & \eta y_{GNSS1_i} & \eta z_{GNSS1_i} & 1 & 0 & 0 \\ \vdots & \vdots & \vdots & \vdots & \vdots & \vdots \\ \eta x_{GNSS1_{N_1}} & \eta y_{GNSS1_{N_1}} & \eta z_{GNSS1_{N1}} & 1 & 0 & 0 \\ \eta x_{GNSS2_i} & \eta y_{GNSS2_i} & \eta z_{GNSS2_i} & 0 & 1 & 0 \\ \vdots & \vdots & \vdots & \vdots & \vdots & \vdots \\ \eta x_{GNSS2_{N_2}} & \eta y_{GNSS2_{N_2}} & \eta z_{GNSS2_{N_2}} & 0 & 1 & 0 \\ \eta x_{GNSS3_i} & \eta y_{GNSS3_i} & \eta z_{GNSS3_i} & 0 & 0 & 1 \\ \vdots & \vdots & \vdots & \vdots & \vdots & \vdots \\ \eta x_{GNSS3_{N_3}} & \eta y_{GNSS3_{N_3}} & \eta z_{GNSS3_{N_3}} & 0 & 0 & 1 \end{bmatrix} \quad (2.40)$$

where the subscript $i = 1, 2, \ldots N_j$ present the i^{th} satellite used in position computation and N_j represent the maximum number of satellite in view from the j^{th} GNSS system. In this case, the states estimated are receiver position and receiver-GNSS clock-offsets for each constellation, thus, $\hat{\boldsymbol{x}} = [x_R \; y_R \; z_R \;\; b_{GNSS1} \;\; b_{GNSS2} \;\; b_{GNSS3}]^T$. In this example, these six unknown parameters are to be estimated by the receiver at each epoch.

Alternatively, instead of estimating the system clock-offset for each GNSS constellation, the receiver can estimate the clock-offset of a reference system and inter-system clock-offset between the reference system and the additional system. In this case, the design matrix changes to the following:

$$H = \begin{bmatrix} \eta x_{GNSS1_i} & \eta y_{GNSS1_i} & \eta z_{GNSS1_i} & 1 & 0 & 0 \\ \vdots & \vdots & \vdots & \vdots & \vdots & \vdots \\ \eta x_{GNSS1_{N_1}} & \eta y_{GNSS1_{N_1}} & \eta z_{GNSS1_{N1}} & 1 & 0 & 0 \\ \eta x_{GNSS2_i} & \eta y_{GNSS2_i} & \eta z_{GNSS2_i} & 1 & 1 & 0 \\ \vdots & \vdots & \vdots & \vdots & \vdots & \vdots \\ \eta x_{GNSS2_{N_2}} & \eta y_{GNSS2_{N_2}} & \eta z_{GNSS2_{N_2}} & 1 & 1 & 0 \\ \eta x_{GNSS3_i} & \eta y_{GNSS3_i} & \eta z_{GNSS3_i} & 1 & 0 & 1 \\ \vdots & \vdots & \vdots & \vdots & \vdots & \vdots \\ \eta x_{GNSS3_{N_3}} & \eta y_{GNSS3_{N_3}} & \eta z_{GNSS3_{N_3}} & 1 & 0 & 1 \end{bmatrix} \quad (2.41)$$

In this case, the state estimates are receiver-satellite position, receiver-GNSS clock-offset of the reference GNSS constellation and inter-system clock-offsets between reference system and the other GNSS. The estimated states vector can thus be written as $\hat{\boldsymbol{x}} = [x_R\ y_R\ z_R\ \ b_{GNSS1}\ \ \Delta b_{GNSS12}\ \ \Delta b_{GNSS13}]^T$ where GNSS1 is the reference system in this case. The design matrix for the three GNSS constellations as stated in (2.40) and (2.41) can be generalized into other multiple GNSS constellations combinations.

When the inter-system clock-offset, Δb_{GNSS12} and Δb_{GNSS13}, are either broadcast by the GNSS or obtained by other means, the receiver can use these values as additional measurements along with their estimated accuracies as constraints. In such a case, the design matrix manifest as:

$$H = \begin{bmatrix} \eta x_{GNSS1_i} & \eta y_{GNSS1_i} & \eta z_{GNSS1_i} & 1 & 0 & 0 \\ \vdots & \vdots & \vdots & \vdots & \vdots & \vdots \\ \eta x_{GNSS1_{N_1}} & \eta y_{GNSS1_{N_1}} & \eta z_{GNSS1_{N1}} & 1 & 0 & 0 \\ \eta x_{GNSS2_i} & \eta y_{GNSS2_i} & \eta z_{GNSS2_i} & 0 & 1 & 0 \\ \vdots & \vdots & \vdots & \vdots & \vdots & \vdots \\ \eta x_{GNSS2_{N_2}} & \eta y_{GNSS2_{N_2}} & \eta z_{GNSS2_{N_2}} & 0 & 1 & 0 \\ \eta x_{GNSS3_i} & \eta y_{GNSS3_i} & \eta z_{GNSS3_i} & 0 & 0 & 1 \\ \vdots & \vdots & \vdots & \vdots & \vdots & \vdots \\ \eta x_{GNSS3_{N_3}} & \eta y_{GNSS3_{N_3}} & \eta z_{GNSS3_{N_3}} & 0 & 0 & 1 \\ 0 & 0 & 0 & 1 & -1 & 0 \\ 0 & 0 & 0 & 1 & 0 & -1 \end{bmatrix} \tag{2.42}$$

where the last two rows represent constraints in the form of direct observations of the inter-system time-offsets. In this case, the GNSS1 is the *reference system time-offset*. The measurement covariance matrix in this case is:

$$R = \begin{bmatrix} \sigma^2_{GNSS1\rho_i} & 0 & \cdots & \cdots & \cdots & \cdots & \cdots & \cdots & \cdots & \cdots & 0 \\ 0 & \ddots & & & & & & & & & \vdots \\ \vdots & & \sigma^2_{GNSS1\rho_{N1}} & & & & & & & & \vdots \\ \vdots & & & \sigma^2_{GNSS2\rho_i} & & & & 0 & & & \vdots \\ \vdots & & & & \ddots & & & & & & \vdots \\ \vdots & & & & & \sigma^2_{GNSS1\rho_{N2}} & & & & & \vdots \\ \vdots & & & & & & \sigma^2_{GNSS3\rho_i} & & & & \vdots \\ \vdots & & & 0 & & & & \ddots & & & \vdots \\ \vdots & & & & & & & & \sigma^2_{GNSS1\rho_{N3}} & & \vdots \\ \vdots & & & & & & & & & \sigma^2_{\Delta b_{GNSS12}} & 0 \\ 0 & \cdots & \cdots & \cdots & \cdots & \cdots & \cdots & \cdots & \cdots & 0 & \sigma^2_{\Delta b_{GNSS13}} \end{bmatrix} \tag{2.43}$$

where $\sigma^2_{GNSSj\rho_i}$ is the uncertainty in range measurements i^{th} $(i = 1, 2, \dots, N_j)$ from satellite in j^{th} $(j = 1, 2, 3)$ constellation and the uncertainty associated with the inter-system clock-offset parameters of the two additional systems with GNSS1 as reference system clock-offset is represented by $\sigma^2_{\Delta b_{GNSS12}}$ and $\sigma^2_{\Delta b_{GNSS13}}$ parameters.

Parameterizing the clock-offsets as one clock-offset and two nearly constant biases has advantages if Kalman filtering is used instead of epoch-by-epoch least-squares. In this case the inter-system time-offsets can be modelled as random constants while the remaining clock-offset can be modelled depending on the oscillator used. Using the first approach (multiple clock-offsets) in a Kalman filter would require that all of the clock-offsets be modelled as processes with highly correlated process noise, since their variability from epoch to epoch depends primarily on the physical behaviour of the single oscillator in the receiver. Filtering could then be applied so that the system could initially estimate each of the receiver-GNSS clock-offsets during the times when the receiver-satellite geometry is good and when there are sufficient number of satellites in the view. Then at a later time when the number of satellites is reduced, the receiver can use the initially estimated clock-offset parameters as a priori information. In this case when an a priori clock-offset for each constellation is available and is used by the position solution algorithm as a constraint, the design matrix can be expressed as:

$$H = \begin{bmatrix} \eta x_{GNSS1_i} & \eta y_{GNSS1_i} & \eta z_{GNSS1_i} & 1 & 0 & 0 \\ \vdots & \vdots & \vdots & \vdots & \vdots & \vdots \\ \eta x_{GNSS1_{N_1}} & \eta y_{GNSS1_{N_1}} & \eta z_{GNSS1_{N1}} & 1 & 0 & 0 \\ \eta x_{GNSS2_i} & \eta y_{GNSS2_i} & \eta z_{GNSS2_i} & 0 & 1 & 0 \\ \vdots & \vdots & \vdots & \vdots & \vdots & \vdots \\ \eta x_{GNSS2_{N_2}} & \eta y_{GNSS2_{N_2}} & \eta z_{GNSS2_{N_2}} & 0 & 1 & 0 \\ \eta x_{GNSS3_i} & \eta y_{GNSS3_i} & \eta z_{GNSS3_i} & 0 & 0 & 1 \\ \vdots & \vdots & \vdots & \vdots & \vdots & \vdots \\ \eta x_{GNSS3_{N_3}} & \eta y_{GNSS3_{N_3}} & \eta z_{GNSS3_{N_3}} & 0 & 0 & 1 \\ 0 & 0 & 0 & 1 & 0 & 0 \\ 0 & 0 & 0 & 0 & 1 & 0 \\ 0 & 0 & 0 & 0 & 0 & 1 \end{bmatrix} \tag{2.44}$$

It might appear that with a priori clock-offsets for all GNSS constellations, only 3 satellites are required to obtain a position solution. While this is true in principle, is not the case in practise, as clock drift, mainly due to receiver frequency offset, usually leads to rapid deviation of the true clock-offset values from their initial estimates. This can be mitigated by estimating the frequency offset (or clock drift), d, which can be done easily by estimating user velocity and clock drifts parameters $(\dot{x}, \dot{y}, \dot{z}, d_{GNSS1}, d_{GNSS2}, d_{GNSS3})$ using Doppler measurements. Assuming that all three GNSS are subject to the same clock drift (due to the frequency error of the single oscillator in the receiver) a minimum of four satellites is required to estimate $(\dot{x}, \dot{y}, \dot{z}, d)$ parameters. This results in the design matrix having to be modified to incorporate the Doppler measurements as follows:

$$
H = \begin{bmatrix}
\eta x_{GNSS1_i} & \eta y_{GNSS1_i} & \eta z_{GNSS1_i} & 0 & 0 & 0 & 0 & 1 & 0 & 0 \\
0 & 0 & 0 & \dot{\eta} x_{GNSS1_i} & \dot{\eta} y_{GNSS1_i} & \dot{\eta} z_{GNSS1_i} & 1 & 0 & 0 & 0 \\
\vdots & \vdots & \vdots & \vdots & \vdots & \vdots & \vdots & \vdots & \vdots & \vdots \\
\vdots & \vdots & \vdots & \vdots & \vdots & \vdots & \vdots & \vdots & \vdots & \vdots \\
\eta x_{GNSS1_{N_1}} & \eta y_{GNSS1_{N_1}} & \eta z_{GNSS1_{N1}} & 0 & 0 & 0 & 0 & 1 & 0 & 0 \\
0 & 0 & 0 & \dot{\eta} x_{GNSS1_{N_1}} & \dot{\eta} y_{GNSS1_{N_1}} & \dot{\eta} z_{GNSS1_{N1}} & 1 & 0 & 0 & 0 \\
\eta x_{GNSS2_i} & \eta y_{GNSS2_i} & \eta z_{GNSS2_i} & 0 & 0 & 0 & 0 & 0 & 1 & 0 \\
0 & 0 & 0 & \dot{\eta} x_{GNSS2_i} & \dot{\eta} y_{GNSS2_i} & \dot{\eta} z_{GNSS2_i} & 1 & 0 & 0 & 0 \\
\vdots & \vdots & \vdots & \vdots & \vdots & \vdots & \vdots & \vdots & \vdots & \vdots \\
\vdots & \vdots & \vdots & \vdots & \vdots & \vdots & \vdots & \vdots & \vdots & \vdots \\
\eta x_{GNSS2_{N_2}} & \eta y_{GNSS2_{N_2}} & \eta z_{GNSS2_{N_2}} & 0 & 0 & 0 & 0 & 0 & 1 & 0 \\
0 & 0 & 0 & \dot{\eta} x_{GNSS2_{N_2}} & \dot{\eta} y_{GNSS2_{N_2}} & \dot{\eta} z_{GNSS2_{N_2}} & 1 & 0 & 0 & 0 \\
\eta x_{GNSS3_i} & \eta y_{GNSS3_i} & \eta z_{GNSS3_i} & 0 & 0 & 0 & 0 & 0 & 0 & 1 \\
0 & 0 & 0 & \dot{\eta} x_{GNSS3_i} & \dot{\eta} y_{GNSS3_i} & \dot{\eta} z_{GNSS3_i} & 1 & 0 & 0 & 0 \\
\vdots & \vdots & \vdots & \vdots & \vdots & \vdots & \vdots & \vdots & \vdots & \vdots \\
\vdots & \vdots & \vdots & \vdots & \vdots & \vdots & \vdots & \vdots & \vdots & \vdots \\
\eta x_{GNSS3_{N_3}} & \eta y_{GNSS3_{N_3}} & \eta z_{GNSS3_{N_3}} & 0 & 0 & 0 & 0 & 0 & 0 & 1 \\
0 & 0 & 0 & \dot{\eta} x_{GNSS3_{N_3}} & \dot{\eta} y_{GNSS3_{N_3}} & \dot{\eta} z_{GNSS3_{N_3}} & 1 & 0 & 0 & 0 \\
0 & 0 & 0 & 0 & 0 & 0 & 0 & 1 & 0 & 0 \\
0 & 0 & 0 & 0 & 0 & 0 & 0 & 0 & 1 & 0 \\
0 & 0 & 0 & 0 & 0 & 0 & 0 & 0 & 0 & 1
\end{bmatrix} \tag{2.45}
$$

where $\dot{\eta}$ is the design matrix element corresponding to velocity states. The corresponding measurement covariance matrix in this case is:

$$R = \begin{bmatrix}
\sigma^2_{GNSS1\rho_i} & 0 & \cdots & \cdots & \cdots & \cdots & \cdots & \cdots & \cdots & \cdots & \cdots & \cdots & \cdots & \cdots & \cdots & 0 \\
0 & \sigma^2_{GNSS1\Phi_i} & & & & & & & & & & & & & & \vdots \\
\vdots & & \ddots & & & & & & & & & & & & & \vdots \\
\vdots & & & \sigma^2_{GNSS1\rho_{N1}} & & & & & & & & & & & & \vdots \\
\vdots & & & & \sigma^2_{GNSS1\Phi_{N1}} & & & & & & & & & & & \vdots \\
\vdots & & & & & \sigma^2_{GNSS2\rho_i} & & & & & & 0 & & & & \vdots \\
\vdots & & & & & & \sigma^2_{GNSS2\Phi_i} & & & & & & & & & \vdots \\
\vdots & & & & & & & \ddots & & & & & & & & \vdots \\
\vdots & & & & & & & & \sigma^2_{GNSS1\rho_{N2}} & & & & & & & \vdots \\
\vdots & & & & & & & & & \sigma^2_{GNSS1\Phi_{N2}} & & & & & & \vdots \\
\vdots & & & & & & & & & & \sigma^2_{GNSS3\rho_i} & & & & & \vdots \\
\vdots & & & & & & & & & & & \sigma^2_{GNSS3\Phi_i} & & & & \vdots \\
\vdots & & & & & & & & & & & & \ddots & & & \vdots \\
\vdots & & & & & 0 & & & & & & & \sigma^2_{GNSS1\rho_{N3}} & & & \vdots \\
\vdots & & & & & & & & & & & & & \sigma^2_{GNSS1\Phi_{N3}} & & \vdots \\
\vdots & & & & & & & & & & & & & & \sigma^2_{b_{GNSS1}} & \vdots \\
\vdots & & & & & & & & & & & & & & \sigma^2_{b_{GNSS2}} & 0 \\
0 & \cdots & \cdots & \cdots & \cdots & \cdots & \cdots & \cdots & \cdots & \cdots & \cdots & \cdots & \cdots & \cdots & \cdots 0 & \sigma^2_{b_{GNSS3}}
\end{bmatrix} \tag{2.46}$$

where $\sigma^2_{GNSSj\Phi_i}$ is the uncertainty in Doppler measurements, Φ, and $\sigma^2_{b_{GNSSj}}$ represent the uncertainty associated with an a priori clock-offset for the j^{th} constellation. The design matrix for the three GNSS constellations as stated in (2.42) and (2.45) as well as the measurement covariance matrix R as stated in (2.43) and (2.46) can be generalized into other multiple GNSS constellations combinations.

2.7 Number of Satellites Requirements

In order to estimate user position and multiple clock-offsets, one additional observation is required for every additional GNSS. In this case, the additional observation is only able to uniquely determine the additional clock-offset and has no effect on the position estimate. If at least two observations are available from each GNSS, it will be possible to perform the global test but with only one degree of freedom, the local test is not possible. In order to detect and exclude faulty measurements when using measurements from multiple GNSS constellations, at least three satellites from each constellation are required to identify faulty signals when the inter-system time-offsets (or receiver-GNSS clock-offsets) are estimated by the receiver at each epoch. This is because with only two measurements from a system, the standardized residuals, $\boldsymbol{r}_s$, obtained by:

$$r_{s_{i,i}} = \frac{r_i}{\sqrt{(C_r)_{i,i}}} \tag{2.47}$$

will be equal in magnitude. Since these standardized residuals are also used as the internal reliability test statistic to compute ∇_{MDB_i} expressed in (2.36), the equality of each $r_{s_{i,i}}$ makes it impossible to identify the faulty measurement with only two satellites from a system when the

inter-system clock-offset is estimated by the receiver at each epoch (Hewitson & Wang 2006, O'Keefe et al. 2011).

The least-squares estimation algorithm and statistical tests to detect and identify measurement blunders have been discussed in this chapter. The design matrix for the scenario when using measurements from multiple GNSS constellations has also been presented. The next step is to assess the accuracy and reliably of multi-constellation GNSS positioning in challenging GNSS signal environment when using a limited number of satellites from multiple GNSS constellations and further to assess the benefits of using a priori inter-system clock-offsets information when compute receiver position.

CHAPTER THREE: SIMULATION DESCRIPTION AND RESULTS

One objective of this thesis is to assess the accuracy and reliably of multi-constellation GNSS positioning in urban environments (with small numbers of satellites from each constellation) and further to assess the benefits of inter-system clock-offset information. While this could be accomplished for existing constellations with a large scale data collection campaign, it is simpler to use covariance simulation. The reliability parameters described in Chapter 2 depend only on observation geometry, estimated observation variance, and the test parameters and thus lend themselves to covariance analysis. An added advantage is that the new constellations can be easily tested in simulation. For such a covariance simulation to be valid, the simulation parameters must be realistic.

This chapter is organised in six sections. Section 3.1 describes the simulation scenarios, including various user environments and GNSS constellations. Section 3.2 explains the model parameters used in the covariance simulations. The simulation results and analysis are shown in the remaining four sections. Section 3.3 examines the reliability performance when using signals from GPS and GLONASS systems with and without SBAS corrections applied to GPS measurements. Section 3.4 investigates the availability and reliability of position solution obtains from GPS, GLONASS, BeiDou and Galileo satellites when the clock-offsets for each GNSS are estimated in the receiver at each epoch. Section 3.5 examines the availability and reliability performances of the multiple GNSS constellations when using a priori clock-offsets. Finally, the positioning performance of multi-constellation GNSS when using a priori clock-offsets as constraints with various estimated accuracies is examined in section 3.6.

3.1 Simulation Description

For each simulation scenario, the present GPS and GLONASS constellations are used and system availability as well as MDB and PL (referred to as HPL and VPL for maximum horizontal and vertical protection level) are evaluated using a simulation period of 4 days. The GPS and GLONASS satellite positions are obtained from IGS precise satellite coordinates from 11:00 AM (GPS time) on 27 October 2012 (GPS week 1711). At that time, 30 GPS and 24 GLONASS satellites were in operation. The BeiDou and Galileo constellations are constructed from theoretical orbits as stated in the BeiDou Interface Control Document (BDS-ICD 2012), He et al. (2013) and Van Diggelen (2009) for MEO BeiDou and in ESA (2013a), ESA Fact Sheet (2013), Galileo ICD (2010) and Van Diggelen (2009) for Galileo.

The simulation is carried out over North America from latitude 23^o to 73^o North and longitude from 50^o to 170^o West as shown in Figure 3.1 with a 5^o spacing and an assumed elevation of 500 m. A single frequency (L1/E1/B1) receiver is assumed. Various scenarios have been considered:

- open sky with assumed mask angle of 10^o
- semi-urban areas with assumed mask angle of 30^o
- locations in a north-south running urban-canyon with the road width of 20 m and building height of 15 m
- locations in an east-west running urban-canyon with the same road width and building height.

Figure 3.1: Map of simulation study areas

The satellite combinations considered in this study are combined GPS and GLONASS constellations with:

- partial Galileo constellation
- partial BeiDou constellation
- complete Galileo constellation
- complete MEO BeiDou constellation
- partial Galileo and partial BeiDou constellations
- complete Galileo and MEO BeiDou constellations

The performance of the combined GPS and GLONASS constellations with SBAS corrections applied to GPS measurements also investigated in this study. The system availability for each scenario is examined in terms of position solution availability, fault detection and exclusion availability and 95th percentile values of three reliability parameters: MDB, HPL and VPL (i.e. better than this value 95% of the time) are computed.

3.2 User Equivalent Range Error Model

The measurement variance or user equivalent range error (UERE) can be computed from combining errors from multiple sources as follow:

$$\sigma_{UERE}^2 = \sigma_{URA}^2 + \sigma_{iono}^2 + \sigma_{tropo}^2 + \sigma_{multipath}^2 + \sigma_{noise}^2 \quad (3.1)$$

where the standard deviation of User Range Accuracy σ_{URA} is the error related to satellite clock, orbit and ephemeris errors (Salós et al. 2010c, Sun & Zhang 2009). For GPS, the term User Range Error (URE) is used and the relationship between URE and URA is defined in IS-GPS-200G (2012). The URA is a conservative root mean square (RMS) estimate of the URE assuming a normal distribution with zero mean. According to GPS Standard Positioning Service Performance Standard (GPS-SPS-PS 2008), when using single frequency C/A code, the global average URE is better than 7.8 m 95% of the tine during normal operation. According to Cooley (2013) and Heng et. al. (2012a), however, the URA of within 2 m is observed for most of the GPS satellites in the recent years. Also, the older generation of the navigation satellites, GPS Block IIA (currently 8 satellites from this generation are in operation), has slightly higher URE compared to the newer generation satellites (Cooley 2013). In this study, a conservative σ_{URA} value of 3.9 m as used by Salós et al. (2010b) and Salós et al. (2010c) is assumed.

The σ_{URA} value used by Salós et al. (2010b) and Salós et al. (2010c) also assumed for the SBAS corrected GPS signals and Galileo. The User Differential Range Error (UDRE) of 0.3 m is assumed for GPS with SBAS corrections. The Galileo satellites are assume to have Signal in Space Accuracy (SISA) which equivalent to nominal URA of 0.85 m. For GLONASS, the accuracy of satellite clock corrections in GLONASS-M is 8 ns and the position error due to

broadcast ephemeris from GLONASS is approximately 5 m (GLONASS-ICD 2008, Zinoviev 2005). For all GLONASS-M satellites, the 1σ clock error value was found to be within 5 m (Heng et. al. 2012b). According to this information, the σ_{URA} for GLONASS is assumed to be 8.0 m. It must be noted that an improvement in GLONASS Signal in Space Range Error (SISRE) is evidenced over the past few years (Revnivykh 2010); in this study, however, a conservative assumption is applied. For BeiDou, the satellite broadcast ephemeris accuracy is better than 1.5 m and the clock bias is smaller than 5 ns (China Satellite Navigation Office 2012a, ICAO-China 2012), thus, the σ_{URA} of 3.0 m is assumed for BeiDou.

σ_{iono} is the frequency-dependent error caused by ionosphere code delay. Models to compute this parameter for the GPS and Galileo systems can be found in various literature such as Arbesser-Rastburg (2006), Neri et al. (2011), Salós et al. (2010b) and Salós et al. (2010c). In general, the ionospheric delay, I_ρ, can be computed by:

$$I_\rho = \frac{40.3}{f^2} \times VTEC \times OF(el) \tag{3.2}$$

where $VTEC$ is the vertical total electron content, f is the carrier phase frequency and $OF(el)$ is the obliquity factor as a function of elevation angle, el (in degrees), which can be expressed further as (Arbesser-Rastburg 2006, Misra & Enge 2011):

$$OF(el) = 1.0 + 16.0 \times \left(0.53 - \frac{el}{180}\right)^3 \tag{3.3}$$

The $VTEC$ varies as a function of parameters such as latitude and time of day. The value assumed for the simulation for North America is 40 total electron content units (TECu). In general, GPS broadcast corrections are able to correct 50% of the ionospheric delay (Salós et al.

2010c). For the GLONASS system, if the measurements from GLONASS are used by GPS/GLONASS receiver and the ionospheric correction information from GPS is used by the receiver to perform ionospheric correction for GLONASS measurements then the same amount of ionospheric correction as GPS is assumed for GLONASS. For Galileo, the residual error as a result of ionospheric pseudorange error will not exceed 20 TECu or 30% (Arbesser-Rastburg 2006). According to China Satellite Navigation Office (2012a), when the Klobuchar-8 ionospheric correction model is applied to measurements from BeiDou about 80% of the ionospheric delay can be corrected. In this simulation, a correction of 50% is assumed for measurements from all GNSS constellations and the error due to ionospheric delay can be expressed as:

$$\sigma_{iono} = \frac{40.3}{f^2} \times VTEC \times OF(el) \times M_a \tag{3.4}$$

where M_a is equal to 50% indicating that on average 50% of ionospheric delay is left as an error due to ionospheric code delay. When SBAS corrections are used, the ionospheric error model:

$$\sigma_{iono\ SBAS} = OF(el) \times 0.46 \tag{3.5}$$

is applied (Salós et al. 2010c).

σ_{tropo} is the error due to tropospheric effects on satellite signals. This value can be computed using the model adopted by Choi et al. (2011) and Martineau et al. (2009) as:

$$\sigma_{tropo} = \frac{1.001}{\sqrt{0.002001 + \sin^2(el)}} \times 0.12m \tag{3.6}$$

When SBAS is used, a study over a one-year period for five UK stations found that the RMS EGNOS model zenith tropospheric delay errors range from 4.0 cm to 4.7 cm, with maximum

error ranging from 13.2 cm to 17.8 cm (Penna et al. 2001). Based on this information, a $\sigma_{tropo\ SBAS}$ of 10 cm is assumed during the simulation.

σ_{noise} is the position error due to the noise which depends largely upon factors such as signal strength, user dynamics and quality of the receiver. $\sigma_{multipath}$ is the error due to multipath (which fault detection and elimination algorithms try to detect). The magnitude of multipath error can vary significantly depending on the environment in which the receiver is located. While multipath with magnitudes of few to several tens of centimeters can be expected in an environment with minor signal obstacles (Kaplan & Hegarty 2006), pseudorange multipath with magnitude of several tens of meters is not uncommon in more challenging signal environments (Gerdan et. al. 1995). In urban areas, multipath typically can result in pseudorange error by up to 150 m (Obst & Wanielik 2013).

In this work, the small multipath (few to several tens of centimeters) is considered as a nominal error and is included in the pseudorange noise error budget. The large multipath (several tens of meters) is treated as a form of fault or blunder that the fault detection and elimination algorithm will try to eliminate. According to the information above, the error due to combined noise and small multipath, $\sigma_{noise\ +\ small\ multipath}$, is assumed to be 0.5 m in the nominal error model. The measurement variance model which represents nominal error conditions thus can be expressed as:

$$\sigma^2_{UERE} = \sigma^2_{URA} + \sigma^2_{iono} + \sigma^2_{tropo} + \sigma^2_{noise\ +\ small\ multipath} \tag{3.7}$$

It must be noted that equation (3.7) does not imply an assumption that large multipath does not exist in the environment where the receiver is located. This equation, however, indicates that in this study the large multipath is not considered as part of a contribution to nominal signal error but it is one of the faults that the blunder detection process tries to detect and eliminate. By using this UERE value as an error budget in statistical testing, residuals exceeding this would be identified as errors due to large multipath. Although the faults could be due to other factors such as satellite faults, in challenging GNSS environments such as urban scenarios when there are many signal reflectors, errors due to multipath are the main source of outliers.

The σ_{UERE} and $\sigma_{UERE\ iono,tropo\ only}$ (error as a result of ionospheric and tropospheric only) values for GPS, GLONASS, BeiDou, Galileo, and GPS corrected with SBAS adopting the models and parameters listed above are shown in Figure 3.2. For the statistical analysis, a confidence level of 95% (α = 5%) and a power of the test of 90% (β = 10%), resulting in a non-centrality parameter of δ_0 = 3.24 is assumed.

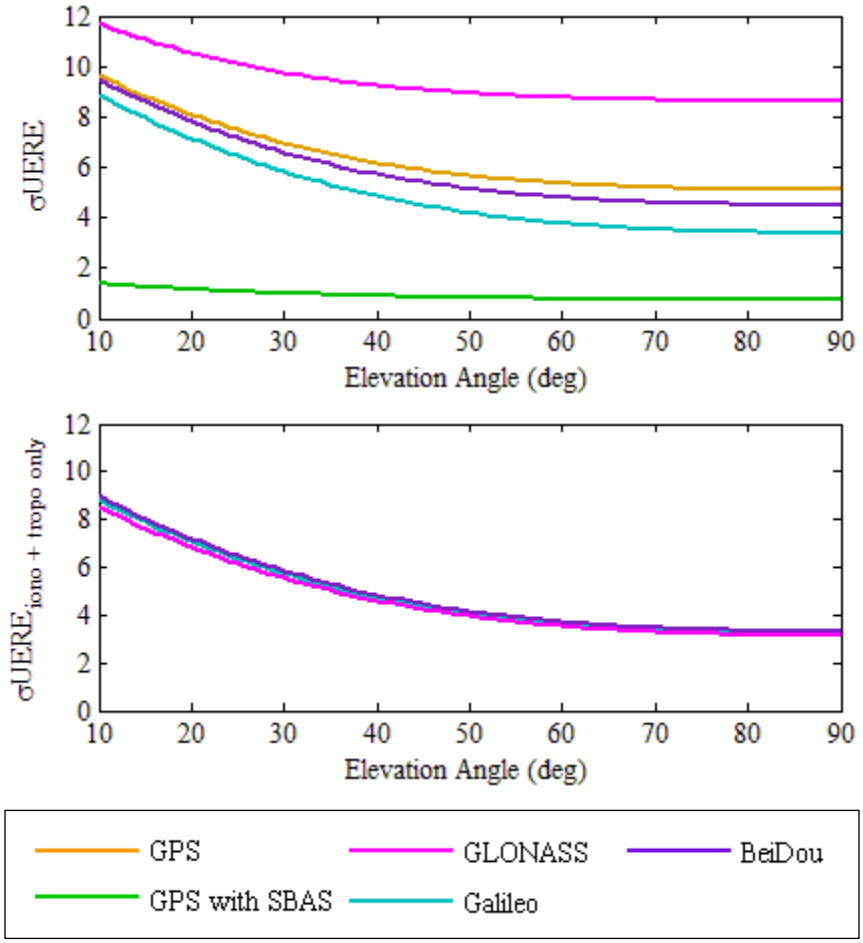

Figure 3.2: σUERE for GPS, GPS with SBAS correction, GLONASS, Galileo and BeiDou (top) and σUERE ionospheric and tropospheric only for GPS, GLONASS, Galileo and BeiDou (bottom)

The simulation scenarios have been discussed and the model parameters have been explained. The simulation results for each scenario using these model parameters are presented in the following sections.

3.3 Positioning Reliability When Using GPS and GLONASS with SBAS Corrections

In order to improve integrity and accuracy of GNSS signals, SBAS corrections can be applied to GNSS signals to reduce the effect of atmospheric errors, however not all SBAS currently support all GNSS. To test the effects of using an SBAS that does not provide corrections for all available GNSS, this section examines the MDB and protection levels when position solutions are computed using signals from combined GPS and GLONASS satellites with SBAS corrections applied to only GPS measurements. In this subsection, the system clock-offsets are estimated at the receiver at each epoch.

Average number of satellites in view and percentage of time when position and FDE are unavailable are shown in Figure 3.3. Covariance simulations are carried out to examine MDB, HPL and VPL when using measurements from GPS and GLONASS satellites with and without SBAS corrections; the results are shown in Figure 3.4 to Figure 3.6.

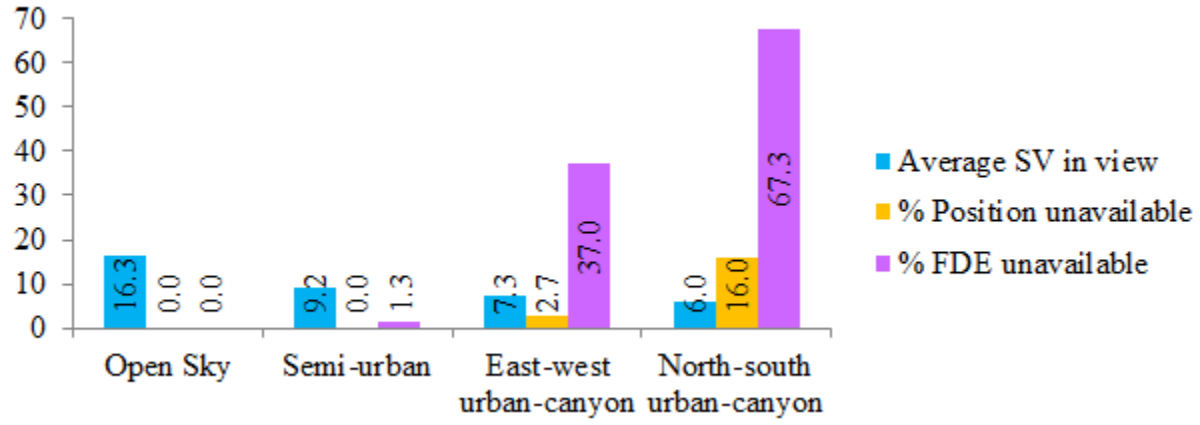

Figure 3.3: Average number of satellites (SV) in view and percentage of time when position solution and FDE are unavailable when using signals from GPS and GLONASS satellites in various environments

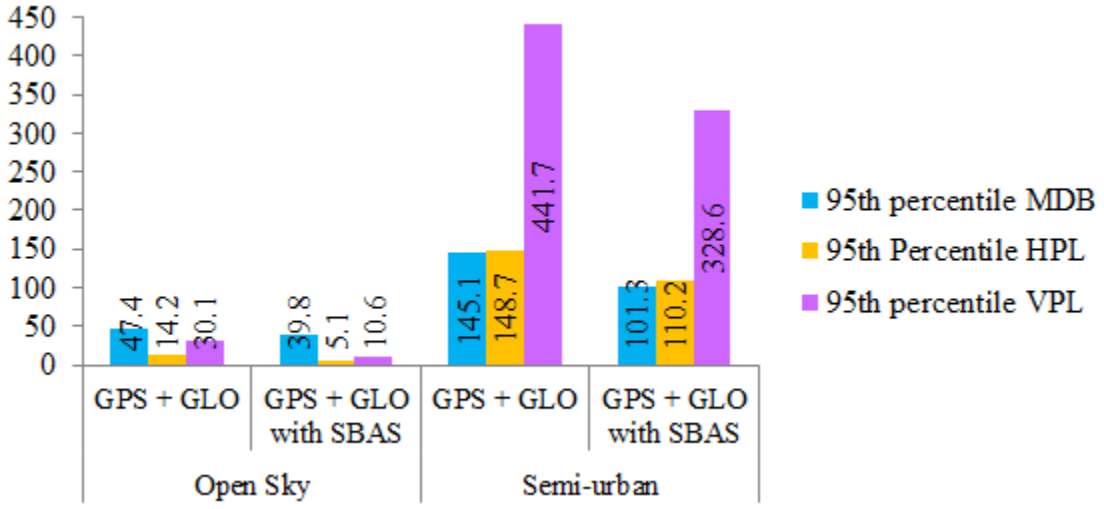

Figure 3.4: 95th Percentile MDB (m) and PLs (m) when using measurements from GPS and GLONASS satellites without and with SBAS corrections applied to GPS measurements (the inter-system clock-offsets are estimated at the receiver at each epoch)

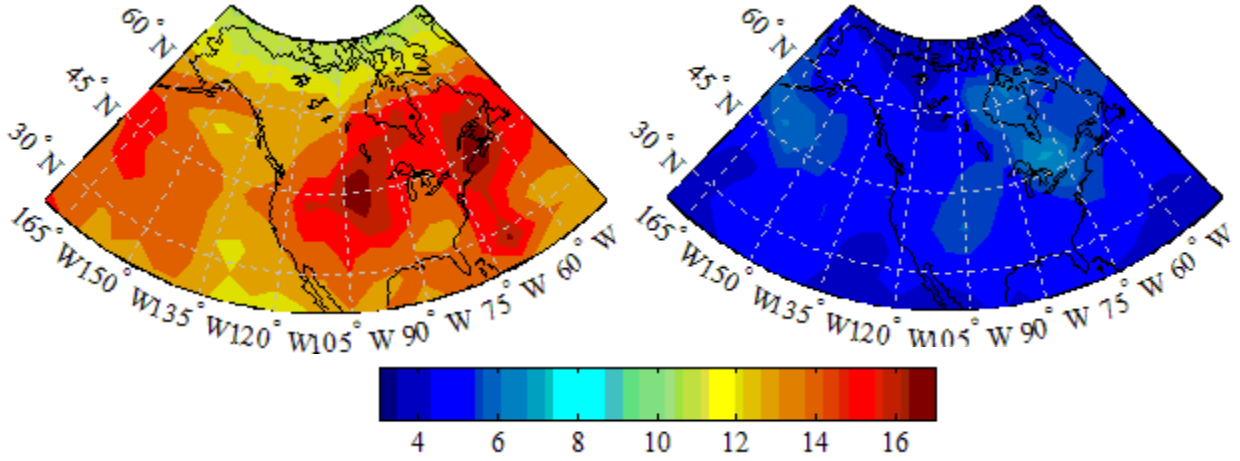

Figure 3.5: 95th Percentile HPL (m) when using signals from combined GPS and GLONASS constellations when SBAS corrections are not applied (left) and are applied (right) to GPS measurements in open sky environment (the inter-system clock-offsets are estimated at the receiver at each epoch)

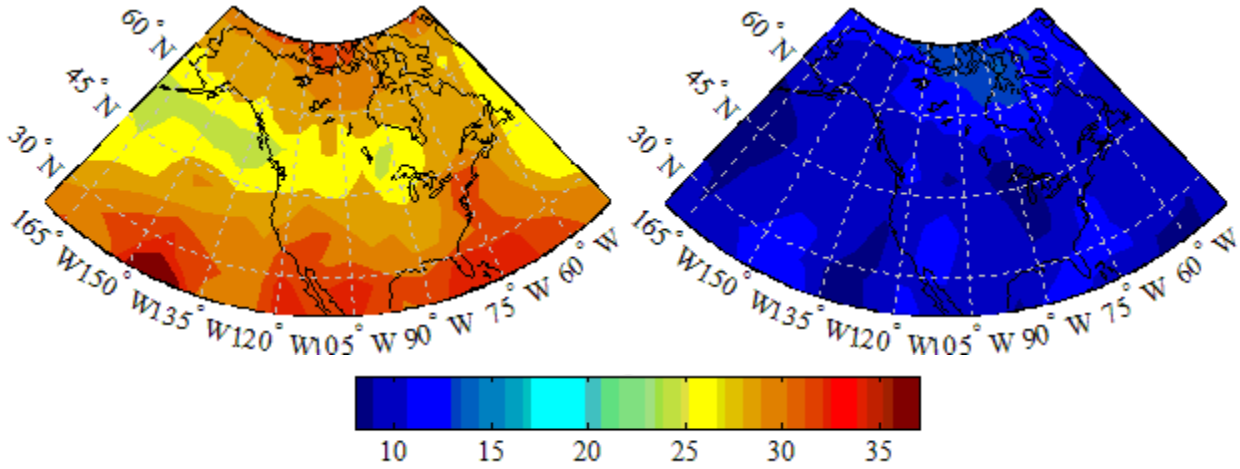

Figure 3.6: 95th Percentile VPL (m) when using signals from combined GPS and GLONASS constellations when SBAS corrections are not applied (left) and are applied (right) to GPS measurements in open sky environment (the inter-system clock-offsets are estimated at the receiver at each epoch)

When using signals from GPS and GLONASS constellations, the GNSS user in the open sky environment can be expected to see, on the average, 16 satellites in view which allows position solution and FDE to be available at all times. This situation is illustrated in Figure 3.3. When the user is in the semi-urban environment, however, the average number of satellites in view reduces to 9 leading to FDE unavailability of just above 1% of the time. The situation becomes more challenging when the receiver is located in an urban-canyon. When using the combined GPS and GLONASS constellations, on average, only 7 and 6 satellites are visible to the users in the east-west and north-south running urban-canyons respectively. This leads to the FDE unavailability of 37% in the east-west running urban-canyon and 67% in the north-south running urban-canyon.

The performance of the combined GPS and GLONASS constellations, with and without applying SBAS corrections to GPS measurements, is then evaluated and the results are shown in Figure 3.4. When SBAS corrections are applied to GPS measurements, the reduction in MDB and PLs are evident in both the open sky and semi-urban environments. For the open sky scenario, without SBAS corrections, the position solutions obtained from GPS and GLONASS measurements has 95^{th} percentile MDB of 47 m. With SBAS corrections, the 95^{th} percentile MDB reduces to below 40 m. As a result of the improvement in MDB, the 95^{th} percentile value of HPL improves from 14 m to 5 m and the 95^{th} percentile VPL improves from 30 m to 11 m.

The performance of the combined GPS and GLONASS constellations, with and without SBAS corrections, in the open sky environment is examined in detail and shown in Figure 3.5 and Figure 3.6. When using SBAS corrections, the 95^{th} percentile HPL improves from above 10 m to lower than 7 m in most of the locations. More significant improvement is in the vertical

protection level. With SBAS corrections, the 95th percentile VPL improves from above 24 m to lower than 14 m in most of the locations.

In the semi-urban environment, without SBAS corrections applied to GPS measurements, position solution obtained from the combined GPS and GLONASS constellations has a 95th percentile MDB of 145 m as shown in Figure 3.4. When applying SBAS corrections to GPS measurements, the 95th percentile MDB reduces to about 100 m. As a result of the improvement in MDB, the 95th percentile value of HPL reduces from almost 150 m to 110 m and the 95th percentile VPL improves from over 440 m to lower than 330 m.

Although the results reveal that when SBAS corrections are applied to GPS measurements the results are improvements in MDB and PLs in both the open sky and semi-urban environments, it must be noted, however, that users in urban-canyon environments will face a challenge of limited GNSS observations due to signals blockage. As demonstrated in Figure 3.3, when the receiver is located in the north-south or east-west running urban-canyons, with signals from two constellations, users can be expected to see on average only 7 and 6 satellites in these environments respectively. With the combined GPS and GLONASS constellations, it is expected that the number of satellites are not sufficient to perform fault detection and exclusion 67% of the time in the north-south running urban-canyon. This situation motivates the need for additional ranging sources from new constellations.

3.4 Performance of GPS, GLONASS, BeiDou and Galileo Constellations

As all planned signals from the BeiDou and Galileo constellations are not yet available, it is of interest to assess, through simulations, the benefit the users would achieve when using measurements from GPS and GLONASS satellites together with additional ranging signals from partial BeiDou and Galileo constellations. This subsection investigates the availability, MDB and PLs of position solutions in challenging signal environments when using measurements from GPS, GLONASS, BeiDou and Galileo constellations when the inter-system clock-offsets are estimated at the receiver at each epoch. The average numbers of satellites in view in the semi-urban and urban-canyon environments when using signals from the combined GPS and GLONASS systems with various combinations of additional signals from the Galileo and BeiDou systems are shown in Figure 3.7.

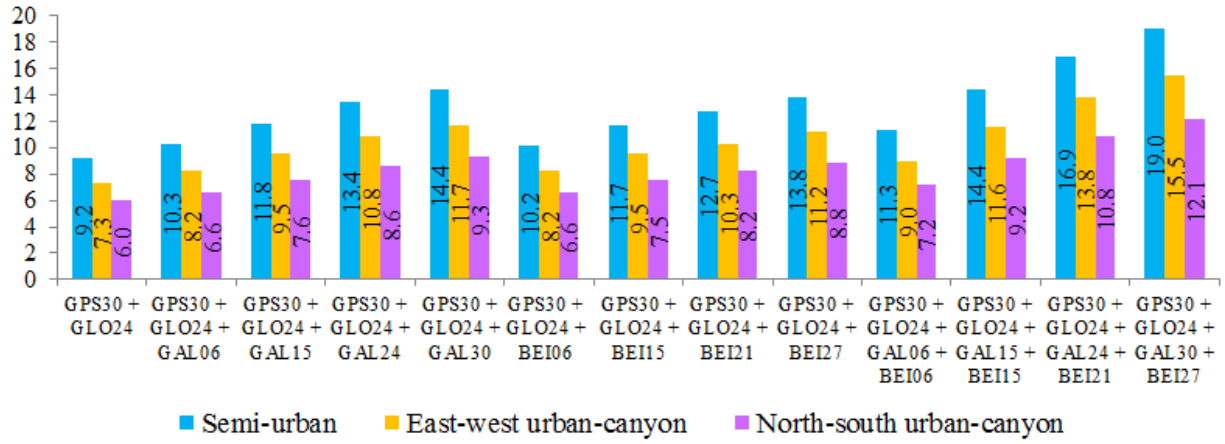

Figure 3.7: Average number of satellites in view

It can be seen that, for the semi-urban scenario, the average number of satellites in view ranges from 9 with the combined GPS and GLONASS constellations to 19 with the complete four GNSS constellations. For the urban-canyon environments, the east-west urban-canyon offers more visibility satellites on the average compared to the north-south urban-canyon. If the signals from GPS and GLONASS are used when the receiver is placed in the north-south running urban-canyon environment, the GNSS users can expect to see on average only 6 satellites. This number is expected to improve up to 12 satellites when all four GNSS constellations are completely operational. The results indicate that the improvement in number of ranging sources would particularly benefit GNSS users in signal challenging locations where position solution would otherwise not at all be possible using only GPS and GLONASS signals.

The dilutions of precision for the semi-urban scenario using satellites from various combinations of constellations are shown in Figure 3.8. The average east and north DOPs are expected to reduce by half when the signals from all the four GNSS constellations become available compared to when using range measurements from only GPS and GLONASS satellites. With the signals from all four GNSS constellations, the average VDOP is expected to improve from 6 to less than 3. When using signals from the combined GPS and GLONASS systems with either full-constellation BeiDou or Galileo in the semi-urban environment, the user can expect average EDOP and NDOP to be about 1 and average VDOP to be less than 4.

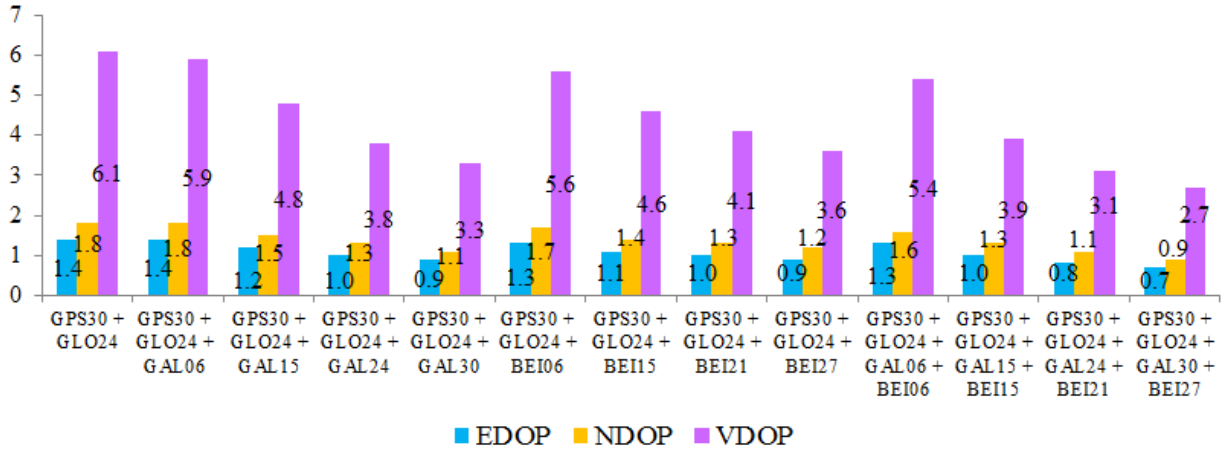

Figure 3.8: Average DOPs for semi-urban environment when the inter-system clock-offsets are estimated at the receiver at each epoch

The reliability performance of the combined GPS and GLONASS constellations with signals from partial Galileo and BeiDou in the semi-urban environment is examined in detail. The number of satellites in view, availability of the FDE and protection levels obtained from using the combined GPS and GLONASS constellations are compared with the performance of GPS and GLONASS with additional signals from 15 Galileo and 15 BeiDou satellites. The results are illustrated in Figure 3.9 to Figure 3.12.

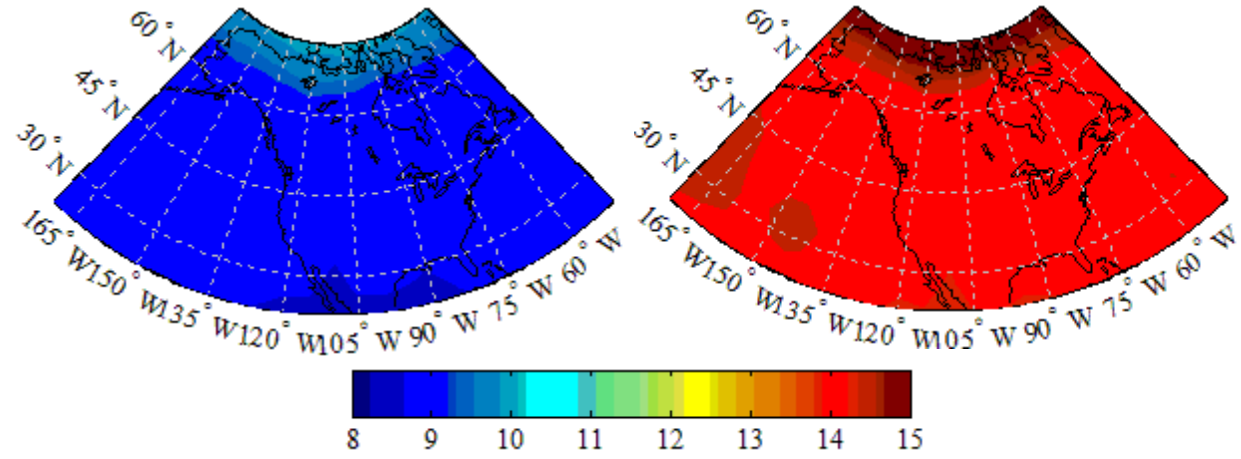

Figure 3.9: Average number of satellites in view when using signals from GPS and GLONASS (left) and when using signals from GPS, GLONASS and 15 satellites from each of the Galileo and BeiDou constellations (right) in semi-urban environment

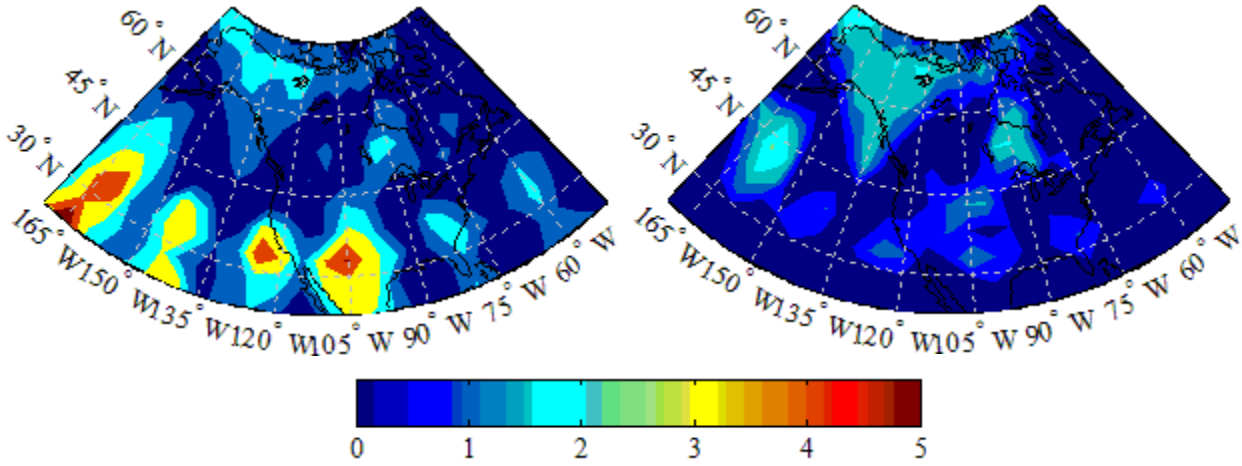

Figure 3.10: Percentage of time when FDE is unavailable in semi-urban environment when using signals from GPS and GLONASS (left) and when using signals from GPS, GLONASS and 15 satellites from each of the Galileo and BeiDou constellations (right)

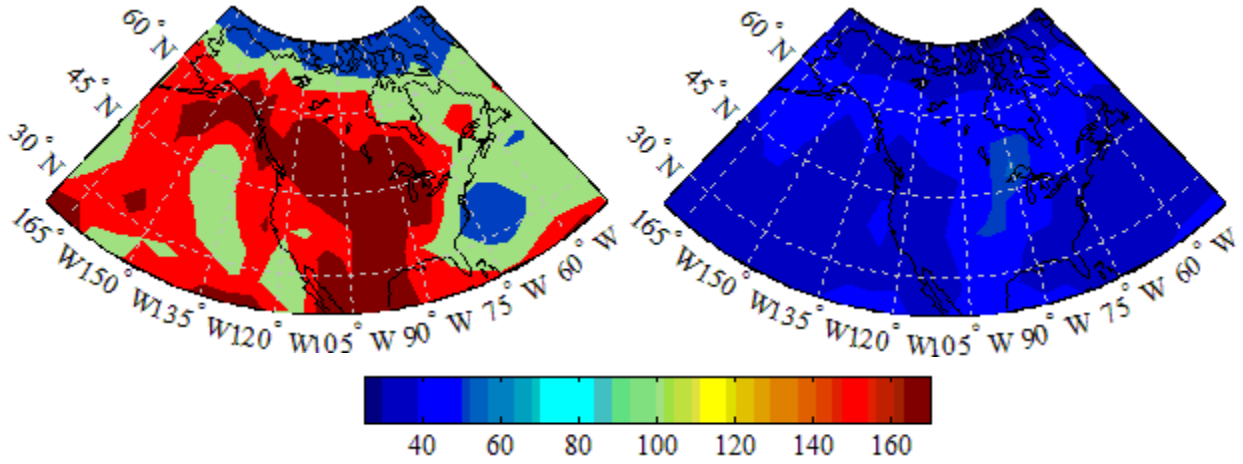

Figure 3.11: 95th Percentile HPL in semi-urban environment when using signals from GPS and GLONASS (left) and when using signals from GPS, GLONASS and 15 satellites from each of the Galileo and BeiDou constellations (right), the inter-system clock-offsets are estimated at the receiver at each epoch

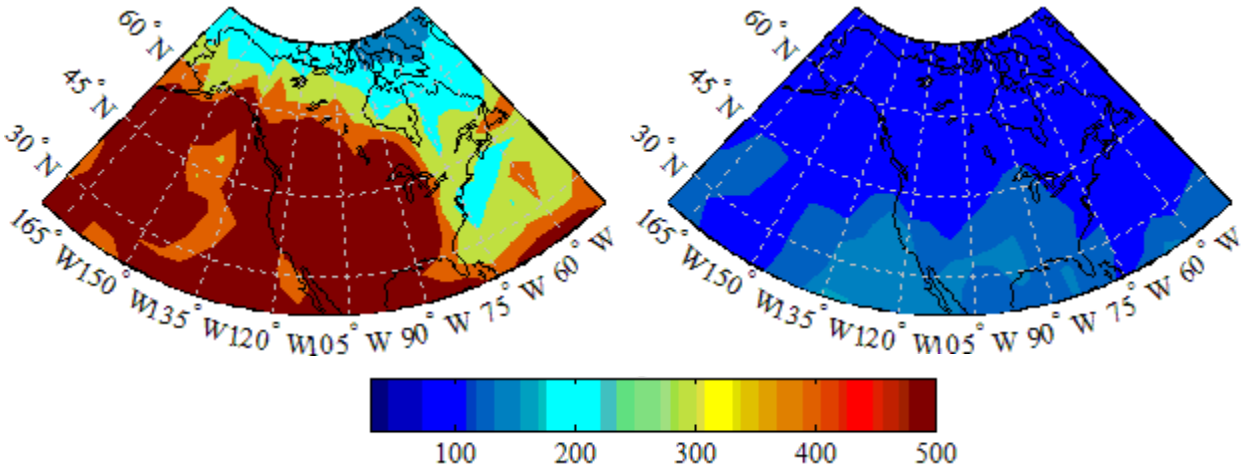

Figure 3.12: 95th Percentile VPL in semi-urban environment when using measurements from GPS and GLONASS (left) and when using signals from GPS, GLONASS and 15 satellites from each of the Galileo and BeiDou constellations (right), the inter-system clock-offsets are estimated at the receiver at each epoch

When the inter-system time-offsets are estimated at the receiver level at each epoch, with an average of at least 8 satellites in view in all study locations in the semi-urban environment, the position solution is always available. This is also the case even when range measurements from only GPS and GLONASS are used. It can be noted in Figure 3.10, in the semi-urban environment, FDE is unavailable less than 5% of the time in most locations when the ranging signals from the combined GPS and GLONASS constellations are used. The value reduces to less than 2% in most locations when measurements from partial Galileo and BeiDou constellations are available. These percentages of unavailability are considered small for most applications.

Significant improvements as a result of the increase in the number of ranging sources are evident in the HPL and VPL as shown in Figure 3.11 and Figure 3.12 respectively. With 15 additional satellites from each of the Galileo and BeiDou systems, the 95^{th} percentile HPL reduces from 90 m or greater to less than 50 m in most of the simulation locations. The 95^{th} percentile VPL also improves from 200 m or higher to less than 130 m in most of the study areas when signals from partial Galileo and BeiDou constellations are used.

The availability of FDE and the 95^{th} percentile MDB and PLs in the semi-urban environment when using signals from GPS, GLONASS, Galileo and BeiDou are investigated. The corresponding results are shown in Figure 3.13 and Figure 3.14.

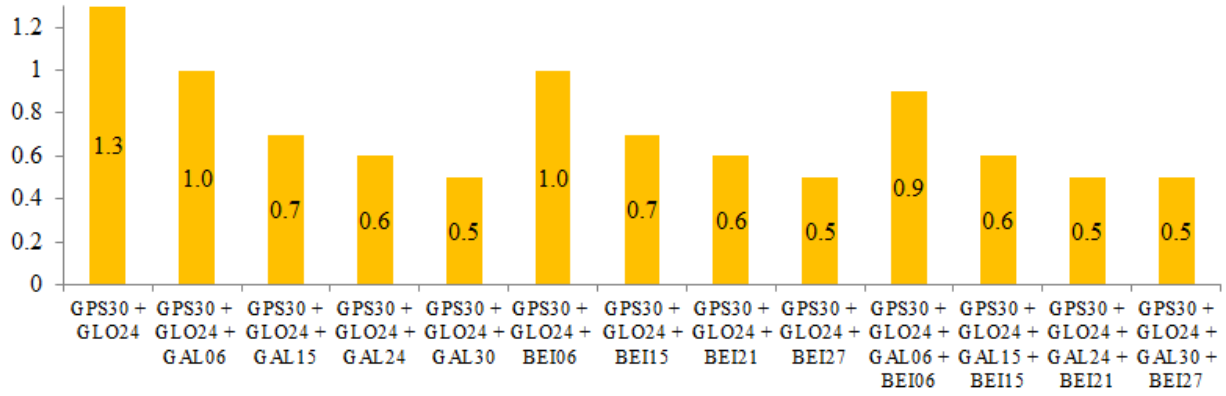

Figure 3.13: Percentage of time when FDE unavailable in semi-urban scenario (position is always available in this scenario)

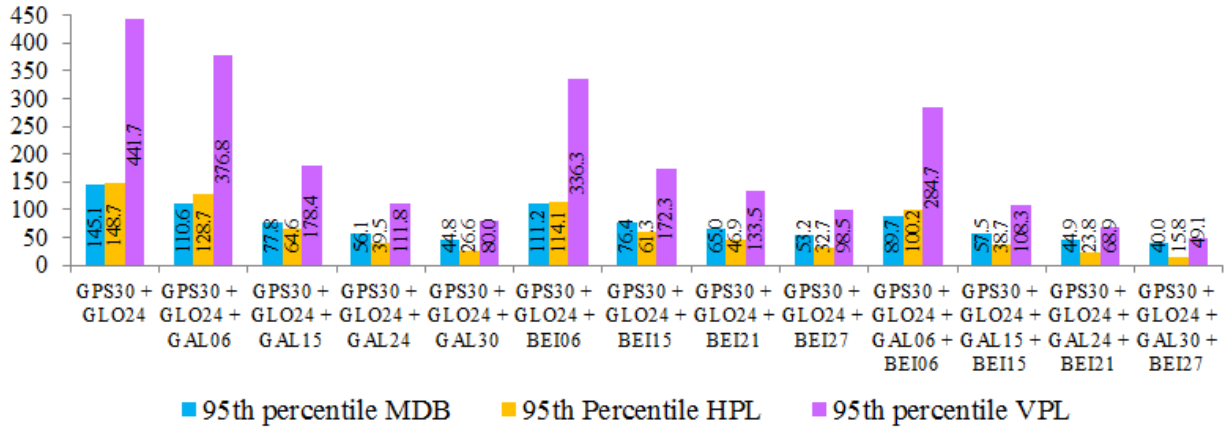

Figure 3.14: 95th Percentile MDB and PLs in semi-urban scenario (the inter-system clock-offsets are estimated at the receiver at each epoch)

Figure 3.13 shows that, in the semi-urban environment, the percentage of FDE unavailability reduces from 1.3% when using range measurements from GPS and GLONASS constellations down to 0.5% when using signals from the combined GPS and GLONASS together with measurements from either complete Galileo or BeiDou constellations. Significant improvements in MDB and PLs are observed with additional ranging sources. When using signals from the

combined GPS and GLONASS systems with additional measurements from either full-constellation Galileo or BeiDou the GNSS users in the semi-urban environment can expect the 95th percentile MDB to reduce to about one-third of its value when using only GPS and GLONASS signals. It is evident from Figure 3.14 that 95th percentile of the HPL and VPL reduce to about one-fourth of their value when complete constellation from either Galileo or BeiDou becomes available. With four complete GNSS constellations, the 95th percentile MDB is expected to improve from 145 m to 40 m. The corresponding 95th percentile HPL is expected to reduce from 149 m with GPS and GLONASS down to 16 m. Similarly, the VPL is expected to reduce from 442 m to 49 m.

Traditionally SBAS signals are used to provide corrections to GPS measurements thereby improving reliability. It is of interest to compare the improvement in protection levels achievable from applying SBAS corrections to GPS measurements to the improvement achievable by using additional ranging sources from the new constellations. To this end, Figure 3.15 shows the protection levels obtained for a selection of combinations of multiple GNSS constellations and PLs obtained when using signals from GPS and GALILEO constellations with SBAS corrections applied to GPS measurements.

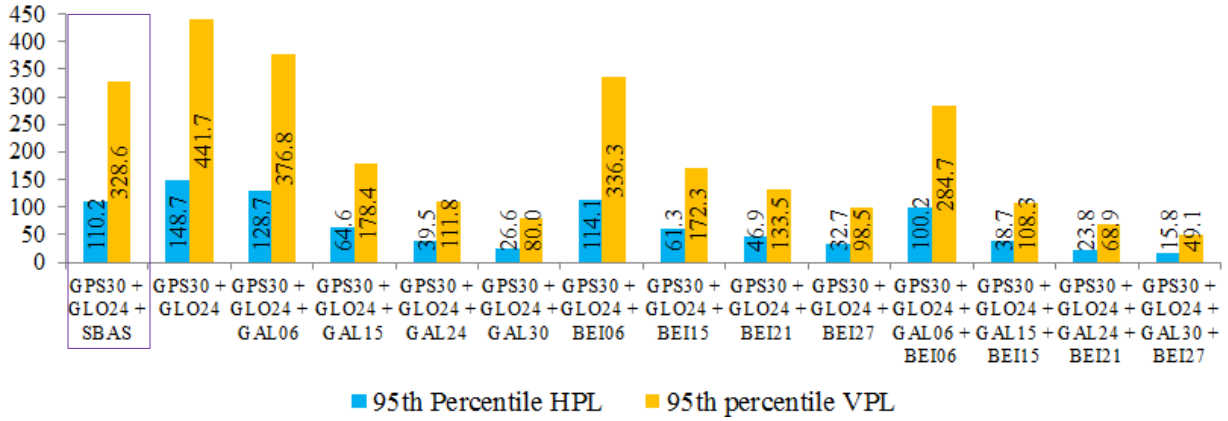

Figure 3.15: 95th Percentile PLs when using GPS and GLONASS with SBAS corrections applied to GPS measurements (purple box) and when using signals from GPS, GLONASS, BeiDou and Galileo in semi-urban environment (the inter-system clock-offsets are estimated at the receiver at each epoch)

Figure 3.15 shows that the improvement in 95th percentile HPL and VPL as a result of using signals from GPS and GLONASS with SBAS corrections is similar to the performance achieved using signals from GPS, GLONASS and 6 additional measurements from either Galileo or BeiDou constellations. It must be noted that in this simulation SBAS corrections are assumed to be applied to GPS measurements in all locations over the region of interest which is the North American region. Currently, however, WAAS which provides corrections to GPS measurements over the North America region does not have coverage over a large part of north-eastern region. The performance of the partial constellations, on the other hand, would also depend on the order of placement and orbital planes of the new operational satellites in each constellation.

In addition to the open sky and semi-urban environments, the multi-constellation GNSS performance in urban-canyons was also investigated in detail. It is revealed in Figure 3.7 that the

north-south running urban-canyon see the least number of satellites in view on the average, hence this scenario is the most challenging environment for GNSS receivers. The system availability, the 95th percentile MDB and the 95th percentile PLs when using measurements from the combined GPS and GLONASS systems with additional signals from Galileo and BeiDou constellations for receiver located in this this environment are shown in Figure 3.16 and Figure 3.17.

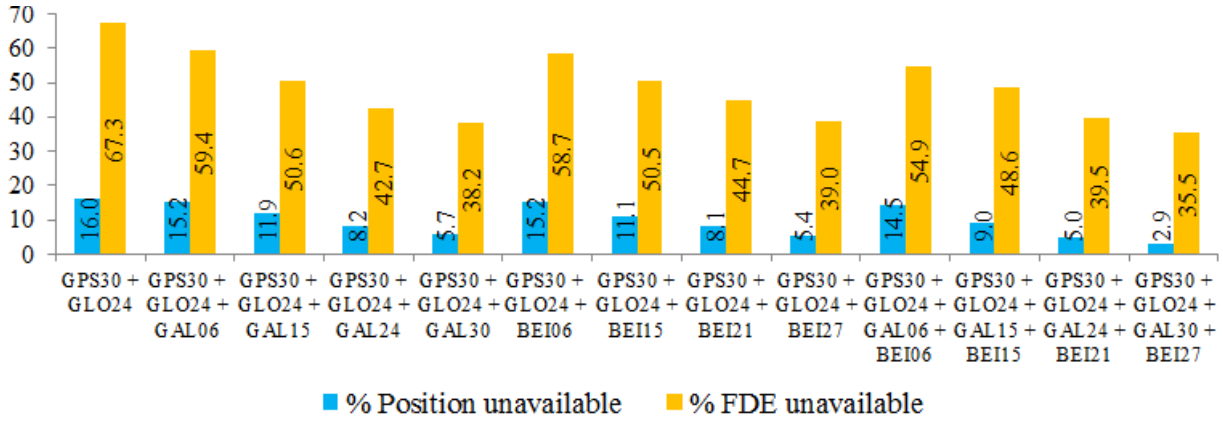

Figure 3.16: Percentage of time when position and FDE are unavailable in north-south running urban-canyon scenario

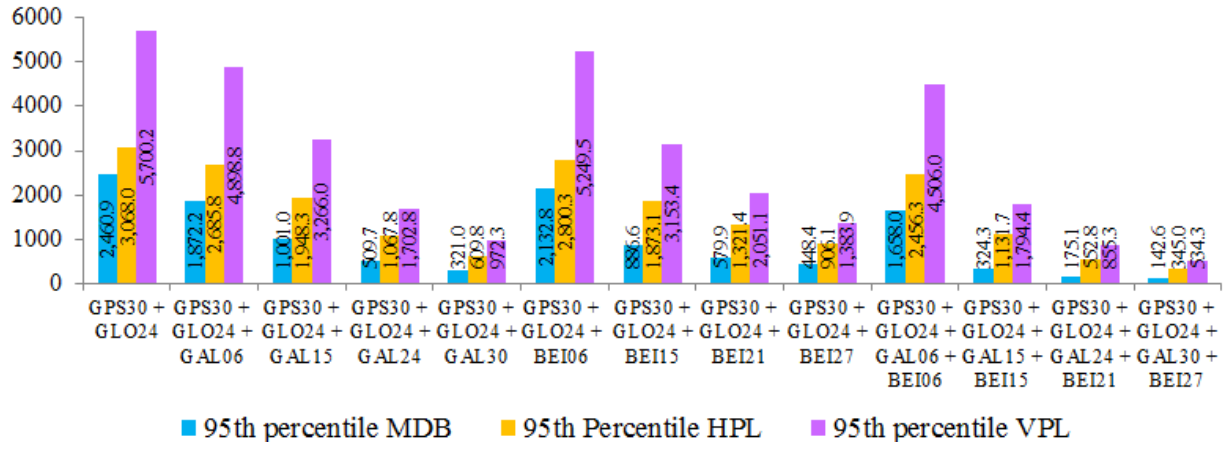

Figure 3.17: 95th Percentile MDB and PLs in north-south running urban-canyon (the inter-system clock-offsets are estimated at the receiver at each epoch)

Comparing the availability of FDE in the semi-urban environment (Figure 3.13) and in the north-south running urban-canyon environment (Figure 3.16), it is evidenced that the availability of FDE significantly drops when the receiver is placed in the urban-canyon environment.

In the north-south running urban-canyon, without the use of a priori clock-offset constraints, the FDE is unavailable almost 70% of the time when using signals from the combined GPS and GLONASS systems. This improves to 35%, which still considered high, when all the four GNSS constellations are in use. The high percentage of FDE unavailability, even with signal from four GNSS constellations, is due to the fact that without a priori receiver-GNSS system time-offset constraints, at least 3 satellites from each constellation are required to achieve fault detection and exclusion.

Significant increase in MDB and PLs in the urban-canyon environment (Figure 3.17) compared to the semi-urban environment (Figure 3.14) can also be observed. When using ranging signals from the combined GPS and GLONASS constellations in the north-south running urban-canyon, the 95^{th} percentile MDB well exceeds 2,000 m which results in a very high 95^{th} percentile HPL of over 3,000 m and a very high 95^{th} percentile VPL of over 5,000 m. When all the signals from four GNSS constellations become available, the 95^{th} percentile MDB, HPL and VPL are expected to be improved to approximately 140, 350 and 530 m respectively which is still considered large.

The high percentage of time when FDE is unavailable and the large MDB and PLs values in the urban-canyon environment demonstrates the need for the receiver to incorporate inter-system

clock-offsets as a priori knowledge if a reliable position solution is to be achieved in challenging GNSS signal environments. The performance improvements achievable via a priori system clock-offsets are detailed in the next section.

3.5 Availability and Reliability Performance of Multiple GNSS Constellations with a Priori Inter-system Clock-offset Constraints

Although various GNSS constellations rely on their proprietary methods for timing and synchronisation, fundamentally all systems follow International Systems of units (SI) for representation of the time. This has an interesting implication that the fundamental unit of time is still the same in all systems. However, there might be a constant or slow-time-varying offsets across the systems. These offsets can be monitored and made available to the multi-constellation GNSS receiver via network links. This section explains how these inter-system time-offsets can be utilised to provide improved GNSS availability and reliability performance.

During the normal operation of a multi-constellation GNSS receiver, the inter-system time-offsets needs to be estimated as state variables in the position solution. This requires j additional measurements for j constellations. However, when the inter-system time-offsets are available (either broadcast from GNSS or by having the receiver initially estimate the offsets at an earlier epoch with better satellite availability for the use at later epochs), they can be used as additional constraints (or pseudo-observations) in the position estimation algorithm thus reducing the number of pseudorange measurements required to obtain a position solution. As a result, the availability and fault detection and exclusion capability is enhanced. The reliability performance of the combined GPS and GLONASS constellations with additional signals from BeiDou and

Galileo systems when using a priori inter-system clock-offsets is investigated in this following. The percentage of time when position solution and FDE are unavailable and the 95th percentile protection levels when using signals from the four GNSS constellations in the north-south running urban-canyon scenario are shown in Figure 3.18 to Figure 3.21.

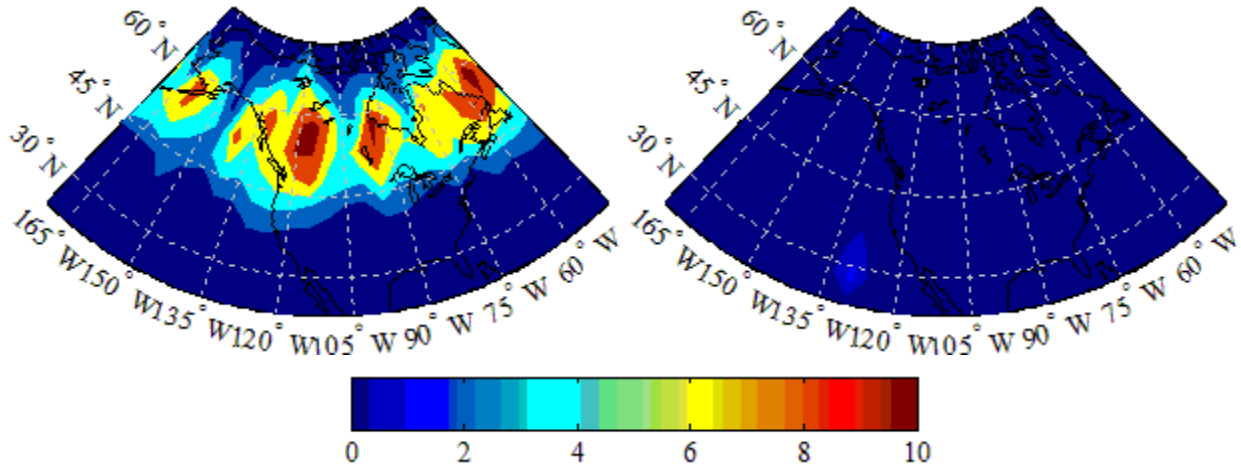

Figure 3.18: Percentage of time when position solution is unavailable in north-south running urban-canyon when using signals from four-constellation without (left) and with (right) a priori clock-offset constraints

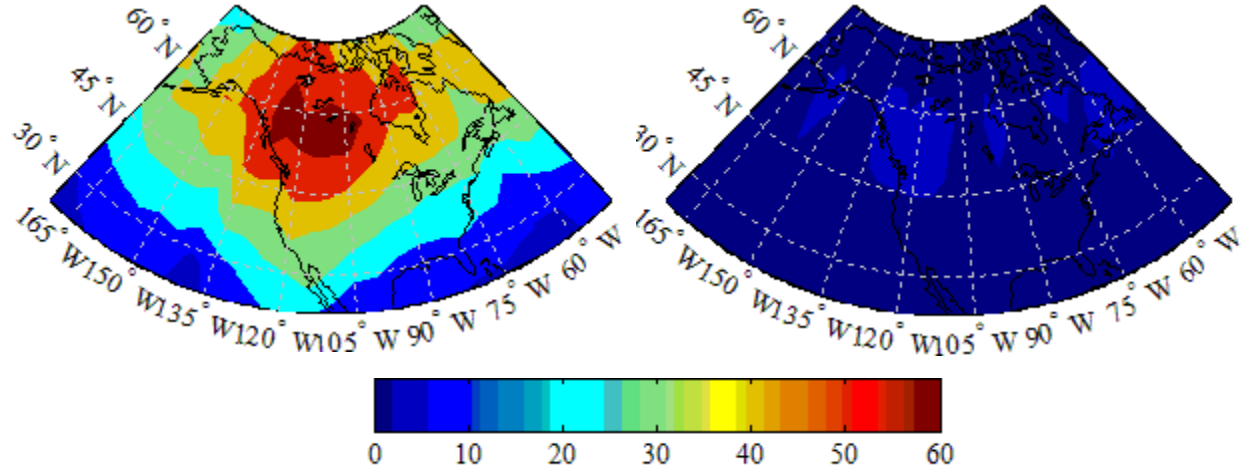

Figure 3.19: Percentage of time when FDE is unavailable in north-south running urban-canyon when using signals from four-constellation without (left) and with (right) a priori clock-offset constraints

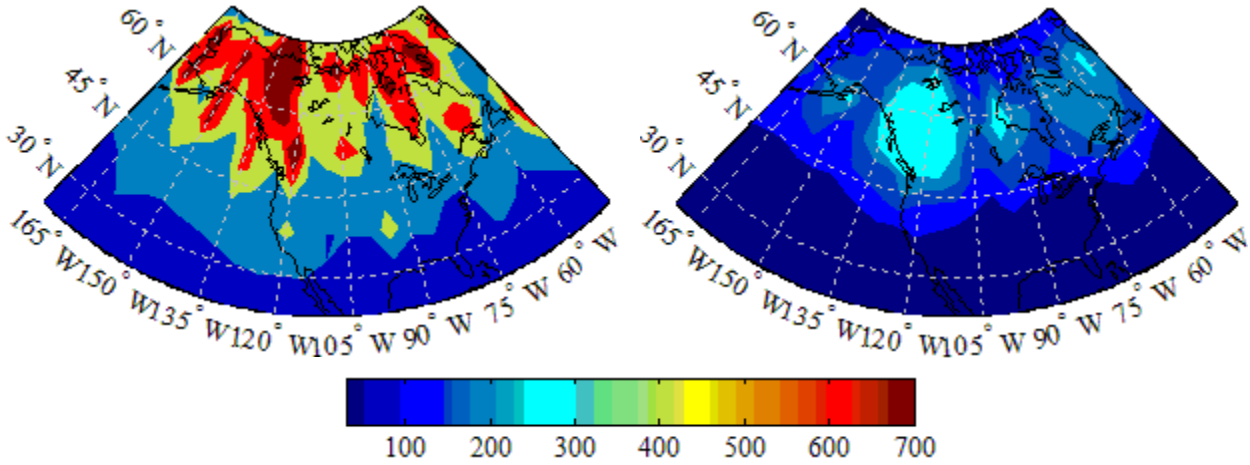

Figure 3.20: 95th Percentile HPL in north-south running urban-canyon when using signals from four-constellation without (left) and with (right) a priori clock-offset constraints

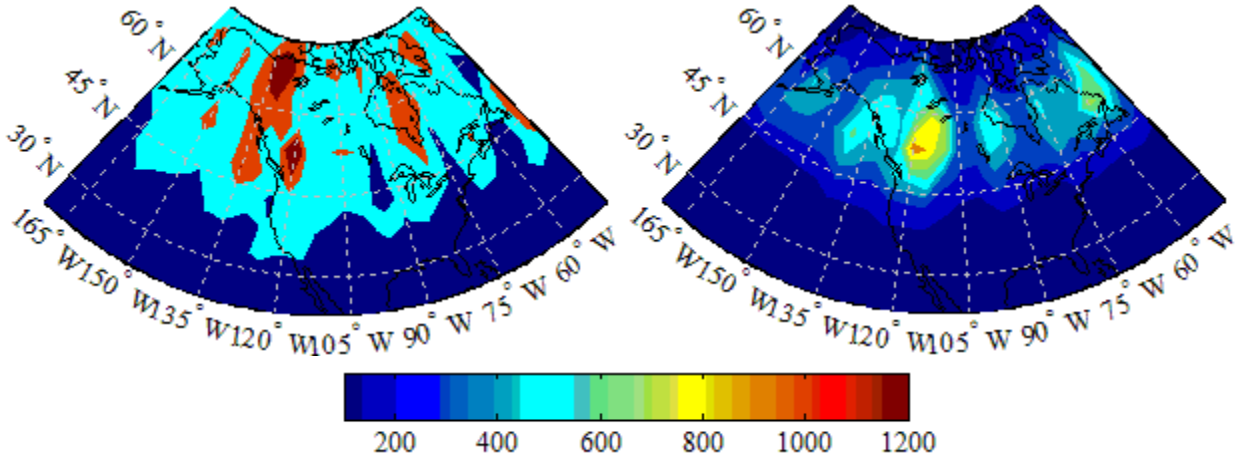

Figure 3.21: 95th Percentile VPL in north-south running urban-canyon when using signals from four-constellation without (left) and with (right) a priori clock-offset constraints

For the north-south running urban-canyon scenario, when using signals from the four GNSS constellations without the use of a priori inter-system clock-offsets, the position solution is unavailable up to about 10% in some locations as demonstrated in Figure 3.18. When using a priori inter-system clock-offsets, the percentage of time when position solution is unavailable reduces to below 2% in all locations. Similar improvements are also observed in the availability of FDE as illustrated in Figure 3.19. The percentage of time when FDE is unavailable improves from over 50% in some locations to less than 5% in all study locations, which is primarily the result of a reduction in number of minimum number of satellites required, when using a priori inter-system clock-offsets.

The improvement in the 95th percentile HPL as a result of the use of a priori inter-system clock-offsets is evidenced in Figure 3.20. Without the use of a priori clock-offsets, large areas with high 95th percentile HPL exceeding 500 m are observed. When a priori clock-offsets are used,

the 95th percentile HPL improves to below 360 m in all locations. Improvements also evidence in the 95th percentile VPL as demonstrate in Figure 3.21. Without the use of a priori inter-system clock-offsets, most of the locations has 95th percentile VPL of 500 m or greater with some areas have very high 95th percentile VPL exceed 1,000 m. This value improves to within 1,000 m in all study locations when using a priori inter-system clock-offsets with majority of the locations having 95th percentile VPL less than 400 m.

The effect of a priori clock-offsets on the percentage of time when position solution and FDE are unavailable in the semi-urban and in the north-south running urban-canyon is examined in the following. In the semi-urban environment, when using a priori clock-offset constraints, the position solution and FDE are always available even when signals from only GPS and GLONASS constellations are used. This is not the case, however, without the use of a priori clock-offset constraints as demonstrated in Figure 3.13 when the FDE is unavailable 1.3% of the time when using signals from the combined GPS and GLONASS constellations. Also, in this case FDE is unavailable 0.5% of the time even when signals from at least three GNSS constellations are available.

The reduction in 95th percentile MDB and PLs in the semi-urban environment when using a priori inter-system clock-offset constraints is also observed from scenarios with various satellites combinations. With signals from the four full GNSS constellations, the 95th percentile MDB improves from 40 m when not using a priori clock-offset constraints (Figure 3.14) to 37 m when using a priori clock-offset constraints (Figure 3.22) and the corresponding 95th percentile HPL and VPL reduces from 16 m and 49 m down to 14 m and 42 m respectively when using a priori

clock-offset constraints. More significant improvements are observed when the receiver uses signals from a limited number of satellites. When using signals from GPS and GLONASS satellites only, in the semi-urban environment, the use of an a priori inter-system clock-offset results in a reduction in the 95th percentile MDB from 145 m to 91 m. The 95th percentile PLs also reduces by about 50 % of what would be achievable without the use of a priori clock-offset constraints.

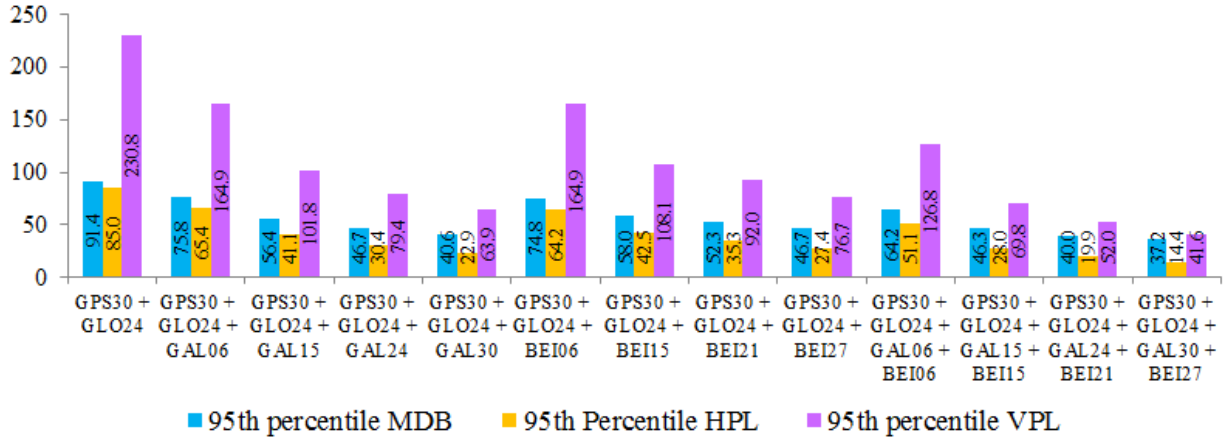

Figure 3.22: 95th Percentile MDB and PLs in semi-urban when using a priori clock-offset constraints

The benefit of using an inter-system broadcast time-offset as a measurement is particularly clear when the receiver is located in areas where the signals from GNSS satellites are limited such as in an urban-canyon. Referring to the results presented in Figure 3.16, even with the complete four GNSS constellations the FDE is unavailable 35% of the time without using a priori clock-offset constraints in the north-south running urban-canyon. With the use of a priori clock-offset

constraints, however, the percentage of time when FDE is unavailable reduces to below 1% and the position solution is always available (Figure 3.23).

Although when the signals from the four full GNSS constellations are available, only marginal improvements in protection levels can be obtained when using a priori clock-offset in the semi-urban environment; this is, however, not the case when receiver is located in the urban-canyon with a very limited number of satellites in view. Comparing the 95th percentile PLs in the north-south running urban-canyon without the use of a priori clock-offsets for the four GNSS constellation scenario (Figure 3.17) to the result when using a priori clock-offsets (Figure 3.24), it is evidenced that the sizes of the 95th percentile HPL and VPL are reduced by more than 50 % when using a priori inter-system clock-offsets. As evidenced in these two figures, the protection levels for all other satellites combinations also shows significant improvements with a priori clock-offset constraints in the urban-canyon environment.

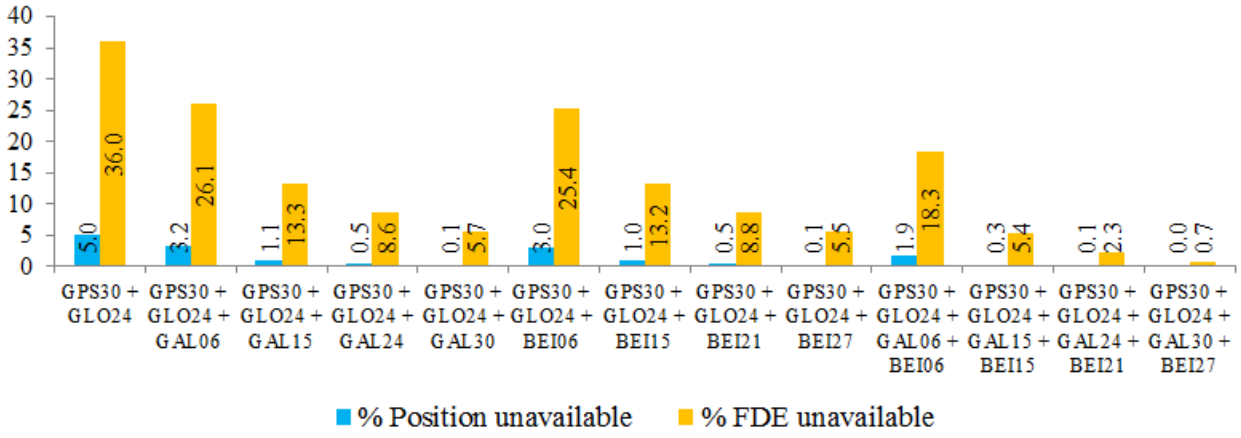

Figure 3.23: Percentage of time when position and FDE are unavailable in north-south running urban-canyon scenario when using a priori clock-offset constraints

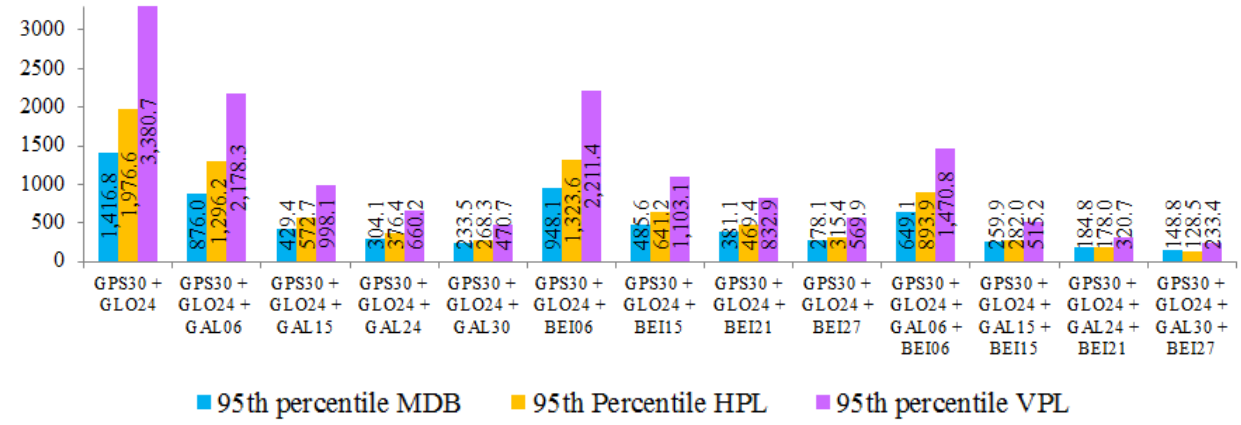

Figure 3.24: 95th Percentile MDB and PLs in north-south running urban-canyon when using a priori clock-offset constraints

3.6 The Use of a Priori Inter-system Clock-offsets with Different Accuracies

It must be noted that the improvements achievable via a priori clock-offset constraints also depend on the accuracy of the constraints themselves. This subsection expands the analysis for various accuracies of the clock-offset constraints. The protection levels obtained from the four GNSS constellations without a priori clock-offsets and with a priori clock-offsets with accuracies of 9, 3 and 0.75 m are compared and the results are shown in Figure 3.25. Protection levels when the receiver is located in the semi-urban and the urban-canyon environments are examined in this figure.

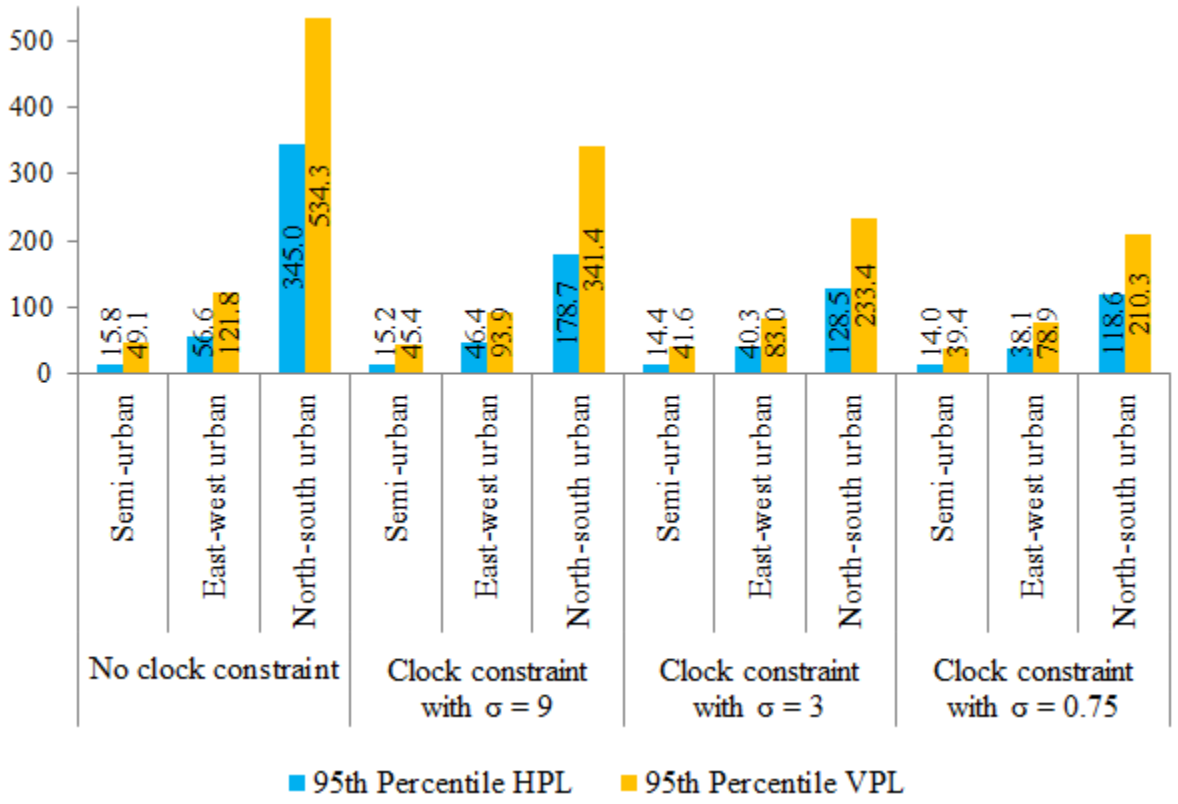

Figure 3.25: 95th Percentile HPL and VPL when using signals from four-constellations without and with a priori clock-offset constraints with accuracies of 9, 3 and 0.75 m

Figure 3.25 shows improvements in PL values even when using a priori clock-offsets with accuracy of 9 m compared to when a priori clock-offset is not used at all. The HPL improves from 345 m when not using a priori clock-offset constraints in the north-south running urban-canyon down to 179 m when using a priori clock-offset constraints with accuracy of 9 m. This value further reduces to 129 m and 119 m when using a priori clock-offsets with accuracy of 3 m and 0.75 m respectively. As revealed in the same figure, the value of VPL also showed similar improvements. The VPL improves from 534 m when not using a priori clock-offset constraints down to 341 m when using a priori clock-offset constraints with accuracy of 9 m. This value

further improves to 233 m and 210 m with the a priori clock-offset constraints with accuracy of 3 m and 0.75 m respectively.

The availability and reliability of position solutions obtain from GPS, GLONASS, BeiDou and Galileo satellites with and without a priori clock-offset constraints have been examined using covariance simulation. The next step is to assess the positioning performance when using and not using a priori receiver-GNSS clock-offsets when a limited number of satellites from multiple GNSS constellations are available using live data. These analyses are carried out in the next chapter.

CHAPTER FOUR: REAL DATA PROCESSINGS AND RESULTS

In order to further demonstrate the results shown in Chapter 3, this chapter assess the positioning accuracy and blunder detection capability when using signals from a limited number of satellites from multiple GNSS constellations. This chapter is organised in five sections. Section 4.1 describes the data sets containing measurements from GPS, GLONASS, BeiDou and Galileo satellites used to compute position solutions. Section 4.2 explains data processing procedures and the software modification process in order to examine the accuracy of the position solution when using and not using a priori receiver-GNSS clock-offset constraints. Three types of analysis are performed using real data in this chapter.

Section 4.3 examines position solutions obtained from three GNSS constellations using a limited number of satellites. Solutions obtained from data processing using a priori receiver-GNSS clock-offsets are compared with positions when processed without a priori clock-offsets. The stability of the clock-offsets parameters are also examined in this section. Section 4.4 investigates the fault detection and exclusion capability when using a limited number of satellites from multiple GNSS constellations. Finally, section 4.5 explores the use of a priori clock-offsets to obtain position solutions in situations when signals from four satellites, one from each of the GPS, GLONASS, BeiDou and Galileo constellations, are available.

4.1 Data Set Descriptions

Two sets of static data were collected to examine the performance of multiple GNSS constellations with and without the use of a priori time-offsets. The data were collected in open sky environment using NovAtel GPS-703-GGG triple-frequency antenna. The first set of data was collected on 12th August 2013 and contains pseudorange and Doppler measurements from GPS, GLONASS and BeiDou, there were no healthy Galileo signals at the time of this data collection. It was assumed that a land vehicle could undergo up to 15 minutes of seeing a limited number of satellites in view (such as the case when a vehicle is driving through a dense urban-canyon) and as such the duration of this first data set was limited to approximately 20 minutes. GPS, GLONASS and BeiDou satellites with an elevation angle above 35^{o} were selected to simulate an urban-canyon environment. Details of each scenario are shown in Table 4.1 and the sky plot of these high elevation angle satellites is shown in Figure 4.1.

In order to examine position solutions obtained from combined GPS, GLONASS, BeiDou and Galileo constellations in limited signal environments, second set of data containing pseudorange and Doppler observations from all four constellations was collected on 11th September 2013. At this time, the Galileo satellites were again in service. The duration of data collection was approximately 10 minutes. Four high elevation angle satellites of at least 35^{o}, one from each of the GPS, GLONASS, BeiDou and Galileo constellations, were selected to use in the position computation. (This satellite combination is referred to as scenario 4(b) in Table 4.1.) A sky plot of the satellites in this scenario is shown in Figure 4.2.

Table 4.1: Total number of satellites (SVs) and satellites' Pseudo Random Noise (PRN) number used to compute position solutions in each scenario

Scenario Total SVs	Data Set	PRN used to compute position solutions			
		GPS	GLONASS	BeiDou	Galileo
8	12 Aug 2013	4, 12, 17	10, 11, 19	11, 12	-
7	12 Aug 2013	4, 12, 17	10, 11, 19	12	-
6(a)	12 Aug 2013	4, 12, 17	10, 11, 19	-	-
6(b)	12 Aug 2013	4, 17	11, 19	11, 12	-
4(a)	12 Aug 2013	4, 12	10	12	-
4(b)	11 Sep 2013	29	21	11	19

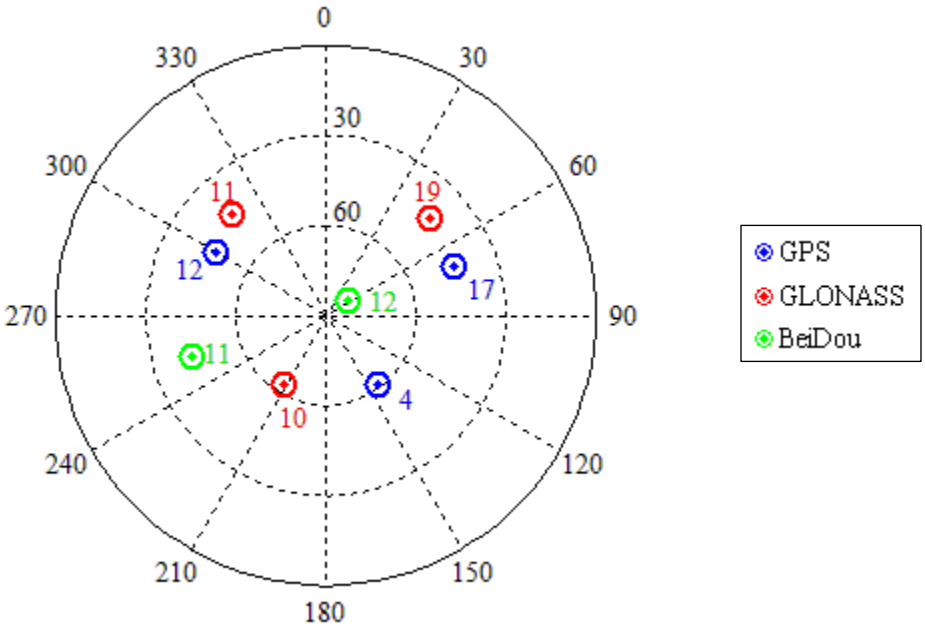

Figure 4.1: Sky plot of satellites with elevation angle above 35^{o} from data collected on 12th August 2013

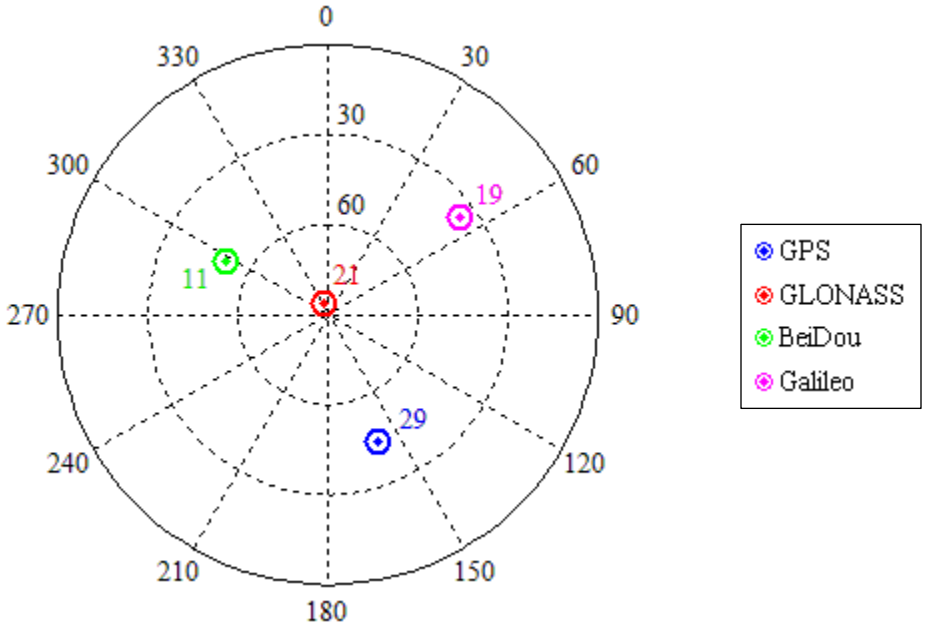

Figure 4.2: Sky plot of selected satellites with elevation angle above 35^{o}, one SV from each of the GPS, GLONASS, BeiDou and Galileo constellations. Data collected on 11th September 2013

4.2 Software Receiver and Data Processing

The intermediate frequency data was processed using the GNSS Software Navigation Receiver (GSNRx^{TM}) developed by PLAN group at the University of Calgary. The GSNRx^{TM} navigation receiver software was used to compute position solutions in standard operation when the clock-offset parameters from each system are estimated at the receiver level during each epoch along with clock drift. The software was then modified to process ranging signals when the previously estimated clock-offset parameters are used as a priori knowledge by the estimation algorithm.

When there are a limited number of satellites in view from multiple GNSS constellations, a priori receiver-GNSS clock-offsets can be used to reduce number of minimum satellites requirement. In this case, the initial clock-offset parameters for each of the satellite systems were obtained from an initial epoch's least-squares solution and are used in later epochs as a constraint (weighted by their estimated accuracy). The a priori receiver-GNSS clock-offsets for GPS, GLONASS and BeiDou used in the first data set were obtained from a total of 16 satellites (7 GPS, 7 GLONASS and 2 BeiDou satellites) at the initial epoch least-squares solution. The estimated accuracies of a priori system clock-offsets used in this data set are 18 m, 18 m and 23 m for GPS, GLONASS and BeiDou systems respectively. The a priori receiver-GNSS clock-offsets for GPS, GLONASS, BeiDou and Galileo use in the second data set were obtained from a total of 19 satellites (8 GPS, 6 GLONASS, 2 BeiDou and 3 Galileo satellites). The estimated accuracies of a priori receiver-GNSS clock-offsets obtained for this data set are 14 m, 17 m, 18 m and 18 m for GPS, GLONASS, BeiDou and Galileo systems respectively.

The position solution algorithm assumed a single common clock drift among all GNSS systems. When an a priori clock-offset is used, the clock drift parameter is computed using Doppler measurements and the clock-offset values for each GNSS system were updated using the initial clock-offset and computed clock drift values. The measured and estimated (unknown) parameters when using and not using a priori clock-offsets are shown in Table 4.2. The strategy adopted was to assume each constellation has a receiver-GNSS clock-offset, but that all three are subject to the same clock drift (due to the frequency error of the single oscillator in the receiver as discussed in Chapter 2). The clock drift was estimated at each epoch along with the receiver velocity using a minimum of four Doppler observations (from any combination of satellites). The estimated drift was then used to update the three system clock-offsets assuming a constant velocity model.

Table 4.2: Measured and estimated parameters when using and not using a priori clock-offset as constraints

Without a priori clock-offsets		With a priori clock-offsets	
Measured	Estimated	Measured	Estimated
Pseudorange	Position Clock-offsets	Pseudorange	Position
Doppler	Velocity Clock drift	Doppler	Velocity Clock drift

The data sets and data processing procedures have been discussed. Using these datasets and data processing procedures, the positioning performance when using and not using a priori receiver-GNSS clock-offsets when a limited number of satellites from multiple GNSS constellations are available is examined in the following sections.

4.3 The Use of a Priori Clock-offset Constraints in Limited Signal Environment

The accuracy of the position solutions obtained using a priori receiver-GNSS clock-offsets when a limited number of satellites from multiple GNSS constellations are available is examined in this section. The DOPs for 6 satellites (from two and three GNSS constellations) and 8 satellites (from three GNSS constellations) scenarios are shown in Figure 4.3. The details of satellite combination for each scenario are specified in Table 4.1. Figure 4.3 shows that the east dilutions of precision for all scenarios are below 2 throughout the study period. The north dilutions of precision for both 6 and 8 satellites from three GNSS constellation scenarios are below 3 throughout. The NDOP for the two GNSS constellation scenario in the figure, however, varies between 2 to 11. A very high VDOP of almost 50 is observed in the two GNSS constellation scenario. For the three GNSS constellation cases, however, the VDOP are below 6 throughout. The reason for the high VDOP for the two GNSS constellation scenario in this particular receiver-satellite geometry is that none of the 6 satellites (from GPS or GLONASS) are at very high elevation. The vertical results are further degraded by the fact that the vertical position is now highly correlated with not just one, but two poorly determined clock offsets (one of each system) In the three constellation scenarios, BeiDou PRN 12 provides range observations from near zenith (as shown is the sky plot in Figure 4.1).

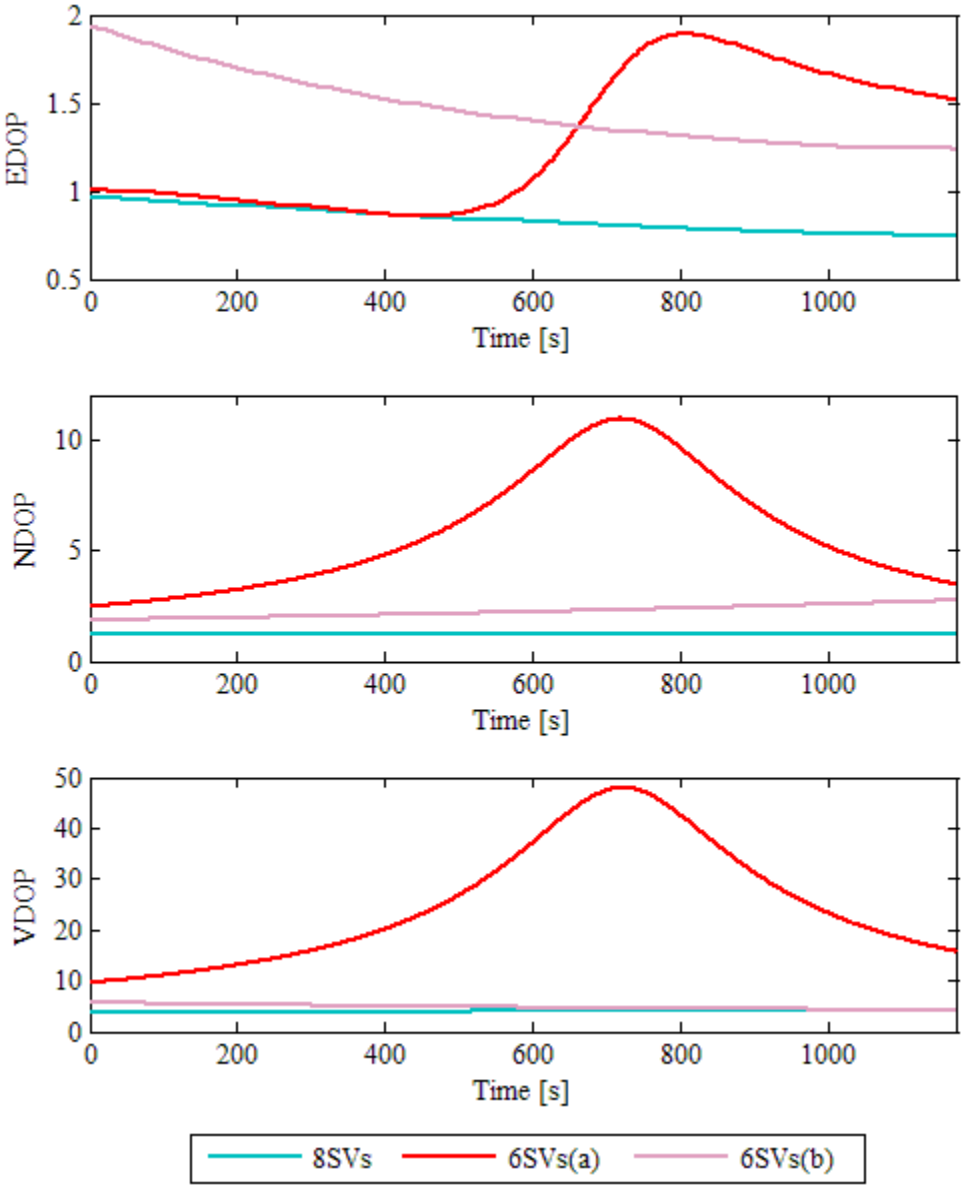

Figure 4.3: DOPs for scenarios using 8 and 6 high elevation angle satellites when position solutions are estimated at each epoch. (Details of satellite combinations are as specified in Table 4.1.)

The position errors (compared to the known receiver position) obtained using 7 and 8 satellites from three GNSS constellations are shown in Figure 4.4. With the limited number of satellites in view, the difference in position solution accuracy with and without an additional measurement can be very significant. This is especially true when the receiver-GNSS time-offsets are estimated by the receiver at each epoch. For the same receiver-satellite geometry, when using a priori time-offset information the difference in the position solutions obtained from using 7 satellites versus 8 satellites are not as significant. With a limited number of satellites in view from multiple GNSS constellations, providing that the duration with limited satellites is reasonably short, the use of a priori time-offset constraints significantly benefits the accuracy and availability of the position solutions.

The reason for a significant difference between using 7 and 8 satellites without the clock-offset constraints is that, for the 7 satellite scenario, the signal from the single BeiDou satellite does not contribute to the position solutions but is used in solving for the BeiDou system time-offset only. Thus, the position solution was obtained from 3 GPS and 3 GLONASS satellites. This situation is further demonstrated in Figure 4.5 where the position solutions from 6 satellites (3 GPS and 3 GLONASS) and position solutions from 7 satellites (3 GPS, 3 GLONASS and 1 BeiDou) are the same when the clock-offset parameters are estimated by the receiver during each epoch. In this figure, the red plots completely overlap with the magenta plots. When the a priori clock-offset is used, the position solution shows noticeable improvement with an additional satellite from the new constellation. The availability of the additional signal directly contributes to the estimation of the position solution.

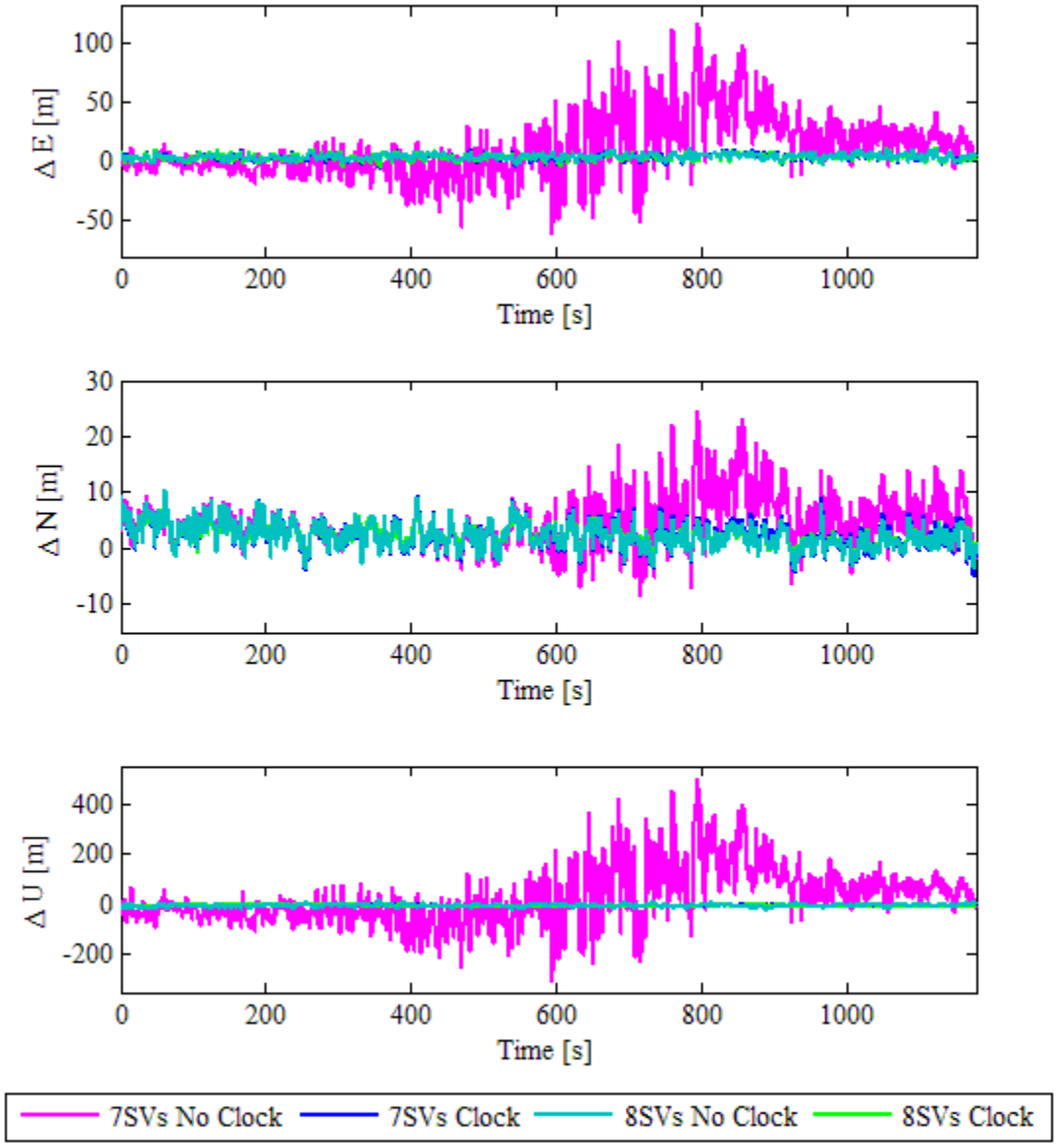

Figure 4.4: Position errors for the 7 and 8 satellite scenarios without a priori clock-offsets (No Clock) and when using a priori clock-offsets (Clock)

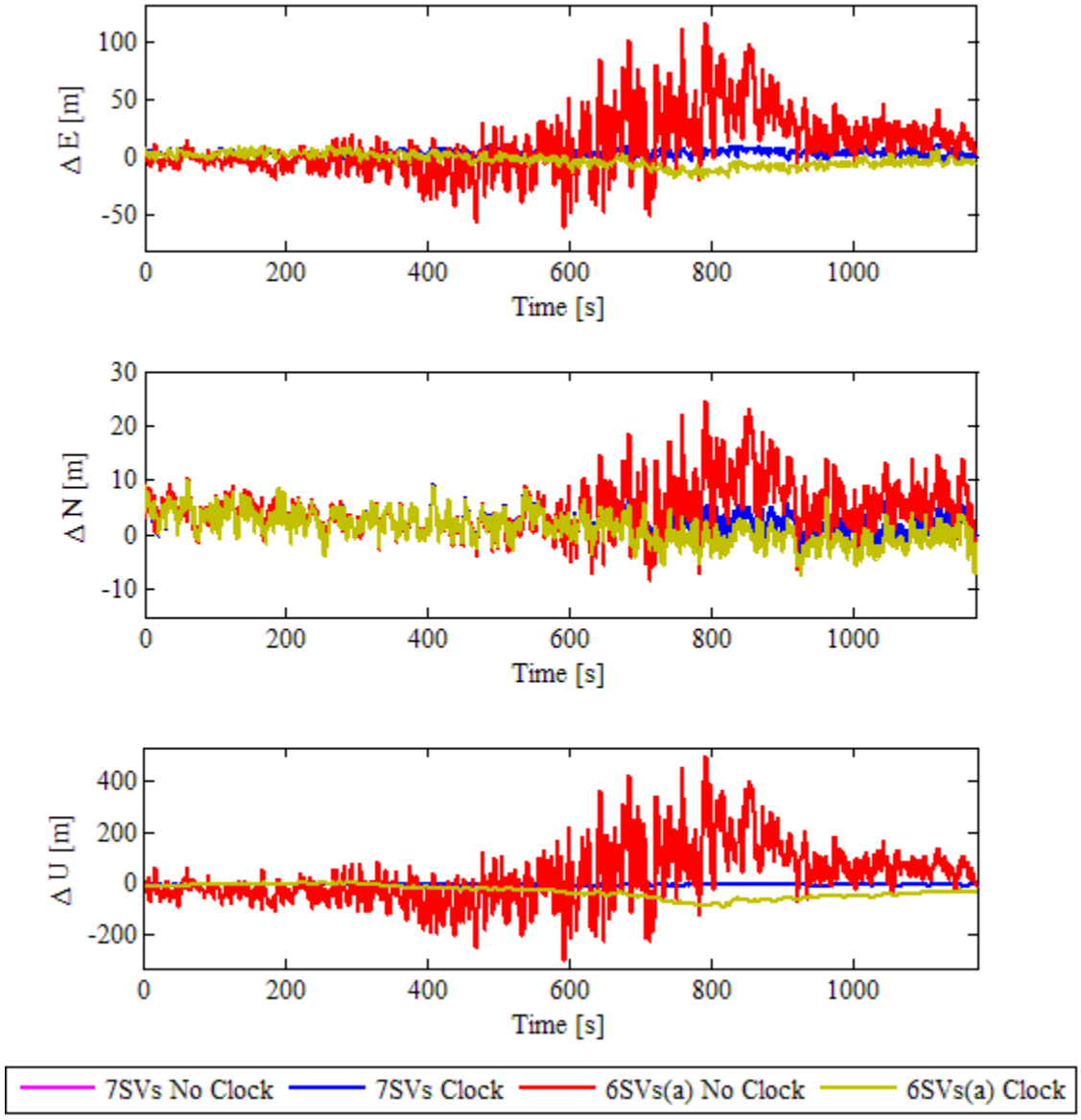

Figure 4.5: Position errors for the 6 and 7 satellite scenarios without a priori clock-offsets (No Clock) and when using a priori clock-offsets (Clock)

Comparing the DOP plots in Figure 4.3 and the position error plots in Figure 4.4 and Figure 4.5, it can be seen that for the 8 satellite scenario, the east, north and vertical DOPs are small throughout the study period. For this scenario, small position errors are observed as shown in

Figure 4.4. In contrast, large DOPs for the 6 satellite from GPS and GLONASS scenario are observed especially after the time 400 seconds. During this time, large position errors for this 6 satellite scenario are observed as illustrated in Figure 4.5.

The residuals for the 8 satellite scenario when using and not using a priori clock-offset constraints are examined. Comparing the residuals from the two data processing methods, it is revealed in Figure 4.6 that for both methods the magnitudes of the residuals are similar for all the satellites. The residuals from all the satellites when not using and using a priori clock-offset constraints have magnitudes within 3.9 m and 4.0 m, respectively, most of the time (2σ).

The residuals for the 7 satellite scenario are displayed in Figure 4.7. It can be seen that, without the use of a priori clock-offset constraints, only residuals for GPS and GLONASS measurements can be obtained. This is because the only BeiDou observation contributes to the estimation of the BeiDou system time-offset; with a single measurement from this constellation there is no measurement redundancy to obtain residuals. Also, with a redundancy of one for each of the GPS and GLONASS system, the residuals are correlated with each other. When using a priori clock-offset constraints, however, residuals for all 7 satellites can be obtained as all the observations contribute to position computation. In this case, there is sufficient measurement redundancy. Furthermore the residuals from all the satellites when not using and using a priori clock-offset constraints for the 7 satellite scenario have magnitudes within 3.1 m and 4.2 m, respectively, most of the time (2σ).

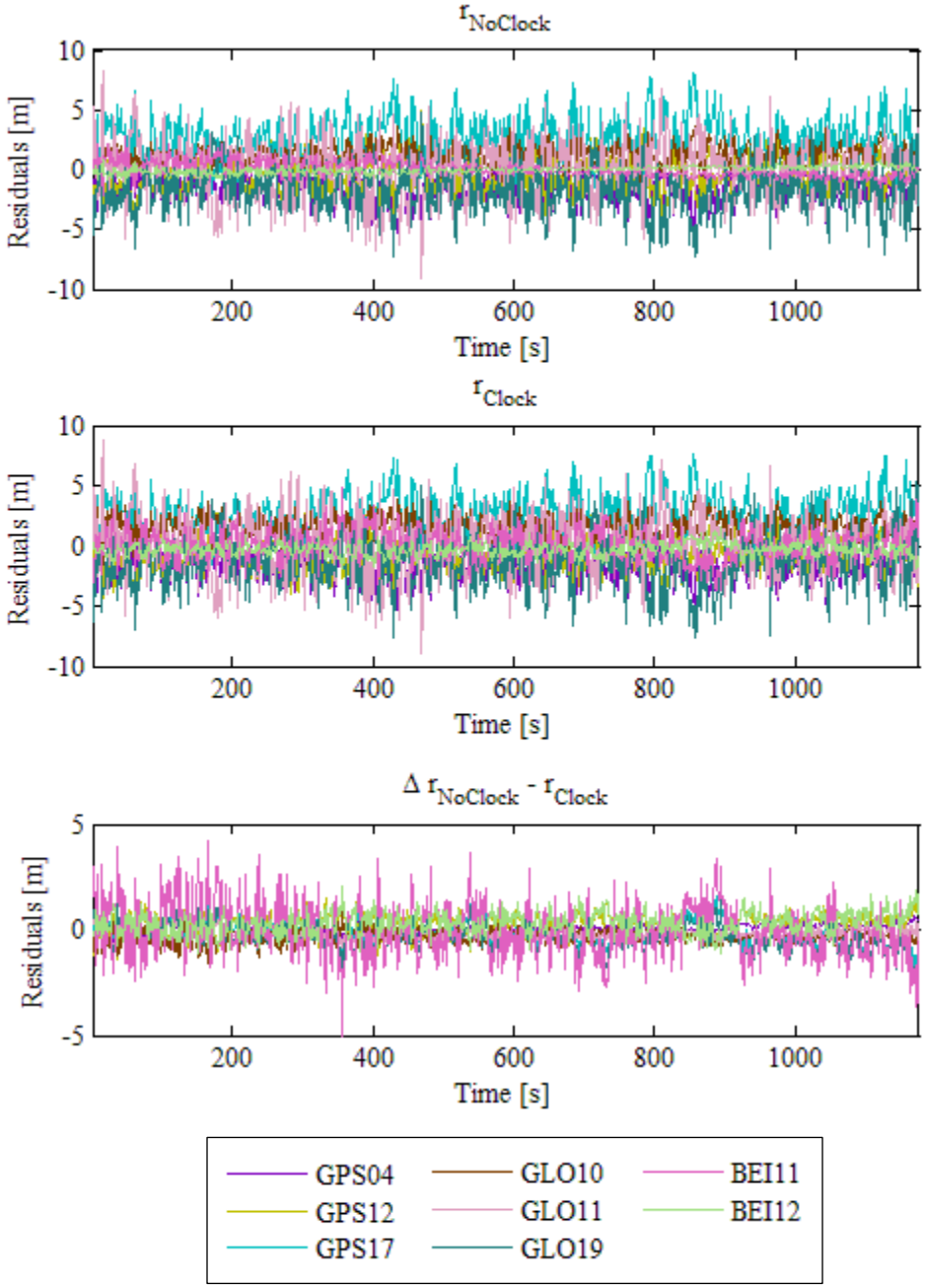

Figure 4.6: Residuals for the 8 satellite scenario when not using (top) and using (middle) a priori clock-offset constraints and the differences between these two sets of residuals (bottom)

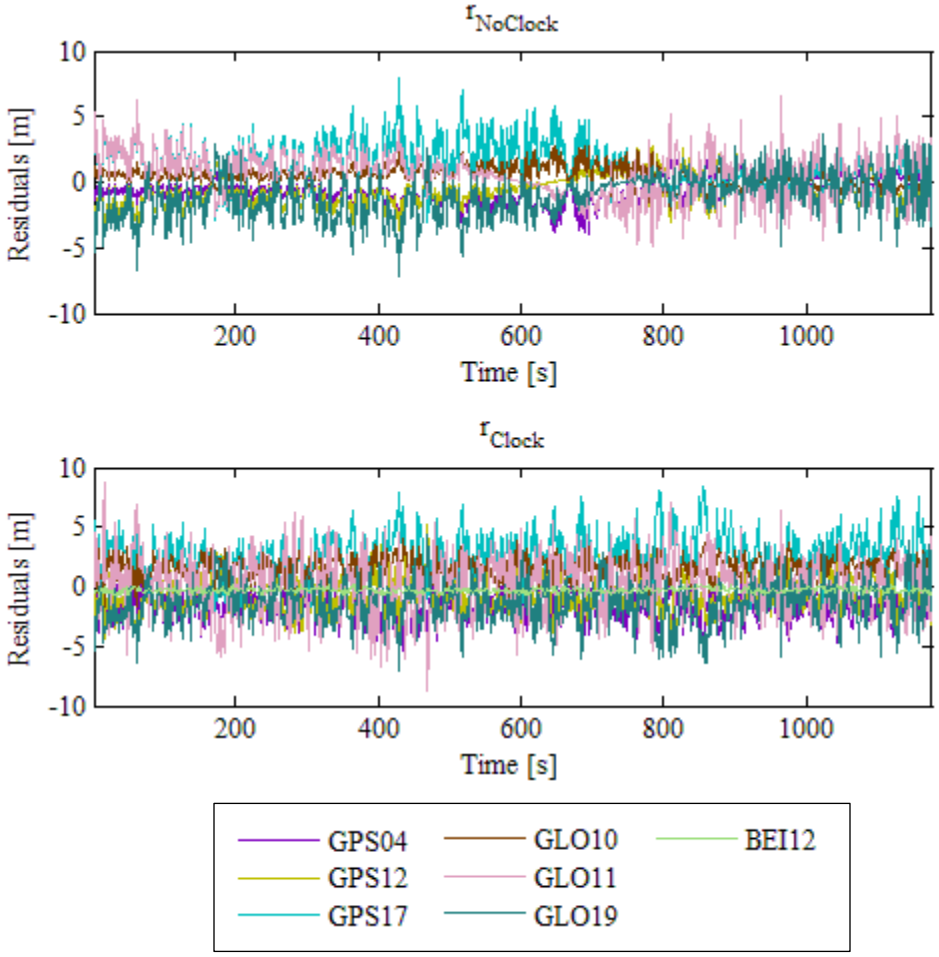

Figure 4.7: Residuals for the 7 satellite scenario when not using (top) and using (bottom) a priori clock-offset constraints

The position solutions obtained in more challenging situations using 6 and 4 satellites from three GNSS constellations were examined. The position solutions from these are then compared with the scenario where ranging signals from 8 satellites were available. The results from these are shown in Figure 4.8.

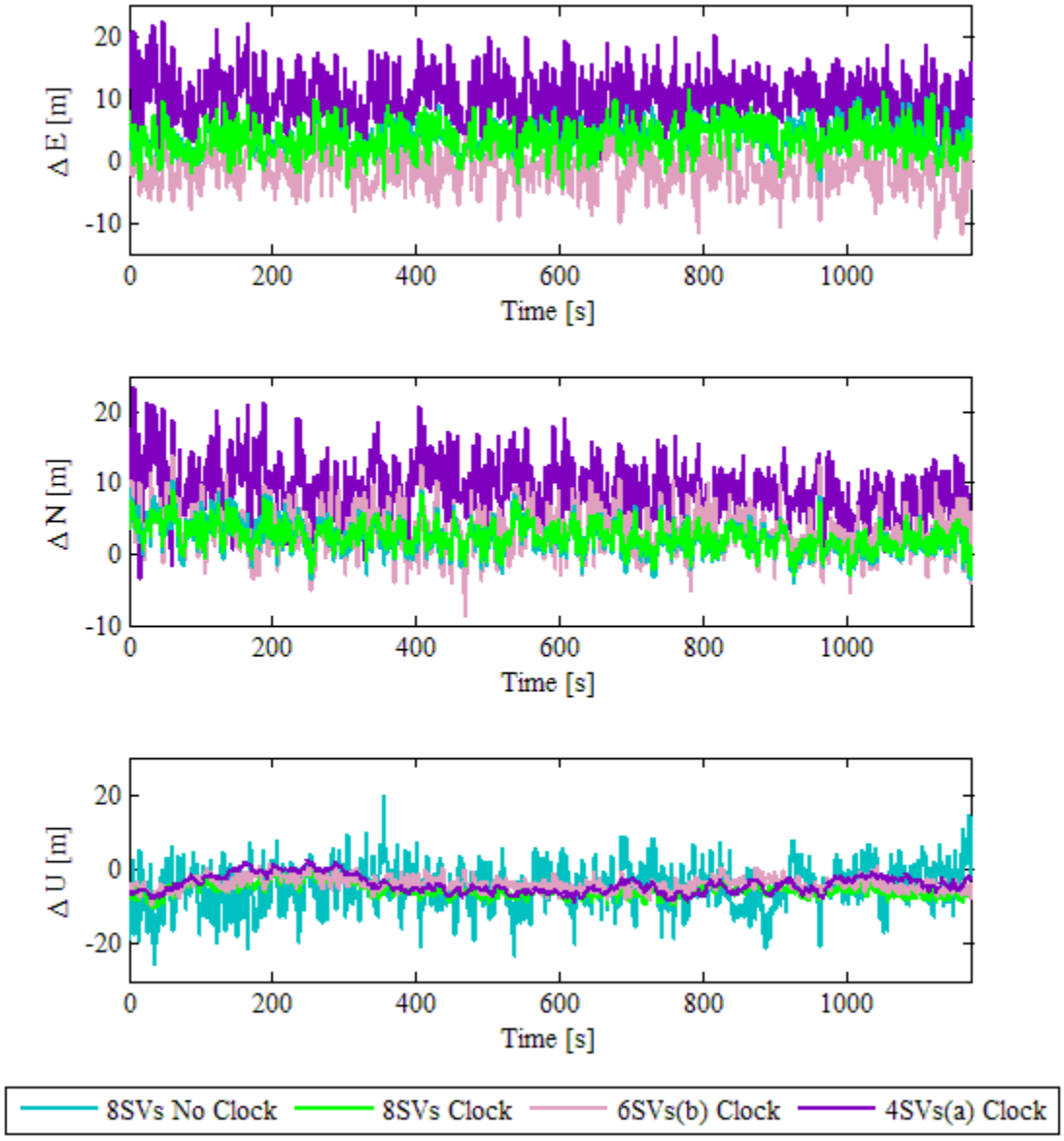

Figure 4.8: Position errors for the 8 satellite scenario when not using a priori clock-offset constraints (No Clock) and position errors for the 4, 6 and 8 satellite scenarios when using a priori clock-offset constraints (Clock)

Figure 4.8 shows that when the a priori clock-offset constraints are used in the 8 satellite scenario, the north and east positions show very similar position accuracy with a slightly smaller error compared to when the clock-offsets are estimated at each epoch. More significant reduction in position error is evident in the vertical position. Without using a priori clock-offset constraints in the 8 satellite scenario the vertical position error exceeds 20 m at times. With the use of a priori clock-offset constraints, the vertical position error for the 8 satellite scenario is within 11 m throughout the data set.

When 6 satellites are used with a priori clock-offset constraints, the results are similar to the 8 satellite with clock-offset constraints scenario but with larger position error fluctuations. With 8 satellites and a priori clock-offsets, maximum east and north position errors of 12 m and 10 m, respectively, are observed. For the 6 satellite scenario, maximum east and north position errors of 13 m and 14 m, respectively, are observed. The maximum vertical position errors for both the 6 and 8 satellite scenarios with a priori clock-offsets are within 11 m throughout.

When 4 satellites are used, however, significantly larger horizontal position errors are observed, with the maximum east and north position errors of 23 m and 24 m respectively. In the 4 satellite scenario the vertical position error is relatively small compared to using 8 satellites without an a priori clock-offset constraint. In this 4 satellite scenario, the vertical position error is within 9 m throughout. It must be noted, however, that although the horizontal position errors in the 4 satellite scenario tend to be quite large, no solution would be available without the clock-offset constraints.

The residuals for the 6 satellite scenario were examined and displayed in Figure 4.9. When using signals from 3 GPS and 3 GLONASS satellites without a priori clock-offsets, there is a residual for each satellite. This is because in this case there are 6 measurements to solve for 5 unknowns (3 unknowns user coordinate parameters and 2 unknowns system clock-offsets), hence, there is a redundant measurement to obtain residuals. With a redundancy of one for each of the GPS and GLONASS system when not using a priori clock-offset constraints, correlations between the residuals are observed. The residuals from all the satellites when not using and using a priori clock-offset constraints have 2σ values within 3.1 m and 4.9 m respectively. It must be noted that, without a priori inter-system clock-offsets, the GPS and GLONASS residuals from this 6 satellite scenario and the 7 satellite scenario (3 GPS, 3 GLONASS and 1 BeiDou in Figure 4.7) are the same.

When the solution is computed using signals from 2 GPS, 2 GLONASS and 2 BeiDou satellites without the use of a priori clock-offset constraints there are 6 unknowns to be estimated (3 unknown user coordinate parameters plus a system clock-offset for each GNSS). In this case, there is no measurement redundancy and the residuals cannot be obtained. The use of a priori clock-offset constraints helps improve measurement redundancy. With the use of a priori clock-offsets, residuals from all 6 satellites from three GNSS constellations can be obtained and the magnitude of residual for all the satellites is within 2.3 m most of the time (2σ).

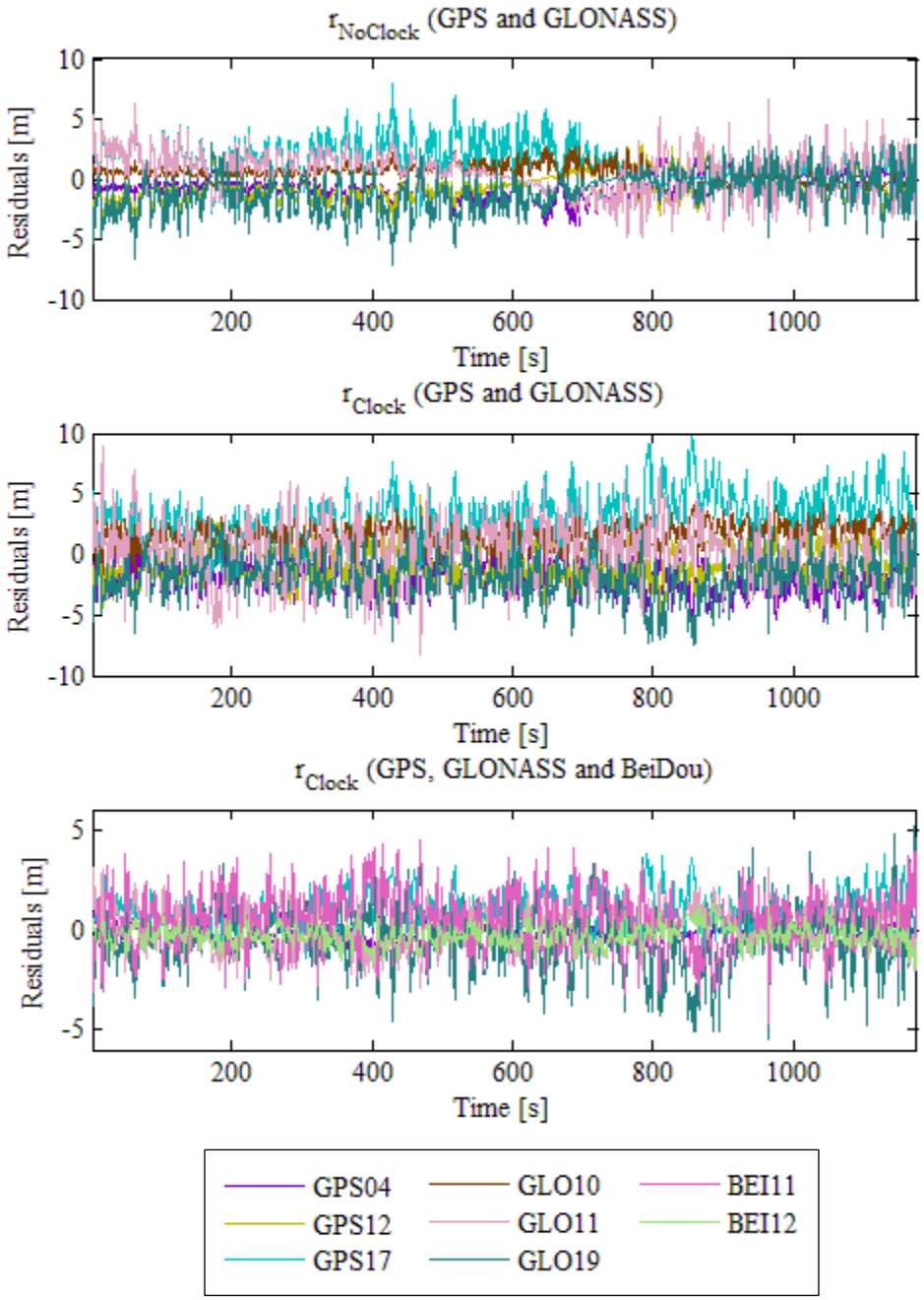

Figure 4.9: Residuals for the 6 satellite scenarios from two constellations when not using a priori clock-offsets (top), and when using a priori clock-offsets (middle); and residuals for 6 satellite from three constellation scenario when using a priori clock-offset (bottom)

The residuals for the 4 satellite scenario are examined and the results are shown in Figure 4.10. When position solutions are computed using 4 satellites from three GNSS constellations with a priori system clock-offsets, residuals for each satellite can be obtained. Correlations between the residuals are observed in this scenario and the residuals from all the satellites have 2σ values of 0.6 m.

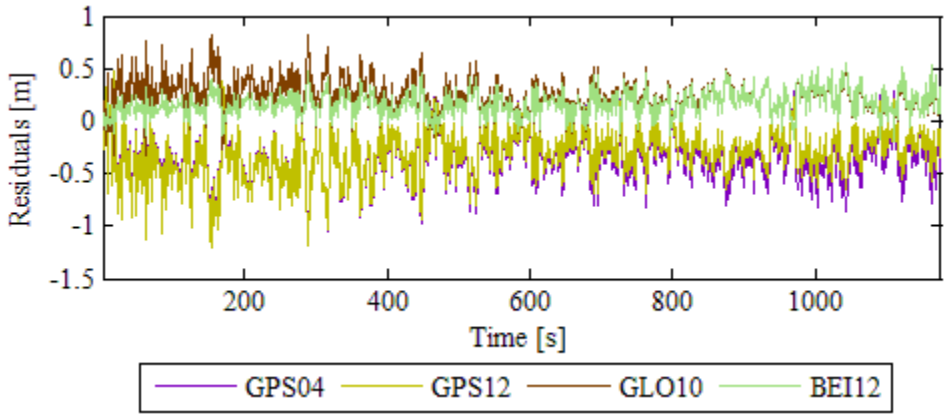

Figure 4.10: Residuals for the 4 satellite from 3 constellation scenario when using a priori clock-offsets

The study further investigates the characteristics of the system clock-offset parameters from the 4, 6 and 8 satellite from three GNSS constellation scenarios. The a priori system clock-offsets for each GNSS constellation (obtained from least-squares estimation at initial epoch then updated using the estimated clock drift) which are used as constraints are compared with clock-offset values computed at each epoch using all in view satellites. The results from theses are presented in Figure 4.11. It is revealed in this figure that the system clock-offset values used as constraints are relatively stable throughout the study period. Also, the clock-offset values are similar for all the scenarios under investigation.

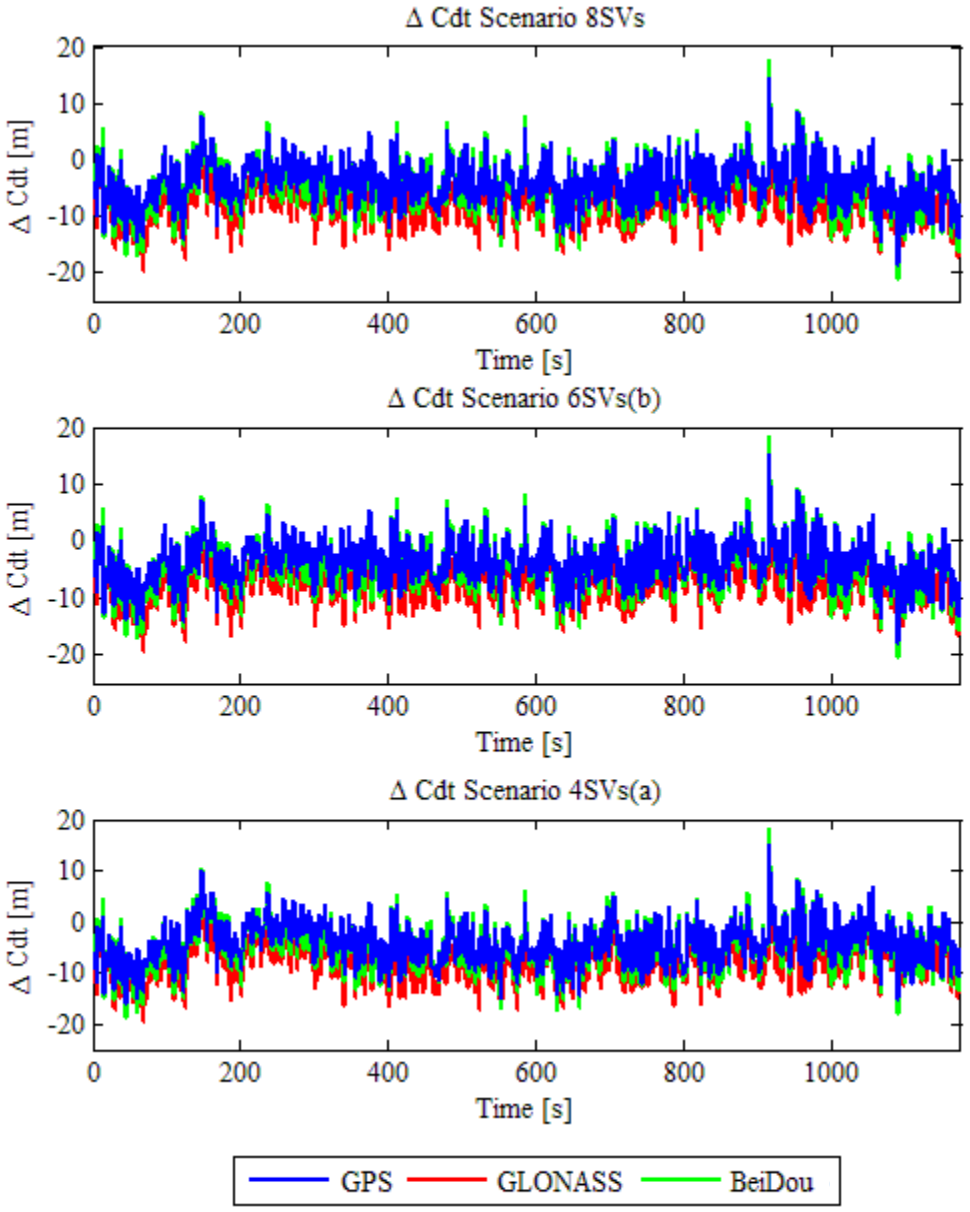

Figure 4.11: The difference between clock-offset values for the 8, 6 and 4 satellite scenarios when the a priori clock-offsets are used and when the clock-offsets are estimated by the receiver at each epoch using all in view satellites with a 10^{o} mask angle

4.4 The Use of a Priori Clock-offset Constraints and Blunder Detection

In order to examine the fault detection and exclusion capability when using measurements from multiple constellations in degraded GNSS signal environments with and without a priori system clock-offsets constraints, a simulated blunder in form of a pseudorange bias of 150 m was added to measurements from BeiDou PRN 11 when position solutions are computed using 2 satellites from each of the GPS, GLONASS and BeiDou systems. The fault starts at time 3 minutes and lasts for 10 minutes. The position errors from these are shown in Figure 4.12 and Figure 4.13 for scenarios when not using and using clock-offset constraints respectively.

Figure 4.12 shows that without the use of the a priori clock-offset, the blunder goes undetected resulting in large position errors. When the fault occurs at this high elevation satellite which positioned to the west of the receiver, the vertical and east-west position errors are large compared to the position error in the north-south direction. The position errors exceed 60 m and 350 m are observed in the east-west and vertical directions respectively.

When the clock constraints were used, the blunder is detected and excluded from the position estimation as shown in Figure 4.13. After rejecting the faulty measurement, a slight increase in position errors compared to when six satellites were used is observed as a result of poorer receiver-satellite geometry. However, the benefit of correctly removing the faulty measurement is outweighs the degraded receiver-satellite geometry. When the blunder is correctly removed, the position errors within 15 m are observed in all the directions.

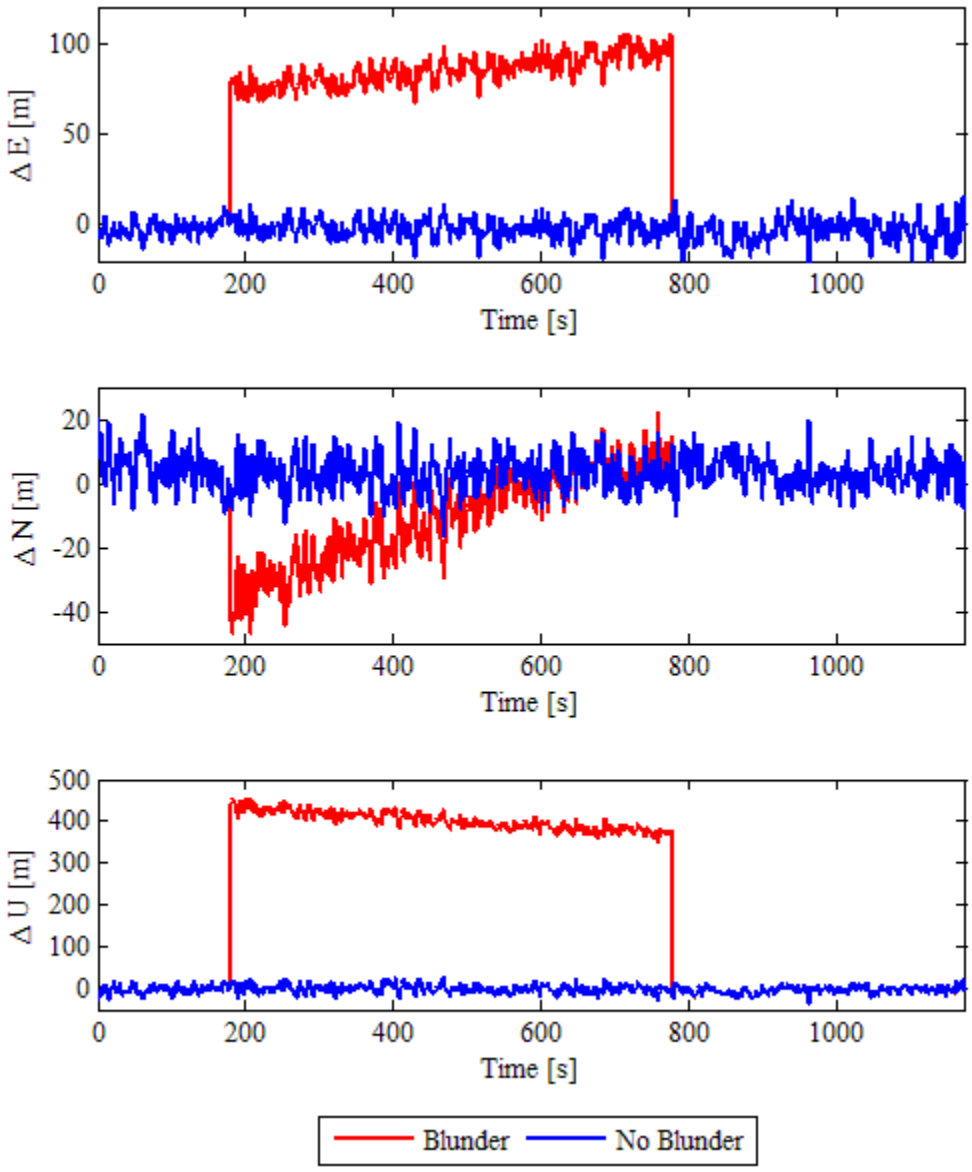

Figure 4.12: Position errors when a simulated blunder in form of a pseudorange bias of 150 m was added to measurements from BeiDou PRN 11 when position solutions are computed using 2 satellites from each of the GPS, GLONASS and BeiDou systems without clock constraint

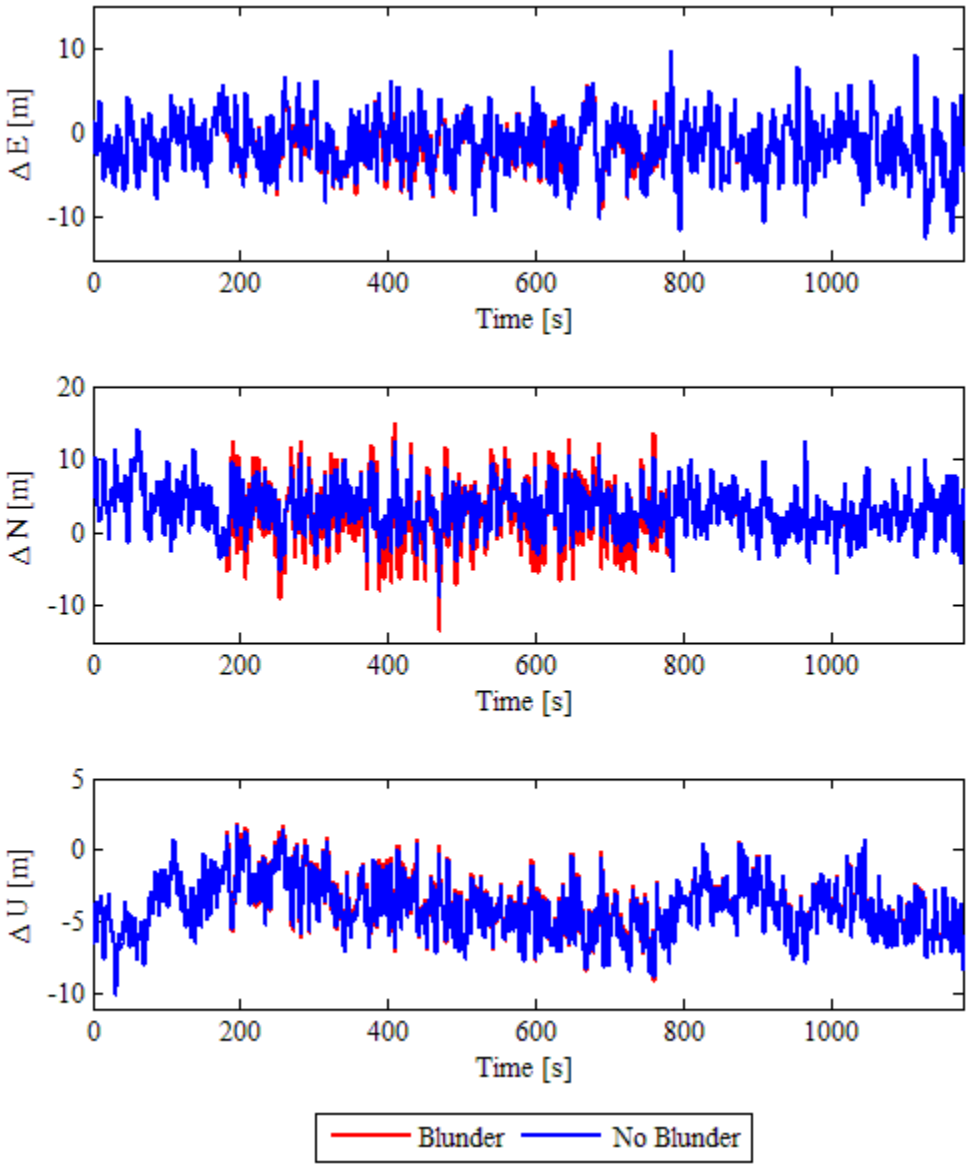

Figure 4.13: Position errors when a simulated blunder in form of a pseudorange bias of 150 m was added to measurements from BeiDou PRN 11 when position solutions are computed using 2 satellites from each of the GPS, GLONASS and BeiDou systems with clock constraints

Standardized residuals for the scenario when using 3 satellites from each of the GPS and GLONASS systems and 2 satellites from BeiDou system are examined. When not using a priori clock-offset constraints, the standardized residuals under the fault-free ($\boldsymbol{r_{s}}_{No\ Clock,No\ Fault}$) and faulty ($\boldsymbol{r_{s}}_{No\ Clock,Fault}$) conditions has elements corresponding to the two BeiDou measurements (printed in blue) having the same magnitude with opposite sign.

$$\boldsymbol{r_{s}}_{No\ Clock,No\ Fault} = \begin{bmatrix} -0.156 \\ 0.156 \\ 0.030 \\ -0.448 \\ 0.222 \\ 0.048 \\ 0.387 \\ -0.434 \end{bmatrix} \tag{4.1}$$

$$\boldsymbol{r_{s}}_{No\ Clock,Fault} = \begin{bmatrix} 2.463 \\ -2.463 \\ -2.292 \\ 1.272 \\ 1.387 \\ 2.167 \\ -2.043 \\ 0.402 \end{bmatrix} \tag{4.2}$$

Although the global and local tests can be used to detect measurement bias, the equality of the two BeiDou standardized residuals makes it impossible to identify the faulty measurement.

When using a priori system clock-offset constraints, the standardized residuals, $\boldsymbol{r_{s}}_{Clock,No\ Fault}$, for each of the measurements has unique value even when only two observations from BeiDou are available.

$$\boldsymbol{r}_{s\ Clock,No\ Fault} \begin{bmatrix} -0.243 \\ -0.030 \\ -0.174 \\ -0.308 \\ 0.528 \\ 0.394 \\ 0.407 \\ -0.713 \end{bmatrix} \tag{4.3}$$

In this case, when the measurement bias occurs in BeiDou PRN 11, the standardized residual ($\boldsymbol{r}_{s\ Clock,Fault}$) with only element corresponding to this satellite has a high value (printed in red). Since these standardized residuals are also used in the test statistic to identify blunders, the use of a priori clock-offsets thus makes it possible to identify the faulty measurement.

$$\boldsymbol{r}_{s\ Clock,Fault} \begin{bmatrix} 7.074 \\ -4.790 \\ -0.687 \\ -2.270 \\ 2.891 \\ -2.096 \\ -0.931 \\ 3.206 \end{bmatrix} \tag{4.4}$$

4.5 Position Solutions Using 4 Observations from 4 GNSS Constellations

A scenario when 4 satellites from four systems are available was tested and position solutions were obtained. In this scenario, one high elevation satellite from each of the GPS, GLONASS, BeiDou and Galileo constellations as shown in the sky plot in Figure 4.2 are used in position estimation with a priori clock-offset constraints. The position solutions obtain from the 4 satellite scenario are then compared against position solutions obtain from using all in view satellites with

mask angles of 10^o and 35^o when the clock-offsets are estimated by the receiver at each epoch. In the mask angle of 35^o case, a total of 13 satellites were used to compute the receiver position. The position errors from these are shown in Figure 4.14.

When the position errors in the north-south and east-west directions were examined, it is revealed that results from using all in view satellites with mask angle of 10^o and 35^o has similar position errors. With the mask angle of 10^o, the position errors in the north-south and east-west directions are within 8 m and 9 m respectively. For the 35^o mask angle scenario, the position errors for the north-south and east-west directions are within 10 m and 13 m respectively. When the number of satellites reduces to 4, the position errors increase noticeably. In this scenario, the north-south position errors are within 39 m and the east-west position errors are within 38 m.

The vertical position error plots reveal that when using all in view satellites with 10^o and 35^o mask angles, the vertical position errors are within 14 m and 31 m respectively. For the 4 satellite scenario, the vertical position errors are 19 m throughout the experimental period.

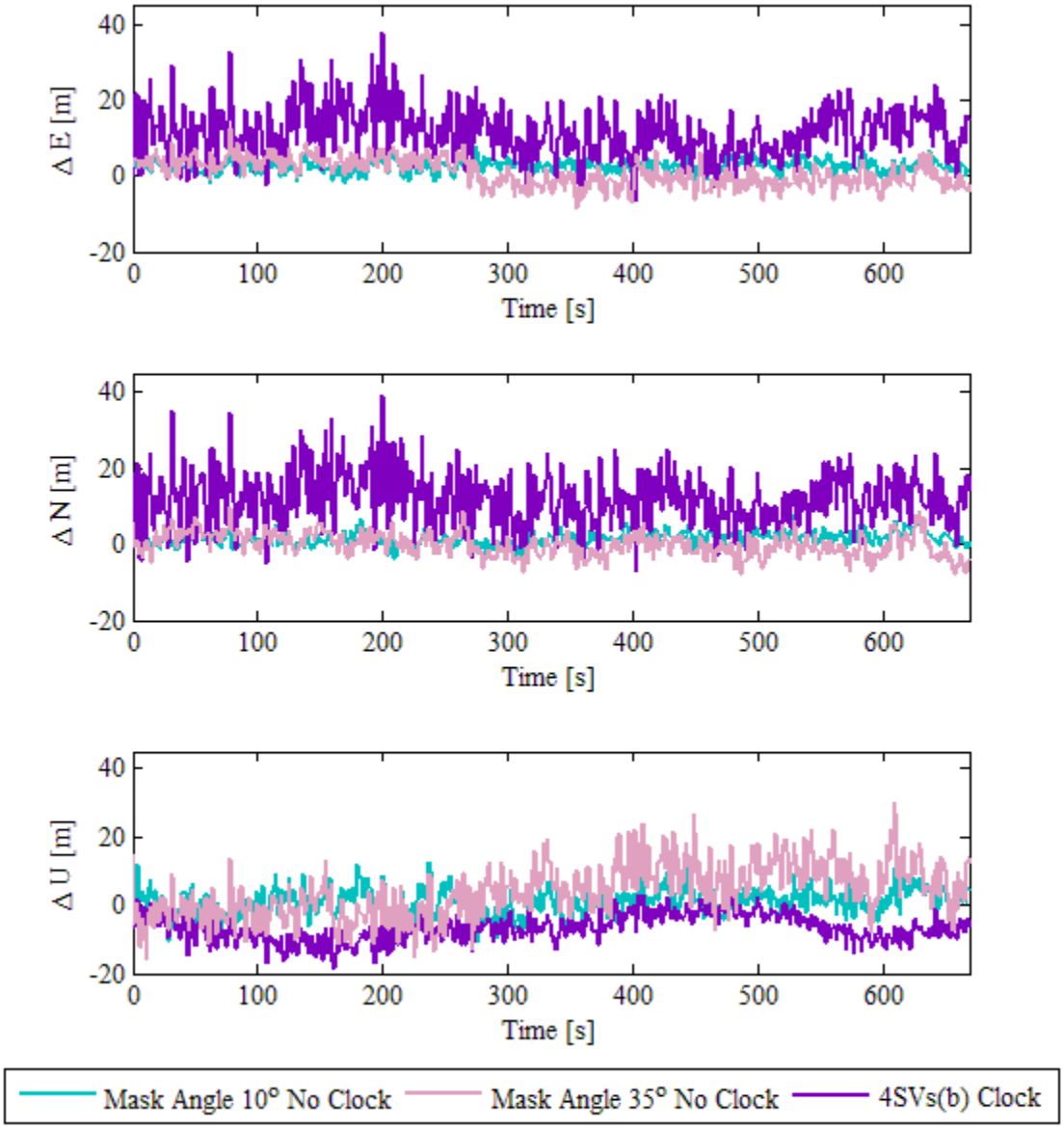

Figure 4.14: Position errors when using all in view satellites with 10^o and 35^o mask angles without a priori system clock-offset constraints (No Clock) and position errors when using 4 satellites from 4 constellations with a priori clock-offset constraints (Clock)

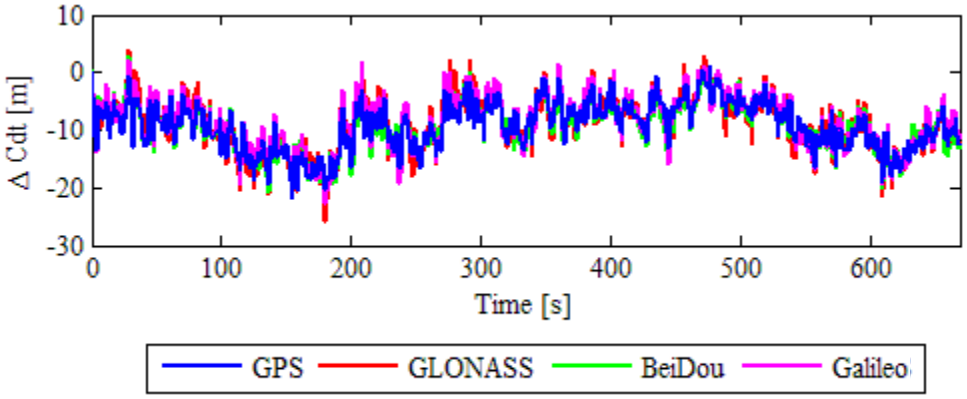

Figure 4.15: The difference between clock-offset values for the 4 satellite from 4 constellation scenario when the a priori clock-offsets are used and when the clock-offsets are estimated by the receiver at each epoch using all in view satellites with a 10^{o} mask angle

The characteristics of the clock-offset parameters are investigated. The a priori system clock-offsets for each GNSS constellation (obtained from least-squares estimation at initial epoch then updated using the estimated clock drift) which are used as constraints for the 4 satellite scenario are compared with clock-offset values computed at each epoch using all in view satellites. The results from theses are presented in Figure 4.15. It is evidenced in this figure that the clock-offset constraint values are relatively stable throughout the study period and the magnitude of a priori clock-offsets for the GPS, GLONASS, BeiDou and Galileo systems are similar.

The availability and reliability of position solutions obtain from multiple GNSS constellations have been examined using covariance simulation in the previous chapter. The positioning accuracy and the benefits from using a priori receiver-GNSS clock-offsets when a limited number of satellites from multiple GNSS constellations are available using live data have been

investigated in this chapter. The following chapter discusses key findings from this study and provides conclusions.

CHAPTER FIVE: CONCLUSIONS AND RECOMMENDATIONS

This chapter presents conclusions and key findings from this study. Recommendations and possible future investigations are also discussed in this chapter.

5.1 Conclusions

The objectives of this study have been achieved through covariance simulations and the examination of position solutions obtained using measurements from GPS, GLONASS, BeiDou and Galileo satellite systems. This section first concludes key findings from simulations performed to examine the availability and reliability of position solutions when using measurements from multiple GNSS constellations. Then, the conclusions from experimental using real observations from GPS, GLONASS, BeiDou and Galileo systems to investigate the benefits of using a priori clock-offset constraints are presented. The main findings from this study are as follows:

- *Reliability of position solutions from GPS and GLONASS with SBAS corrections*

Simulation results revealed that, when SBAS corrections are applied to GPS measurements when using ranging signals from GPS and GLONASS constellations in the semi-urban environment, the 95th percentile HPL reduced from almost 150 m to 110 m. More significant improvement is evident in vertical protection level. With SBAS corrections, the 95th percentile VPL improved from over 440 m to below 330 m.

- *Availability and reliability of position solutions from the combined GPS and GLONASS systems with additional ranging signals from the BeiDou and Galileo satellites*

From simulations it has been found that when using signals from GPS and GLONASS on average 7 satellites are visible to users in the east-west running urban-canyon environment. As a result, the FDE is unavailable 37% of the time. GNSS users in the east-west running urban-canyon see a larger number of satellites on average compared to users in the north-south running urban-canyon. In the north-south running urban-canyon, on average, only 6 satellites are visible when using signals from GPS and GLONASS systems. As a result of limited number of visible satellites in the north-south running urban-canyon environment, the FDE is unavailable 67% of the time.

When ranging signals from the complete BeiDou and Galileo constellations become available, users in the semi-urban environment can expect to see 19 satellites on average when using signals from the four GNSS constellations. In the north-south urban-canyon environment, users can expect to see 12 satellites on average.

In the semi-urban environment, without the use of a priori clock-offset constraints, the 95^{th} percentile HPL is expected to reduce from almost 150 m when using signals from GPS and GLONASS constellations down to below 20 m when all four GNSS constellations become operational. Similarly, the 95^{th} percentile VPL is expected to reduce from over 440 m down to below 50 m.

In the north-south urban-canyon, without the use of a priori clock-offset constraints, the FDE is unavailable almost 70% of the time when using signals from GPS and GLONASS. Simulation results show that this value would be reduced to 35% when ranging signals from all four GNSS constellations become available.

- *Benefits of using a priori clock-offset constraints*

The benefits of using clock-offset constraints are particularly significant when the receiver is located in areas where limited GNSS signals are available such as in the urban-canyon environment. Simulation results show that with the use of a priori inter-system time-offset constraints, in the north-south running urban-canyon, the FDE is unavailable less than 1% of the time when using signals from all four GNSS constellations.

It was found by the simulation that, when using signals from complete four GNSS constellations together with a priori clock-offsets, GNSS users in the north-south running urban-canyon can expect the values of the 95^{th} percentile HPL and VPL to be reduced by about 50 % of what would be achievable without the use of a priori clock-offset constraints.

The inter-system clock-offset parameter can be initially estimated by the receiver at the starting epoch then used as a priori information when computing receiver positions at later epochs. Alternatively, when the inter-system clock-offset is transmitted by GNSS, the receiver can use this broadcast parameter as an additional measurement to reduce number of pseudoranges required. The use of clock-offset information either broadcast by GNSS providers or from initial

estimates by the receiver improves measurement redundancy. This is particularly helpful when using GNSS in signal challenging environment.

The use of clock-offset constraints with small estimated uncertainties results in more reliable position solutions compared to when using clock-offset constraints with large estimated uncertainties. The inter-system clock-offset value estimated at the receiver level could potentially have a larger estimated error compared to inter-system clock-offset values broadcast by GNSS providers. However, during the time when the broadcast inter-system clock-offset is not available, the system availability and reliability would still be improved by using a priori clock-offset constraints obtained by the receiver at an earlier epoch compared to when the clock-offset parameter have to be computed by the receiver at each epoch.

Live data from multiple GNSS constellations were collected. When examining position solutions obtained from GPS, GLONASS and BeiDou systems it is evident that when signals from many satellites from multiple constellations are available; the difference in position solution accuracy when processing data using and not using a priori system clock-offset constraints are not significant. However, this is not the case when signals from a limited number of satellites from multiple GNSS constellations are available. When using a priori clock-offset constraints, all the range measurements directly contribute to the estimation of the position solution. Thus, with a limited number of signals from multiple GNSS constellations, the use of a priori clock-offset constraints helps improve the accuracy and availability of the position solutions. It has also been observed that the a priori clock-offset values which are used as constraints are relatively stable throughout the 20 minutes study period.

A scenario with 4 available satellites, one from each of the GPS, GLONASS, BeiDou and Galileo constellations, was tested and position solutions were obtained when the receiver was using a priori clock-offset constraints. In this scenario large position errors (especially in the horizontal direction) were observed. However, in a limited GNSS signals environment, only few satellites from multiple GNSS constellations could be visible and no solution would be available without the use of a priori clock-offset constraints.

- *Blunder detection and exclusion capabilities when using measurements from multiple GNSS constellations*

A simulated blunder in form of a pseudorange bias of 150 m was added to measurements from one of the BeiDou satellites when position solutions were computed using 2 satellites from each of the GPS, GLONASS and BeiDou systems. The results show that without the use of the a priori clock-offset constraints the blunder was undetected and large position errors were observed. When the clock-offset constraints were used, the blunder was detected and excluded from the position estimation.

5.2 Future Research and Recommendations

The following are recommendations and potential future research on the reliability and availability of position solutions using multiple GNSS constellations:

- The first part of this study compared the minimum detectable blunder and protection levels of the combined GPS and GLONASS constellations with and without SBAS corrections applied to GPS measurements. Further studies could be done to examine the reliability performance of GPS and GLONASS with new constellations such as BeiDou

and Galileo when SBAS corrections are applied to one or more constellations, and when the ranging signals from SBAS satellites are also used in position estimation.

- With the time frame of this study and the limited availability of BeiDou and Galileo satellites at the time of this study, the investigation of position solution accuracies when using signals from multiple GNSS constellations in challenging signal environment was carried out using static data collected in an open sky environment. A high mask angle was chosen to simulate a GNSS user in a limited signals environment. The data collection for future research should be carried out in a dynamic receiver environment such as a receiver placed in a vehicle driving in downtown areas.
- In this study, approximately 20 minutes of collected data containing measurements from GPS, GLONASS and BeiDou is used for algorithm testing. Further studies could be carried out to examine the accuracy of a position solution when using a priori clock-offsets for a longer period of time and for both three and four GNSS constellation scenarios. This will require additional availability of Galileo and BeiDou satellites.
- The a priori system clock-offsets for each GNSS constellation in this study were obtained from the initial estimated clock-offset values from least-squares estimation at the initial epoch. The clock-offsets were then updated at each epoch using estimated clock drift values. Once the new GNSS start to broadcast the inter-system time-offset parameters as is planned by many GNSS providers, further investigations can be performed to examine the accuracy of a position solution obtained when using this broadcast parameter as an additional measurement.

REFERENCES

Alcantarilla, I., D. Porras, A. Tajdine, N. Zarraoa, J.L. Damidaux, D. Flament, and J.C. Lévy, (2006) "The Benefits of Multi-constellation GNSS Augmentations," *Proceedings of the 19th International Technical Meeting of the Satellite Division of The Institute of Navigation*, 26-29 September, Fort Worth, TX, pp. 930-938

Angrisano, A., S. Gaglione, A. Pacifico, and M. Vultaggio (2009) "Multi-Constellation System as Augmentation to GPS Performance in Difficult Environment or Critical Applications," *Atti dell'Istituto Italiano di Navigazione*, vol. 190

Angus, J. E. (2006) "RAIM with Multiple Faults," *Navigation*, vol. 53, no. 4, issue Winter 2006-2007, pp. 249-257

Arbesser-Rastburg, B. (2006) *The Galileo Single Frequency Ionospheric Correction Algorithm*, presented at the 3rd European Space Weather Week, ESA, 13-17 November, Brussels, Belgium

BDS-ICD (2012) *BeiDou Navigation Satellite System (BDS) Signal In Space Interface Control Document (SIS ICD), Open Service Signal B1I*, version 1.0, December, China Satellite Navigation Office

Bestmann, U., S. Batzdorfer, M. Becker, T. Scheide, and P. Hecker (2012) "SBAS in Urban Environment: Scenarios, Applicability and Challenges," *Proceedings of the 25th International Technical Meeting of The Satellite Division of the Institute of Navigation*, 17-21 September, Nashville, TN, pp. 3481-3487

Bhatta, B. (2011) *Global Navigation Satellite Systems: Insight Into GPS, GLONASS, Galileo, Compass and Others*, 1st edition, BS Publications, India

BIPM (2013a) *FTP Server of the Time Department*, Bureau International des Poids et Mesures, http://www.bipm.org/jsp/en/TimeFtp.jsp?TypePub=publication, last accessed 4 December 2013

BIPM (2013b) *International Atomic Time*, Bureau International des Poids et Mesures, http://www.bipm.org/en/scientific/tai/tai.html, last accessed 25 November 2013

Blanch, J., T. Walter, P. Enge, S. Wallner, F. Amarillo Fernandez, R. Dellago, R. Ioannides, I. Fernandez Hernandez, B. Belabbas, A. Spletter, and M. Rippl (2013) "Critical Elements for a Multi-Constellation Advanced RAIM," *Navigation*, vol. 60, no. 1, Spring, pp. 53–69

Blanch, J., T. Walter, P. Enge, S. Wallner, F. Amarillo Fernandez, R. Dellago, R. Ioannides, B. Pervan, I.F. Hernandez, B. Belabbas, A. Spletter, and M. Rippl (2011) "A Proposal for Multi-constellation Advanced RAIM for Vertical Guidance," *Proceedings of the 24th International Technical Meeting of The Satellite Division of the Institute of Navigation*, 20-23 September, Portland, OR, pp. 2665-2680

Blanch, J., M.J. Choi, T. Walter, P. Enge, and K. Suzuki (2010) "Prototyping Advanced RAIM for Vertical Guidance," *Proceedings of the 23rd International Technical Meeting of The Satellite Division of the Institute of Navigation*, 21-24 September, Portland, OR, pp. 284-291

Blanch, J., A. Ene, T. Walter, and P. Enge (2007) "An Optimized Multiple Hypothesis RAIM Algorithm for Vertical Guidance," *Proceedings of the 20th International Technical Meeting of the Satellite Division of The Institute of Navigation*, 25-28 September, Fort Worth, TX, pp. 2924-2933

Bonet, B., I. Alcantarilla, D. Flament, C. Rodriguez, and N. Zarraoa (2009) "The Benefits of Multi-constellation GNSS: Reaching up Even to Single Constellation GNSS users," *Proceedings of the 22nd International Technical Meeting of The Satellite Division of the Institute of Navigation*, 22-25 September, Savannah, GA, pp. 1268-1280

Cai, C. (2008) "A Solution for Combined GPS/GLONASS Navigation in Conditions of Limited Satellite Visibility," *Proceedings of the 21st International Technical Meeting of the Satellite Division of The Institute of Navigation*, 16-19 September, Savannah, GA, pp. 1398-1405

Cai, C., Y. Gao, L. Pan, and W. Dai (2013) "An Analysis On Combined GPS/COMPASS Data Quality and Its Effect On Single Point Positioning Accuracy Under Different Observing Conditions," *Journal of Advances in Space Research*, Available online 7 March 2013, ISSN 0273-1177, http://dx.doi.org/10.1016/j.asr.2013.02.019

Chan, F-C. and B. Pervan (2010) "A Practical Approach to RAIM-based Fault-Tolerant Position Estimation," *Proceedings of the 23rd International Technical Meeting of The Satellite Division of the Institute of Navigation*, 21-24 September, Portland, OR, pp. 3181-3190

Chin, G. Y., J. H. Kraemer, G. C. Nim, and K. L. Van Dyke (1997) "GPS/GLONASS RAIM Augmentation to WAAS for CAT I Precision Approach," *Proceedings of the 53rd Annual Meeting of The Institute of Navigation*, 30 June - 2 July, Albuquerque, NM, pp. 461-472

China Satellite Navigation Office (2012a) *Development of BeiDou Navigation Satellite System*, presented at the 7th Meeting of International Committee on GNSS (ICG), 5 November, Beijing, China

China Satellite Navigation Office (2012b) *Report on the Development of BeiDou Navigation Satellite System*, version 2.1, December

Choi, M., J. Blanch, D. Akos, L. Heng, G. Gao, T. Walter, and P. Enge (2011) "Demonstrations of Multi-constellation Advanced RAIM for Vertical Guidance Using GPS and GLONASS Signals," *Proceedings of the 24th International Technical Meeting of The Satellite Division of the Institute of Navigation*, 20-23 September, Portland, OR, pp. 3227-3234

Cooley, B. (2013) *Global Positioning Systems Directorate: GPS Program Update to ION GNSS+ 2013*, presented at the 26th International Technical Meeting of The Satellite Division of the Institute of Navigation, 18 September, Nashville, TN

Duan, X., K. Jiang, Y. Zheng, J. Yao, and W. Yang (2011) "Combined Integrity Analysis of GPS, Galileo and COMPASS with Comparison of Different Strategies," *Proceedings of the 24th International Technical Meeting of The Satellite Division of the Institute of Navigation*, 20-23 September, Portland, OR, pp. 3217-3226

Dumas, P-Y. (2011) "GLONASS-K for Airborne Applications Issue and Perspectives," *Inside GNSS*, issue July/August, pp. 46-50

EGNOS SDD (2013) *EGNOS Safety of Life (SoL) Service Definition Document (SDD)*, issue 2.0, 28 June, European Union

Ene, A. (2006) "Further Development of Galileo-GPS RAIM for Vertical Guidance," *Proceedings of the 19th International Technical Meeting of the Satellite Division of The Institute of Navigation*, 26-29 September, Fort Worth, TX, pp. 2597-2607

Ene, A., J. Blanch, and T. Walter (2006) "Galileo-GPS RAIM for Vertical Guidance", *Proceedings of the 2006 National Technical Meeting of The Institute of Navigation*, 18-20 January, Monterey, CA, pp. 432-440

ESA (2013a) *Galileo – A Constellation of 30 Navigation Satellites*, European Space Agency, http://www.esa.int/Our_Activities/Navigation/The_future_-_Galileo/Galileo_a_ constellation_of_30_navigation_ satellites, site updated 15 January 2013, last accessed 25 February 2013

ESA (2013b) *Galileo and GPS 'Synchronise Watches': New Time Offset Helps Working Together*, 3 May, European Space Agency, http://www.esa.int/Our_Activities/ Navigation/Galileo_and_GPS_synchronise_watches_new_time_offset_helps_working_ together, last accessed 24 May 2013

ESA (2013c) *Galileo Starts to Tell UTC, The World's Time*, 25 April, European Space Agency, http://www.esa.int/Our_Activities/Navigation/Galileo_starts_to_tell_UTC the_world_s_ time, last accessed 24 May 2013

ESA (2002) *Galileo Mission High Level Definition*, 23 September, European Space Agency

ESA Fact Sheet (2013) *Galileo System Architecture*, European Space Agency, document from http://www.satellite-navigation.eu, updated 15 February 2013

Essen, L. and J.V.L. Parry (1955) "An Atomic Standard of Frequency and Time Interval: A Caesium Resonator," *Nature*, vol. 176, no. 4476, 13 August, pp. 280-282

European Space Agency (2005) *EGNOS Factsheets 12: The Signal EGNOS Explained*, May 2005

Federal Aviation Administration (FAA) U.S. Department of Transportation (2010) *Navigation Programs – WAAS – How It Works*, http://www.faa.gov/about/office_org/ headquarters_ offices/ato/service_units/techops/navservices/gnss/waas/howitworks, last accessed 13 September 2012

Feng, S., C. Milner, A. Jokinen, W. Ochieng, C. Hide, T. Moore, C. Hill, M. Ziebart, M. Bahrami, P. Groves, and Z. Jiang (2011) "A Novel Positioning and Integrity Monitoring Algorithm for a Multiple Constellation Receiver," *Proceedings of the 24th International Technical Meeting of The Satellite Division of the Institute of Navigation*, 20-23 September, Portland, OR, pp. 2681-2688

Galileo ICD (2010) *European GNSS (Galileo) Open Service Signal In Space Interface Control Document (OS SIS ICD)*, issue 1.1, September 2010, European Union

Ge, M., H. Zhang, X . Jia, S. Song, and J. Wickert (2012) "What Is Achievable with the Current Compass Constellation?" *GPS World*, 1 November, http://www.gpsworld.com/what-is-achievable-with-the-current-compass-constellation

Gerdan, G.P., L.J. Coombe, and F. Takac (1995) *The Effects of RF Interference, Multipath and Signal Obstruction on the GPS Observables*, Department of Land Information, Royal Melbourne Institute of Technology, Technical report prepared for the State Data Center, report no. SDC95/1, December, Victoria, Australia, 32 pages

GLONASS-ICD (2008) *Global Navigation Satellite System (GLONASS) Interface Control Document (ICD)*, edition 5.1, Moscow, Russian Institute of Space Device Engineering

GNSS Supervisory Authority (GSA) European GNSS Agency (2011) *What is SBAS?*, http://egnos-portal.gsa.europa.eu/discover-egnos/about-egnos/what-sbas, last accessed 13 September 2012

GPS-SPS-PS (2008) *Global Positioning System Standard Positioning Service Performance Standard*, US Department of Defense and GPS Navstar, 4th edition, September

GPS.GOV (2013a) *New Civil Signals*, website owner: National Coordination Office for Space-Based Positioning, Navigation, and Timing, http://www.gps.gov/systems/gps/modernization/civilsignals, site updated 6 February 2013, last accessed 24 June 2013

GPS.GOV (2013b) *Space Segment*, website owner: National Coordination Office for Space-Based Positioning, Navigation, and Timing, http://www.gps.gov/systems/gps/space, site updated 19 August 2013, last accessed 4 September 2013

Guinot, B. and E.F. Arias (2005) "Atomic Time-keeping from 1955 to The Present," *Metrologia*, vol. 42, no. 3, pp. S20–S30

Hahn, J.H. and E.D. Powers (2005) "Implementation of the GPS to Galileo time offset (GGTO)," *Frequency Control Symposium and Exposition, Proceedings of the 2005 IEEE International*, 29-31 August, pp.33-37

He, L., M. Ge, J. Wang, J. Wickert, and H. Schuh (2013) "Experimental Study on the Precise Orbit Determination of the BeiDou Navigation Satellite System," *Journal of Sensors*, vol. 13, issue 3, pp. 2911-2928

Heng, L., G.X. Gao, T. Walter, and P. Enge (2012a) "GPS Signal-in-Space Integrity Performance Evolution in the Last Decade," *Transactions on Aerospace and Electronic Systems, IEEE*, vol.48, no.4, October, pp. 2932-2946

Heng, L., G.X. Gao, T. Walter, P. Enge (2012b) "Statistical Characterization of GLONASS Broadcast Clock Errors and Signal-In-Space Errors," *Proceedings of the International Technical Meeting (ITM) of The Institute of Navigation*, 30 January – 1 February, Newport Beach, CA, pp. 1697-1707

Hewitson, S. (2003) "GNSS Receiver Autonomous Integrity Monitoring: A Separability Analysis," *Proceedings of the 16th International Technical Meeting of the Satellite Division of The Institute of Navigation*, 9-12 September, Portland, OR, pp. 1502-1509

Hewitson, S. and J. Wang (2006) "GNSS Receiver Autonomous Integrity Monitoring (RAIM) Performance Analysis," *GPS Solutions*, vol. 10, issue 3, pp. 155-170

ICAO-China (2012) *The Development and Application of BeiDou Satellite Navigation System*, Technical report presented by China at the 12th Air Navigation Conference by International Civil Aviation Organization (ICAO), 19-30 November, Montreal, Canada, 4 pages

IGS (2013) *IGS Real-time Service*, International GNSS Service Central Bureau, document from http://www.igs.org/igscb/resource/pubs/IGS_Real_Time_Service_131031.pdf

Inside GNSS (2013) "ESA Adds System Time Offset to Galileo Navigation Message," *Inside GNSS*, issue May/June, published online http://www.insidegnss.com/node/3560

Inside GNSS (2011) "Russia's First GLONASS-K In Orbit, CDMA Signals Coming," *Inside GNSS*, issue March/April, published online http://www.insidegnss.com/node/2487

IS-GPS-200G (2012) *Global Positioning Systems Directorate Systems Engineering & Integration Interface Specification IS-GPS-200*, Navstar GPS Space Segment/Navigation User Interfaces, 5 September

IS-GPS-705C (2012) *Global Positioning Systems Directorate Systems Engineering & Integration Interface Specification IS-GPS-705*, Navstar GPS Space Segment/User Segment L5 Interfaces, 5 September

IS-GPS-800C (2012) *Global Positioning Systems Directorate Systems Engineering & Integration Interface Specification IS-GPS-800*, Navstar GPS Space Segment/User Segment L1C Interface, 5 September

ITU-R TF.460-5 (1997) *Recommendation ITU-R TF.460-5, Standard-frequency and Time-signal Emissions*, International Telecommunication Union

Kaplan, E.D. and C.J. Hegarty (2006) *Understanding GPS: Principles and Applications*, 2nd edition, Artech House, MA, USA

Lee, Y.C. (2013) "New Advanced RAIM with Improved Availability for Detecting Constellation-wide Faults, Using Two Independent Constellations," *Navigation,* vol. 60, no. 1, Spring, pp. 71-83

Lee, Y.C. (2006) "A New Improved RAIM Method Based on the Optimally Weighted Average Solution (OWAS) Under the Assumption of a Single Fault," *Proceedings of the 2006 National Technical Meeting of The Institute of Navigation*, 18-20 January, Monterey, CA, pp. 574-586

Lee, Y.C. (2004) "Investigation of Extending Receiver Autonomous Integrity Monitoring (RAIM) to Combined Use of Galileo and Modernized GPS," *Proceedings of the 17th International Technical Meeting of the Satellite Division of The Institute of Navigation*, 21-24 September, Long Beach, CA, pp. 1691-1698

Lee, Y.C. (1986) "Analysis of Range and Position Comparison Methods as a Means to Provide GPS Integrity in the User Receiver," *Proceedings of The Institute of Navigation, 42nd Annual Meeting*, 24-26 June, Seattle, WA, pp. 1-4

Lee, Y.C. and T. Cashin (2010) "Advanced RAIM Based on Inter-Constellation Comparisons to Detect Consistent Faults for LPV-200," *Proceedings of the 23rd International Technical Meeting of The Satellite Division of the Institute of Navigation*, 21-24 September, Portland, OR, pp. 272-284

Lee, Y.C., R. Braff, J.P. Fernow, D. Hashemi, M.P. McLaughlin, and D. O'Laughlin (2005) "GPS and Galileo with RAIM or WAAS for Vertically Guided Approaches," *Proceedings of the 18th International Technical Meeting of the Satellite Division of The Institute of Navigation*, 13-16 September, Long Beach, CA, pp. 1801-1825

Lewandowski, W. and E.F. Arias (2011) "GNSS Times and UTC," *Metrologia*, vol. 48, no. 4, pp. S219-S224

Lockheed Martin Press Release (2012) *U.S. Air Force Awards Lockheed Martin GPS III Flight Operations Contact*, 31 May 2012, Lockheed Martin Corporation, http://www.lockheedmartin.com/us/news/press-releases/2012/may/0531-ss-gpsIII.html, last accessed 6 September 2013

Madonna, P., S. Viola, and L. Sfarzo (2010) "NIORAIM Algorithm Applied to a Multiconstellation GNSS: Analysis of Integrity Monitoring Performances in Various Phases of Flight," *Proceedings of IEEE/ION PLANS 2010*, 4-6 May, Indian Wells, CA, pp. 1258-1263

Martineau, A., C. Macabiau, and M. Mabilleau (2009) "GNSS RAIM Assumptions for Vertically Guided Approaches," *Proceedings of the 22nd International Meeting of the Satellite Division of the Institute of Navigation*, 22-25 September, Savannah, GA, pp. 2791-2803

Miaoyan, Z., Z. Jun, and Q. Yong (2008) "Multi-Constellation RAIM for Simultaneous Double-Fault Satellite Scenarios," *Proceedings of the 21st International Technical Meeting of the Satellite Division of The Institute of Navigation*, Savannah, 16-19 September, GA, pp. 123-131

Misra, P., and P. Enge (2011) Global Positioning System: Signals, Measurements, and Performance, revised 2nd edition, Ganga-Jamuna Press, Lincoln, MA

Moudrak, A., A. Konovaltsev, J. Furthner, J. Hammesfahr, A. Bauch, P. Defraigne, S. Bedrich, and A. Schroth (2005) "Interoperability on Time: GPS-Galileo Offset Will Bias Position," *GPS World*, March, pp. 24-32

Murphy, T.A. (2005) *Determining the Vertical Alert Limit Requirements for a Level of GBAS Service that is Appropriate to Support CAT II/III operations*, vol. 4, 19 October, Boeing Commercial Airplanes – Electronic Systems, Boeing

Neri, P., L. Azoulai, and C. Macabiau (2011) "Study of the Temporal Behavior of GPS/GALILEO NSE and RAIM for LPV200," *Proceedings of the 24th International Technical Meeting of The Satellite Division of the Institute of Navigation*, 20-23 September, Portland, OR, pp. 3796-3813

Obst, M. and G. Wanielik (2013) "Probabilistic Non-Line-of-Sight Detection in Reliable Urban GNSS Vehicle Localization based on an Empirical Sensor Model," *Proceedings of IEEE Intelligent Vehicles Symposium*, 23-26 June, Gold Coast, Australia, pp. 363-368

O'Keefe, K. (2001) "Availability and Reliability Advantages of GPS/Galileo Integration," *Proceedings of the 14th International Technical Meeting of The Satellite Division of the Institute of Navigation*, 11-14 September, Salt Lake City, UT, pp. 2096-2104

O'Keefe, K., S. Ryan, and G. Lachapelle (2002) "Global Availability and Reliability Assessment of the GPS and Galileo Global Navigation Satellite Systems," *Canadian Aeronautics and Space Journal*, vol. 48, no. 2, June, pp. 123-132

O'Keefe, K., G. Lachapelle, A. Di Fazio, and D. Bettinelli (2011) "Receiver Autonomous Integrity Monitoring in Urban Vehicle Navigation: The Five Satellite Case," *Journal of Global Positioning Systems*, vol. 10, no. 2, pp. 157-164

Penna, N., A. Dodson, and W. Chen (2001) "Assessment of EGNOS Tropospheric Correction Model," *The Journal of Navigation*, vol. 54, issue 1, pp. 37-55

Petovello, M. (2013) "Calculating Time Offsets: How Do You Deal With Timing Differences Between GNSSes?" *Inside GNSS*, issue May/June, pp. 32-37

Petovello, M., S. Pullen, J. Syrjarinne, and L. Wirola (2008) "Quantifying the Performance of Navigation Systems and Standards for Assisted-GNSS," *Inside GNSS*, issue September/October, pp. 20-24

Phelan, J., T. Dass, G. Freed, J. Rajan, J. D'Agostino, M. Epstein (2005) "GPS block IIR clocks in space: current performance and plans for the future," *Proceedings of the IEEE International Frequency Control Symposium and Exposition,* 29-31 August, pp. 19-25

Qian, S. and Z. Jun (2011) "Optimized key parameters on RAIM performance for vertically guided approaches," *IEEE 5th International Conference on Cybernetics and Intelligent Systems*, 17-19 September, Qingdao, China, pp.288-293

Qian, S. and Y. Yuan (2013) "River Information and Navigation Service with BeiDou in China," *Proceedings of the International Technical Meeting (ITM) of The Institute of Navigation*, 28-30 January, San Diego, CA, pp.403-408

Ren, Z., L. Li, J. Zhong, and M. Zhao (2012) "Instantaneous Cycle-Slip Detection and Repair of GPS Data Based on Doppler Measurement," *International Journal of Information and Electronics Engineering*, vol. 2, no. 2, March 2012

Ren, Z., L. Li, J. Zhong, M. Zhao, and Y. Shen (2011) "Real-time Cycle-slip Detection and Repair Method for Single Frequency GPS Receiver," *International Proceedings of Computer Science and Information Technology (IPCSIT)*, vol. 17, IACSIT Press, Singapore, pp. 224-230

Revnivykh, S.G. (2010) *GLONASS Status and Progress*, presented at Civil GPS Service Interface Committee (CGSIC), 21 September, Portland, OR

Russian Federal Space Agency (2013) *GLONASS Constellation Status*, Information-Analytical Centre, http://glonass-iac.ru/en/GLONASS, last accessed 28 May 2013

Sakai, T., H. Yamada, and K. Hoshinoo (2012) "GPS/GLONASS Multi-Constellation SBAS Trial and Preliminary Results for East-Asia Region," *Proceedings of the 25th International Technical Meeting of The Satellite Division of the Institute of Navigation*, 17-21 September, Nashville, TN, pp. 854 -866

Salós, D., C. Macabiau, A. Martineau, B. Bonhoure, and D. Kubrak (2010a) "Analysis of GNSS integrity requirements for road user charging applications," *Proceedings of the 5th ESA Workshop on Satellite Navigation Technologies and European Workshop on GNSS Signals and Signal Processing (NAVITEC)*, 8-10 December, Noordwijk, Netherlands, pp.1-8

Salós, D., C. Macabiau, A. Martineau, B. Bonhoure and D. Kubrak (2010b) "Nominal GNSS Pseudorange Measurement Model for Vehicular Urban Applications," *Proceedings of IEEE/ION PLANS 2010*, 4-6 May, Indian Wells, CA, pp. 806-815

Salós, D., A. Martineau, C. Macabiau, D. Kubrak, and B. Bonhoure (2010c) "Groundwork for GNSS Integrity Monitoring in Urban Road Applications. The Road User Charging Case," *Proceedings of the 23rd International Technical Meeting of The Satellite Division of the Institute of Navigation*, 21-24 September, Portland, OR, pp. 1130-1144

Simon, J., J. Vazquez, A. Madrazo, A. Cezon, and W. Enderle (2010) "Advanced RAIM Scheme and its Evaluation for Non-aeronautical users in Different Environments," *Proceedings of the 23rd International Technical Meeting of The Satellite Division of the Institute of Navigation*, 21-24 September, Portland, OR, pp. 292-300

Sun, Q. and J. Zhang (2009) "RAIM method for improvement on GNSS reliability and integrity," *Proceedings of the 28th Digital Avionics Systems Conference*, IEEE/AIAA, 23-29 October, pp. 7.D.3-1-7.D.3-11

Van Diggelen, F. (2009) *A-GPS: Assisted GPS, GNSS, and SBAS*, 1st edition, Artech House, MA, USA

Vanschoenbeek, I., B. Bonhoure, M. Boschetti, and J. Legenne, (2007) "GNSS Time Offset: Effect on GPS-Galileo Interoperability Performance," *Inside GNSS*, issue September/October, pp. 60-70

Walter, T., J. Blanch, M.J. Choi, T. Reid, and P. Enge (2013) "Incorporating GLONASS into Aviation RAIM Receivers," *Proceedings of the International Technical Meeting (ITM) of The Institute of Navigation*, 28-30 January, San Diego, CA, pp.239-249

Walter, T., P. Enge, J. Blanch, and B. Pervan (2008) "Worldwide Vertical Guidance of Aircraft Based on Modernized GPS and New Integrity Augmentations," *Proceedings of the IEEE*, vol. 96, no. 12, December, pp.1918-1935

Winit, R. and K. O'Keefe (2013) "Four-constellation Reliability in Challenging GNSS Signal Environments and the Estimation of Inter-system Time-offsets," *Proceedings of the 26th International Technical Meeting of The Satellite Division of the Institute of Navigation*, 18-20 September, Nashville, TN, pp. 383-397

Winit, R., K. O'Keefe, A. Di Fazio, D. Bettinelli, and A. Nardi (2013) "Integrity Performance Analysis of GPS-GLONASS with EGNOS for Applications in Complex GNSS Environments," *Proceedings of the International Technical Meeting (ITM) of The Institute of Navigation*, 28-30 January, San Diego, CA, pp. 758-770

Yun, H. and C. Kee (2013) "A New Sequential RAIM Algorithm for Multiple Failures Detection," *Proceedings of the International Technical Meeting (ITM) of The Institute of Navigation*, 28-30 January, San Diego, CA, pp. 234-238

Zhao, Q., J. Guo, M. Li, L. Qu, Z. Hu, C. Shi, and J. Liu, (2013) "Initial Results of Precise Orbit and Clock Determination for COMPASS Navigation Satellite System," *Journal of Geodesy*, vol. 87, issue 5, pp 475-486

Zinoviev, A.E. (2005) "Using GLONASS in Combined GNSS Receivers: Current Status," *Proceedings of the 18th International Technical Meeting of the Satellite Division of the Institute of Navigation*, 13-16 September, Long Beach, CA, pp. 1046-1057